Ph.D. Dissertation of Engineering

Classification of Deforested and Degraded Areas in North Korea Using Phenology-based Indices and Spatiotemporal Data Fusion Method

계절특성 기반의 지수와 시공간 융합기법을 활용한 북한 황폐지역 분류

February 2018

Graduate School of Seoul National University

Interdisciplinary Program in Landscape Architecture

Yihua Jin

Classification of Deforested and Degraded Areas in North Korea Using Phenology-based Indices and Spatiotemporal Data Fusion Method

Advisor: Dong-Kun Lee

A Dissertation Submitted for the Degree of Engineering Doctor of Philosophy

February 2018

Seoul National University

Interdisciplinary Program in Landscape Architecture

Yihua Jin

Approved by Thesis Committee

Chair _____ (Seal)

Vice Chair _____ (Seal)

Examiner _____ (Seal)

Examiner _____ (Seal)

Examiner _____ (Seal)

Abstract

Classification of Deforested and Degraded Areas in North Korea Using Phenology-based Indices and Spatiotemporal Data Fusion Method

Yihua Jin

Interdisciplinary Doctoral Program in Landscape Architecture,

Graduate School, Seoul National University

Supervised by Professor Dong-Kun Lee

Forest ecosystems provide ecological benefits to both humans and biodiversity. Long-term anthropogenic pressure on forests, and frequent disturbance such as forest fires, landslides, and droughts, combined with abiotic factors such as climate variability, create an unsustainable environment. North Korea, suffers from serious forest degradation and deforestation issues. Given that these issues are major threats to the present and future state of forest ecosystems, the country is home to some of the most degraded forests in the world. Poor agricultural practices in North Korea, such as the excessive use of pesticides and fertilizers, are damaging productive capacity of the land. Poor agricultural practices, deforestation, and overgrazing cause soil erosion and forest degradation. Climate change and extreme weather events impact North Korea's deforested lands and degraded

forests considerably, resulting in serious soil loss, landslides, and damage to farmlands and agricultural production. Furthermore, adaptation inerventions (including infrastructure) to extreme climate events, are lacking, and healthy forest ecosystems are essential elements for sustainable environment in North Korea. To provide systemic, prioritized restoration and planning efforts to address these problems, it is essential to establish a classification or monitoring system for typical types of deforestation and degradation.

Because land-cover maps for monitoring deforestation and degradation are among the most fundamental data used in many scientific fields, developing a cost-effective method for classifying forest cover with high accuracy and high spatial and temporal resolution where access to data is difficult or when data are not available, is still challenging and necessary for North Korea. For this purpose, a cost-effective method for classification and monitoring forest cover dynamics in high spatial and temporal resolutions was proposed in this study.

First, to classify types of deforested and degraded areas and to increase accuracy, this study proposed an optimal combination of phenology-based multi-index distinctions, as well as ways to distinguish complex, heterogeneous land cover in forests (such as hillside fields and unstocked forests) from plateau vegetation and natural forests. The outcomes of this research extend beyond those of most previous studies, which have usually been focused only on dryland forest. Previous work also involved the use of single-image classifications based only on spectral data to distinguish types

of deforestation, and consequently, had difficulty capturing the heterogeneous spectral signature of land-cover categories over large areas.

The outcomes of this work can be summarized as follows. 1) The seasonal patterns indicated by three indices (Normalized Difference Vegetation Index, Normalized Difference Soil Index, and Normalized Difference Water Index or NDVI, NDSI, and NDWI, respectively) showed differences typical of each type of vegetative cover in forest land. Thus, it was possible to overcome the reflectance value confusion that occurs when using only one image and increase the classification accuracy. 2) To classify complex land cover and dynamics, Random Forest proved to be a useful tool for classifying a variety of input features. The results highlighted the types of deforested land and their distribution in North Korea. The classification result showed an overall accuracy of 89.38% when phenology-based indices were combined with Random Forest. 3) The phenology-based indices that resulted in classification greater than 20% are the NDSI during the growing season (from March to May), the NDVI during the end of the season (September), and the NDWI during the start and end of the season (March/April and October). Combining these variables can effectively classify or help monitor vegetative cover.

Our method greatly improved accuracies for classification of heterogeneous vegetative cover and presented deforested areas more reliably. Therefore, it should be useful for continued monitoring of variation in forested areas during forest restoration efforts in North Korea. The ecological impacts of forest degradation in the study area should also be urgently considered.

Second, to construct the continuous fine-resolution satellite data using the most accessible datasets, a spatiotemporal data-fusion method was developed to blend satellite images in heterogeneous and spectrum-changing areas. However, previous methods have shown difficulties in predicting spectrum-changed pixels in fine resolution, as each band's value changed in different ways during the period of input and prediction dates. To overcome this limitation, this study proposed a spectrum-correlation-based spatiotemporal data-fusion method (RDSFM), to blend temporally fine-resolution data with temporally dense coarse-resolution data. The RDSFM integrates ideas from unmixing-based methods and a homogeneous index in the FSDAF, IR-MAD, and weighted-function-based method into one framework. The RDSFM was tested using a real landscape and compared to the referred spatiotemporal method, namely FSDAF. The results of the accuracy assessment demonstrate that the RDSFM has higher accuracy, especially in fragmented areas and the NIR band, and the method also maintains more spatial details.

The spectral change of each pixel solved in the RDSFM is more robust than that in the FSDAF because of the strategy of weights based on MAD. MAD addresses detection of nontrivial change in multi-bands and bi-temporal data based on canonical correlation analysis. To estimate the MAD-based weights, the MAD for detecting the temporal change used a fine-resolution image at t1 and a coarse-resolution image at t2. The MAD for detecting the changes occurred using different sensors, with a fine-resolution image at t1 and a coarse-resolution image at t2. This can effectively detect the relative

alteration of each band in one coarse pixel. This method can help accurately predict the pixel value in the areas where the spectrum changes due to land cover or within-class variance. The RDSFM, like other spatiotemporal data-fusion methods, can be applied to analyze land-cover dynamics, monitor vegetation phenology, detect land-cover change, and identify where degradation has occurred.

To determine the effectiveness of the aforementioned proposed methods, the most difficult regions for vegetative cover change monitoring were tested using a simple classifier-unsupervised classification. This part successfully demonstrated the technique's effectiveness and convenience. Using stacked phenology-based multi-variables with the RDSFM is a powerful means of reducing classification errors, and enables better characterization of complex land-cover change status at 30-m resolution. In this manner, the degradation and deforestation that occurred from 2001 to 2014 were detected in three cases: 1) degradation from forest to unstocked forest, 2) degradation from hillside farms to unstocked forest, and 3) deforestation from forest to hillside field. The classification result showed an overall accuracy of 86.1% when using the simple unsupervised classifier. It is clearly effective and convenient to perform annual land-cover change analysis to produce a transition matrix with no information. Finally, various applications for analyzing forest ecosystems were suggested, using information on land cover and detailed forest degradation in fine resolution.

In summary, a combination of phenology-based indices with a spectrum-

correlation-based spatiotemporal data-fusion method can improve the spatial and temporal resolution for classification or monitoring of deforestation and degradation. Furthermore, this study suggested that in monitoring forest cover dynamics, distinguishing forest degradation and deforestation is essential to systemic planning and various analyses of forest ecosystems.

Keywords : Forest degradation, Deforestation, Random forest, Iteratively reweighted multivariate alteration detection (IR-MAD), Unmixing based data fusion, Data fusion, Monitoring forest cover dynamics

Student number : 2014-31476

Table of Contents

List of Tables

List of Figures

I. Introduction

Forest ecosystems provide ecological benefits to both humans and wildlife (MA 2005). Growing global demand for development, food, and fiber is accelerating pressure from agriculture and logging on forest ecosystems around the world (Abood et al. 2015). These pressures have significant impacts on forest ecosystems, which include direct damage to remaining forest ecosystems, as well as changes in plant and animal species diversity through destruction of soil cover and vegetation (MA 2005; Sasaki and Putz 2009). Mapping and monitoring forest cover and vegetation condition is an operational topic that addresses issues such as climate change, biodiversity conservation, and sustainable ecosystem management.

North Korea (the Democratic People's Republic of Korea, [DPRK]) is known to have some of the most degraded forests in the world. Forest degradation and deforestation are considered major threats to the present and future of North Korea ecosystems. Between 1990 and 2015, nearly 40 percent of forests have either been converted to fields for food crop production or logged for wood fuel. In North Korea, there is not sufficient land to farm, and the remaining lands are not suitable for farming, therefore many forests have been converted to farmlands (Engler et al. 2014; Kang and Choi 2013; Lee et al. 2005).

For temporary agriculture, the trees in forests are cut down and burned in order to clear land, the land is used until its productivity declines, at which

point a new plot is selected and the process repeats. In addition, poor agriculture techniques such as the excessive use of pesticides or fertilizers are damaging land productive capacity. Poor agricultural practices, deforestation, and overgrazing cause soil erosion and forest degradation. The hillside farms created by sacrificing forest ecosystems are not sustainable, and ground in once-forested areas in North Korea has become more and more degraded, with denuded forest widely distributed (Engler et al. 2014; Lee et al. 1999). Furthermore, North Korea is heavily influenced by climate change. Recently, North Korea has suffered severe droughts and extreme weather events, and these combined with denuded forest has resulted in serious soil loss and landslides and damaged farmland and agricultural production. When a heavy rain occurs, soil runoff from hillsides is serious. This has resulted in nutrient loss in the soils of forests and other vegetation (Kim and Ryu 2009; Myeong et al. 2008)

Long-term anthropogenic pressure on forests (Baeza et al. 2007; Morris 2010), combined with abiotic factors such as climatic variability (Kosmas et al. 2015; Kumar and Jyoti Das 2014), and frequent disturbances such as fires, landslides, and droughts, create unsustainable environment (Bhatia and Thorne-Lyman 2002; Buma and Wessman 2011; Jucker Riva et al. 2017; Tang et al. 2010; Zheng et al. 1997). Developing countries still lack continuous forest inventories at national or lower levels, as most are carried out in industrialized countries. Therefore, forest management and planning, especially for adaption to extreme climatic events, are essential for a

sustainable environment in North Korea. To provide systematic, prioritized restoration and planning efforts to address these problems, it is important to have a mapping or monitoring system reflecting the regional character of deforestation and degradation (Chazdon 2008; Margono et al. 2012; Miettinen et al. 2014).

In previous studies regarding monitoring forest change in North Korea (Cha et al. 2009; Engler et al. 2014; Jeong et al. 2016b; Jung 2015; Kang and Choi 2013; Yeom et al. 2008; Zheng et al. 1997), the definition of forest degradation and deforestation is not clear; they only classified forest area and non-forest area to analyze reductions in forest, or only classified a deforested area as degradation. Because forest degradation and deforestation are different in their ecological structure and development processes, the impacts of each type on ecosystems should also be considered separately (Hosonuma et al. 2012; Sasaki and Putz 2009). Therefore, efforts to capture not only deforestation but also forest degradation in detail are essential because degradation and deforestation exist simultaneously in North Korea.

While methods for estimating deforestation have progressed in remote-sensing technology, estimating degradation still is subject to several difficulties. The deforestation variable is binary (0, 1), whereas that of degradation is not. The Food and Agriculture Organization (FAO) (2003) defined deforestation as "a decrease in the area covered by forest," and "degradation is not involving a reduction of the forest area, but rather a quality decrease in its condition, generally to its functioning." For estimating

degradation, continuous data are essential for monitoring vegetation condition and detecting degraded areas.

Land-cover maps for estimating deforestation, which are vital for monitoring, understanding, and predicting the effects of complex human-nature interaction, are one of the most fundamental information sources used in many scientific fields and are often produced from remotely sensed images (Bartholomé and Belward 2005; Friedl et al. 2002; Jucker Riva et al. 2017). A wide variety of remote-sensing systems have been developed; thus, images are available of different spatial and temporal resolutions, thereby allowing the production of land-cover maps at different spatial and temporal scales.

How to obtain satellite images of high spatial and temporal resolution is among the difficult problems in analyzing degradation and deforestation. Moderate Resolution Imaging Spectroradiometer (MODIS) data provide dense images at a coarse-resolution, and they are helpful for successive events, such as degradation. However, there are cases where several types of land cover are mixed into one coarse pixel, and this will cause errors in deforestation or other land-cover classification on a regional scale. In contrast, there are several types of satellite images of fine spatial resolution and low temporal resolution, such as Landsat images. They are helpful in classifying land cover in more detail, but there are difficulties in analyzing continuous events, such as degradation. Thus, mapping and monitoring forest cover of a high spatial and temporal resolution with high accuracy, in areas difficult to access such as North Korea, are still challenging tasks.

Rapid assessment of land-cover change and monitoring vegetation condition, such as deforestation and degradation, requires frequent measurements if it is to be incorporated into management and policy decisions. To meet all these requirements, developing a cost-effective method for processing satellite images of high spatial and temporal resolution is essential for periodic monitoring of land-cover change and vegetation condition.

In spite of numerous developed methods for mapping or monitoring land cover, mapping and monitoring deforestation and degradation with high accuracy and spatial and temporal resolution are still challenging tasks. Therefore, the objective of this research is to propose cost-effective methods for mapping and monitoring deforestation and degradation in North Korea.

This study proposed two types of methods for mapping and monitoring deforestation and degradation. First, we suggested key phenology-based indices for mapping deforestation in North Korea. To improve the accuracy in vegetative cover classification each year, this study found an optimal combination of phenology-based variables to effectively classify and monitor land-cover change and deforestation in North Korea. From this, the main results are a land-cover map reflecting deforestation status in North Korea at a coarse-resolution. Moreover, a key phenology-based variables combination derived from this work can be applied to classify or monitor land-cover dynamics with high accuracy and conveniently.

Second, to build continuous satellite data in fine resolution, using the most

accessible datasets, this study proposed a new concept of a spatiotemporal data-fusion method that can effectively predict in areas of spectrum-changed pixels. The spatiotemporal data-fusion method proposed here can improve the accuracy of spectral changes by phenology in heterogeneous vegetative cover. Through the proposed spatiotemporal data-fusion method, this study can create time-series, Landsat-like images at a MODIS time-resolution. The time-series fine-resolution data were applied to map deforestation and degradation in more detail. They were also used for monitoring degradation in fine resolution.

This study aims to answer the following research questions: 1) What is the optimal combination of variables for effectively mapping confusing vegetative cover? 2) How does one improve spatiotemporal data-fusion accuracy in spectrum-changed pixels? 3) What is the extent of degraded forest and deforestation in North Korea? 4) How have degradation rates changed from 1990 to 2016, and what are the drivers? 5) Are the proposed methods able to effectively detect deforestation and degradation?

II. Literature review

1. Studies of degradation and deforestation in North Korea

Forest degradation and deforestation are distinctly different processes. Deforestation involves the conversion of forest to another land-cover type, while forest degradation results when forests remain forests but lose their ability to provide ecosystem services (MA 2005; Sasaki and Putz 2009) or decrease in canopy cover (Wang et al. 2005a). However, previous research regarding forest cover in North Korea has not separated these two kinds of disturbances.

There are several studies (Cha and Park 2007; Jeong et al. 2006; Kang and Choi 2013; Lee et al. 2007; Lee et al. 1999; Lee et al. 2005) that have resulted in a land-cover map of North Korea, but they only classified low-level land-cover types (built-up, forest, farmland, open water, etc.), and detected the forest cover change analyzing the forest degradation or deforestation that occurred during the study period. For estimating deforestation where forest was converted to a hillside field, Jeong et al. (2016b) classified the deforestation with a standard of farmland with a slope greater than 16 degrees. Yoo et al. (2011) also detected the deforestation area with a slope greater than 8 degrees. But these studies used different thresholds of slope, and the slope standard for separating hillside fields and farmlands is not clear. Some studies have examined forest area dynamics. Zheng et al. (1997), Engler et al. (2014) and Kang and Choi (2013) analyzed forest cover trends from the past.

However, they only estimated area of forest disturbance, or only analyzed the change in forest cover, and did not consider deforestation and degradation separately.

In previous studies of forest cover in North Korea, researchers addressed forest degradation and deforestation as a comprehensive issue. Because forest degradation and deforestation are distinctly different processes, there is a need to distinguish degradation and deforestation from satellite imagery, to aid in planning or various analyses of forest ecosystems.

2. Studies for forest degradation monitoring

Forest degradation is the reduction in the capacity of a forest or of canopy cover and stocking to provide goods and services (FAO 2010). Monitoring and detecting forest degradation is more difficult than observing deforestation (Asner et al. 2005; Joshi et al. 2006; Matricardi et al. 2007; Mon et al. 2012; Panta et al. 2008), especially reduction in canopy cover, which is the main indicator to measure deforestation and forest degradation. (Mon et al. 2012).

Remote sensing can be used for the mapping of deforestation of a dynamic landscape, covering broad areas but retaining detail in the spatial distribution of target parameters. Several studies have mapped the land cover of North Korea using remote-sensing images. (Cha and Park 2007; Jeong et al. 2016b; Kim et al. 2010; Lee et al. 2007; Yoo et al. 2011). These studies only classified basic land-cover types, using a traditional classification method, such as

ISODATA or the maximum-likelihood method. Forest cover types in North Korea, natural forest, plateau vegetation, unstocked forest, hillside farmland, and farmland in flatland, have similar reflectance values at a particular time. Therefore, the use of one-image information to classify land cover that has a similar reflectance value will result in many errors.

In addition, many studies have successfully mapped species-level classification, mainly at highly localized spatial scales (Carleer and Wolff 2004; Immitzer et al. 2012; Ke et al. 2010; Martin et al. 1998). These studies typically depended on data that had intensive hyperspectral or high-spatial resolution imagery, such as Ikonos, QuickBird, WorldView-2, and LiDAR, limiting their applicability to land-cover classification across larger regions where it is difficult to acquire data.

Phenology information has been widely used for regional-to-global scale vegetation trends and change analysis (Funk and Budde 2009), and land cover classification (de Jong et al. 2011; Demir et al. 2013; Fensholt and Proud 2012; Fensholt and Rasmussen 2011; Fensholt et al. 2009). For land-cover classification based on time-series data, various methods have been developed.

Kalensky and Scherk (1975) suggested that using multi-date images selected on the basis of spectral patterns can significantly improve image classification rather than on the basis of image availability alone. Wolter et al. (1995) achieved relatively accurate species type classification using multiple Landsat image dates to capture phenological changes of different tree species.

Hill et al. (2010) determined an autumn image with an image from both the green-up and full-leaf phases was the optimal combination to derive an improved tree species map. They demonstrated the usefulness of multiple image dates to capture significant phenology differences which improved classification results among the species.

To achieve more detailed information on phenology in different types of landscapes, dense temporal images, such as MODIS images, are actively utilized. Yan et al. (2015) successfully classified various vegetative cover types using vegetation phenological characteristics from time series of MODIS-derived NDVI and EVI. Tuanmu et al. (2010), Kiptala et al. (2013), Akçakaya et al. (2009) are also demonstrated phenological information derived from MODIS images can improve the classification accuracy of various landscapes.

Through these previous studies, we can see phenological information is helpful to improve vegetative cover classification based on phenologically significant differences among landscape types, especially among vegetative covers that have similar reflectance in one satellite image. However, although phenological analysis and time-series classification have been widely used, the connections between these two techniques have been rarely investigated in the literature, and most methods need numerous continuous satellite images to derive phenologically different variables.

However, there is no satellite sensor that provides dense time-series images in fine spatial resolution. Therefore, there is a high urgency to find key

phenology-based indices for classification or monitoring vegetative cover and conduct phenology-driven classification with minimal datasets. To obtain dense time-series images in fine resolution applicable to achieve phenological information in fine resolution, a technique for enhancing spatial and temporal resolution is also necessary to obtain continuous satellite images in fine resolution.

3. Techniques for remote sensing data classification

Most previous land-cover classification studies have been focused on the classification of broad land-cover types, such as deforested areas or sand. In the classification algorithm, traditional classification methods, such as ISODATA (Wilson and Sader 2002; Zheng et al. 1997) and maximum likelihood (Cha and Park 2007), were used for classification of degraded forests for mapping. However, these are not appropriate for the classification of combined multi-date images because of the heterogeneous spectral signature of land-cover categories over large areas (Gómez et al. 2016).

Previous studies of land cover and land-cover change mapping have provided valuable insight into vegetation status and dynamics. However, these insights cannot be used directly because the definition of forest varies widely among studies and does not provide sufficient levels of information for detection of subtle differences.

Recently, machine-learning algorithms, such as neural network (Souza et al.

2013), support vector machines (SVM) (Adam et al. 2014), and random forest (RF), have been used to overcome these problems Among these algorithms, RF classification accuracy for mapping (Baccini et al. 2012; Grimm et al. 2008) or neural network has been shown to be better than a support vector machine or a neural network. Thus, RF could help overcome the shortcomings of using multiple parameters (Adam et al. 2014; Clark et al. 2010; Clerici et al. 2012; Eisavi et al. 2015; Senf et al. 2013). RF can be used in mountainous areas, where topographic variables tend to be highly collinear; thus, RF could improve forest classification (Franklin et al. 1994; Gartzia et al. 2013).

Thus, RF combined with phenological information could improve the classification of farmland and semi-arid vegetation by capturing specific seasonal patterns of each landscape type (Dymond et al. 2002; Senf et al. 2013). Synthetically, RF and phenological information could be used to improve the accuracy of the mapping of specific forest-cover types using various phenology-based indices.

4. Techniques for enhancing spatial and temporal resolution

Dense time-series data composed of satellite images with frequent coverage are important sources for studying land-surface dynamics, such as for monitoring phenology of vegetation (Jin and Eklundh 2014; Liu et al. 2015;

Shen et al. 2011), mapping deforested and degraded areas (Grinand et al. 2013; Jacques et al. 2014; Renó et al. 2011; Rishmawi and Prince 2016), and detecting land cover and land use change (Yang and Lo 2002; Zhu et al. 2012). Obtaining phenological information also requires dense time series fine-resolution data. However, no single satellite sensor currently provides global coverage of dense time-series data with fine spatial resolution due to the tradeoff between pixel size and swath width as cloud contamination (Gevaert and García-Haro 2015; Zhu et al. 2016).

There are two types of satellite images easily acquired and applicable over the past several decades, one with frequent coverage of every one or two days, but a coarse spatial resolution of from 250 m to 1 km, such as MODIS images (hereafter "coarse-resolution images"), and the other with fine spatial resolution of from 10 m to 30 m, but with a long revisit cycle of 16 days, such as Landsat images (hereafter "fine-resolution images"). The spatiotemporal data-fusion methods have been developed to fuse these two types of satellite images to generate data with both fine spatial resolution and frequent coverage(Fu et al. 2013; Gao et al. 2006; Gevaert and García-Haro 2015; Hilker et al. 2009; Huang and Zhang 2014; Song and Huang 2013; Zhu et al. 2010; Zurita-Milla et al. 2008). These synthesized data can support the continuous information of land surface dynamics (Zhu et al. 2016).

Data-fusion offers a possible solution to the current available images of different resolutions. Existing spatiotemporal data-fusion methods can be categorized into three groups: STARFM-based, unmixing-based, and

machine-learning-based. All of these methods need one or more observed pairs of coarse-(e.g., MODIS) and fine-(e.g., Landsat) resolution images for training and a coarse-resolution image of prediction data as input data.

The Spatial and Temporal Adaptive Reflectance Fusion Model (STARFM), first proposed by Gao et al. (2006), detects reflectance through similar neighboring pixels weighted by spectral, temporal, and spatial distances. It blends Landsat and MODIS data to generate Landsat-like imagery on a daily basis. Enhanced STARFM (ESTARFM) (Zhu et al. 2010) and Spatial Temporal Adaptive Algorithm for Mapping Reflectance Change (STAARCH) (Hilker et al. 2009) have been developed to overcome STARFM's limitations. The STARFM-based, or weighted-function-based, approaches are particularly suited to reflectance changes caused by time, but not changes from land-cover change (e.g., the conversion of forested areas to built-up areas) (Zhu et al. 2016). However, STARFM-based methods proposed recently are strongly related to changes in similar pixels selected from input imagery, so that they are not effective in predicting spectrum-changed pixels that are sudden or are caused by phenology (e.g., a farmland spectral change from spring to summer or fall), or are not observed in input imagery (Fu et al. 2013; Gao et al. 2006; Zhu et al. 2010).

The Multisensory Multiresolution Technique (MMT), was proposed by Zhukov et al. (1999), as the first one to fuse images acquired at different sensors and different resolutions. MMT unmixes the coarse pixel with endmember fractions of each coarse pixel; it can also be called an unmixing-

based method. Several studies have modified MMT and tried to improve the accuracy of the blending (Gevaert and García-Haro 2015; Zhu et al. 2016; Zurita-Milla et al. 2008). Unmixing-based fusion methods also require that no land-cover type change occur between the input and prediction dates (Gevaert and García-Haro 2015; Zhukov et al. 1999; Zurita-Milla et al. 2008). The Flexible Spatiotemporal Data Fusion Method (FSDAF) proposed by Zhu et al. (2016) is one of the advanced models that predict fine-resolution images in heterogeneous areas more accurately using minimal input data. However, it cannot capture how reflectance values have changed within a range in each band of input imagery. For landscapes such as farmland, grassland or other vegetative cover, the spectrum responds in a different way through seasonal change. However, in the FSDAF, it provides the same weights to bands in the target pixel, causing errors especially in land cover changes in in-class areas. Thus, there is an urgent need for the development of novel fusion methods that can achieve high prediction accuracy regardless of a spectral change by phenology or land-cover change.

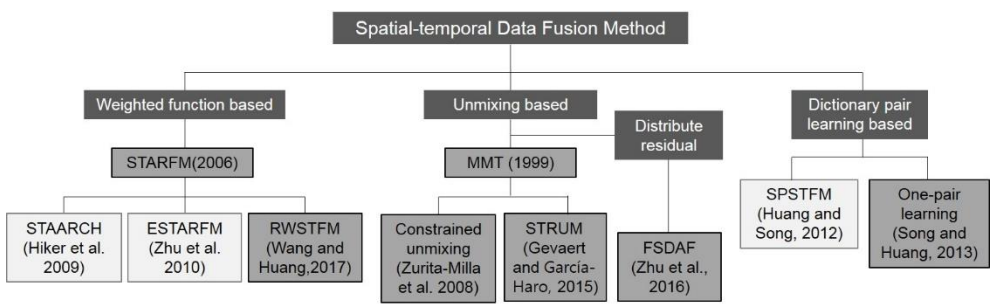

Figure 1. Summary of previous spatiotemporal data-fusion models. The light gray models need two fine-resolution images for input, and the dark gray models need one fine-resolution image for input.

III. Methods and materials

This study proposes two methods for mapping and monitoring deforestation and degradation as follows: 1) determining key phenology-based indices and suggest an optimal combination that can effectively classify or monitor deforestation and degradation in North Korea; and 2) proposing a residual-distribution-based spatiotemporal data-fusion model to monitor vegetative cover change in fine resolution. Figure 2 is the workflow of this study, and the details of each part are as follows.

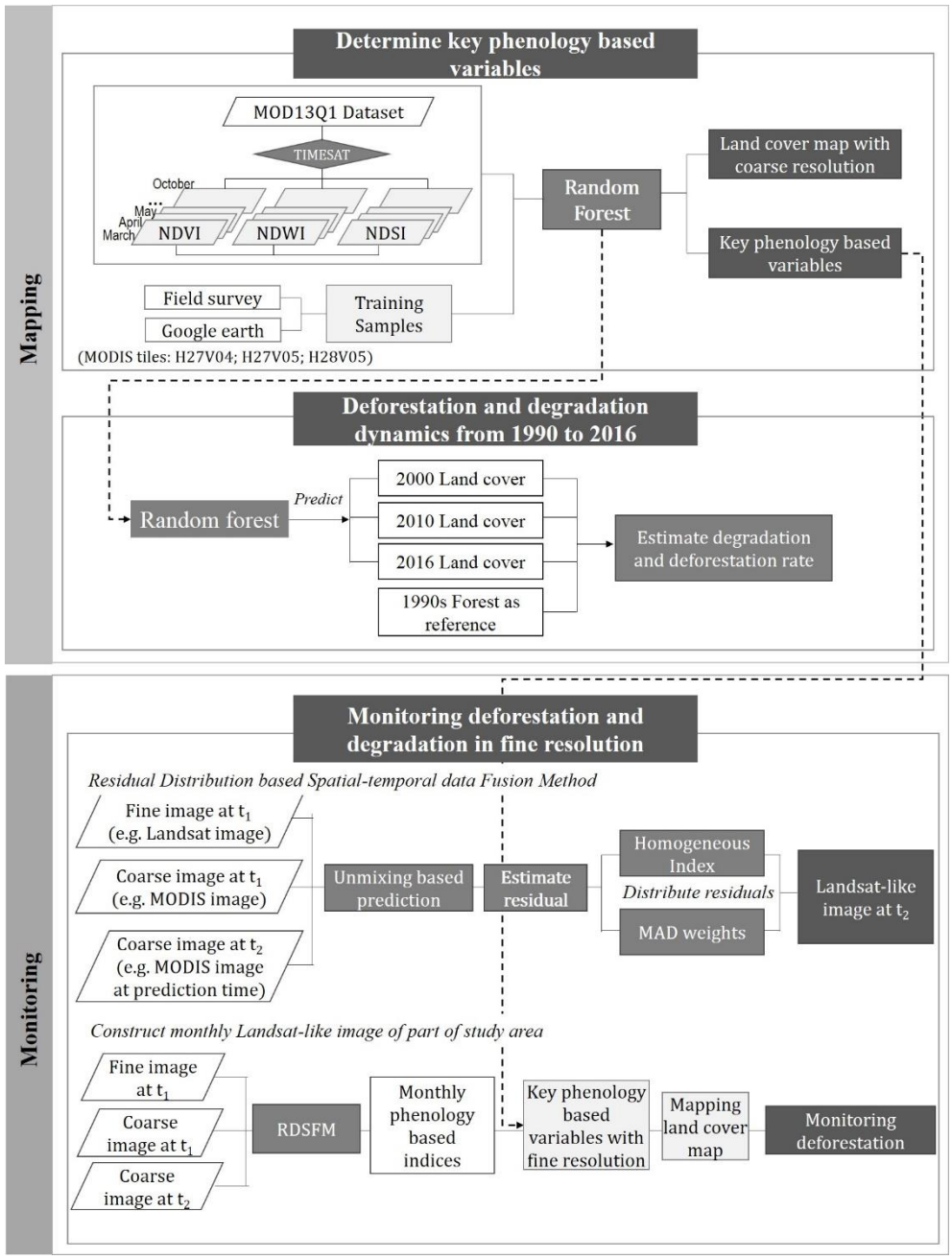

Figure 2. Workflow of this study

1. Study area

To determine the relevant variables for classifying the total main land-cover types in North Korea, the study area for the first part was chosen as the whole of North Korea as shown in Figure 3. North Korea encompasses approximately 123,138 km2 of land in far eastern Asia. The country is surrounded by rivers and ocean that comprise its borders with China and Russia in the north, and the 38th parallel forms its southern border with South Korea. North Korea has four distinct seasons: spring, summer, autumn, and winter.

The majority of the land cover in North Korea is mountain forest. There are mountain ranges in the north and east regions of the country that have plateaus that rise above 2,000 m. Examples of high plateau areas include the Gaema and Baeckmu plateaus, which are dominated by shrubs and grasses (Cha et al. 2009). The stocked forests are temperate broadleaf, conifer, and mixed forest. In response to extreme pressure to provide adequate food and energy, the size of the forested area in North Korea has shown a clear decreasing trend starting in the 1990s (Schoene et al. 2007). This region is experiencing one of the highest deforestation rates in the world. Moreover, there is a high probability of continued forest degradation due to shifting, slash and burn fields for crop cultivation, and logging. Annually, approximately 127 thousand hectares have been deforested, and forests in North Korea are already known to be among the most degraded in the world (LCLUC). The characteristic deforested land in North Korea includes areas in which crops

are cultivated after logging of the trees, and to which cultivation is then shifted onto terrace fields with slopes >16 degrees to produce food and fuel (Bhatia and Thorne-Lyman 2002; Tang et al. 2010; Zheng et al. 1997). In hillside fields, corn is the main crop. It is an annual plant with shallow roots, and is planted more densely on hillsides than is typical in flat land fields, which causes soil erosion and nutrient loss.

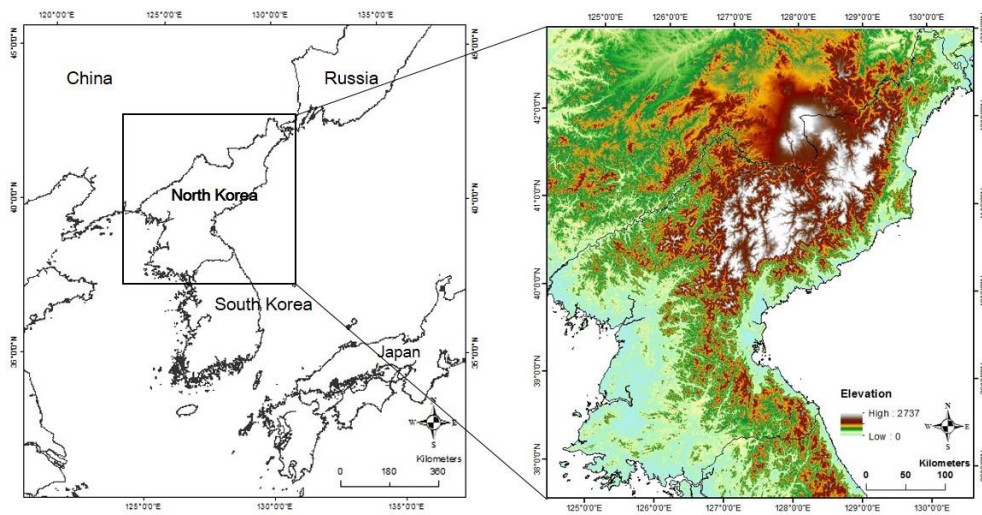

Figure 3. Study site

Unstocked forest (defined by the standard of South Korea, which is an area where the crown cover is <20% because of slash and burn), is covered with grasses and shrubs. In the flat lands the main land use types are paddies for rice production, fields for producing other crops such as potatoes and other vegetables, and built-up areas. This means that each type of vegetative cover presents a different phenological characteristic. More specifically, the farmland on the hillsides and the unstocked forests have different phenology from the woody and plateau vegetation (Thompson et al. 2013).

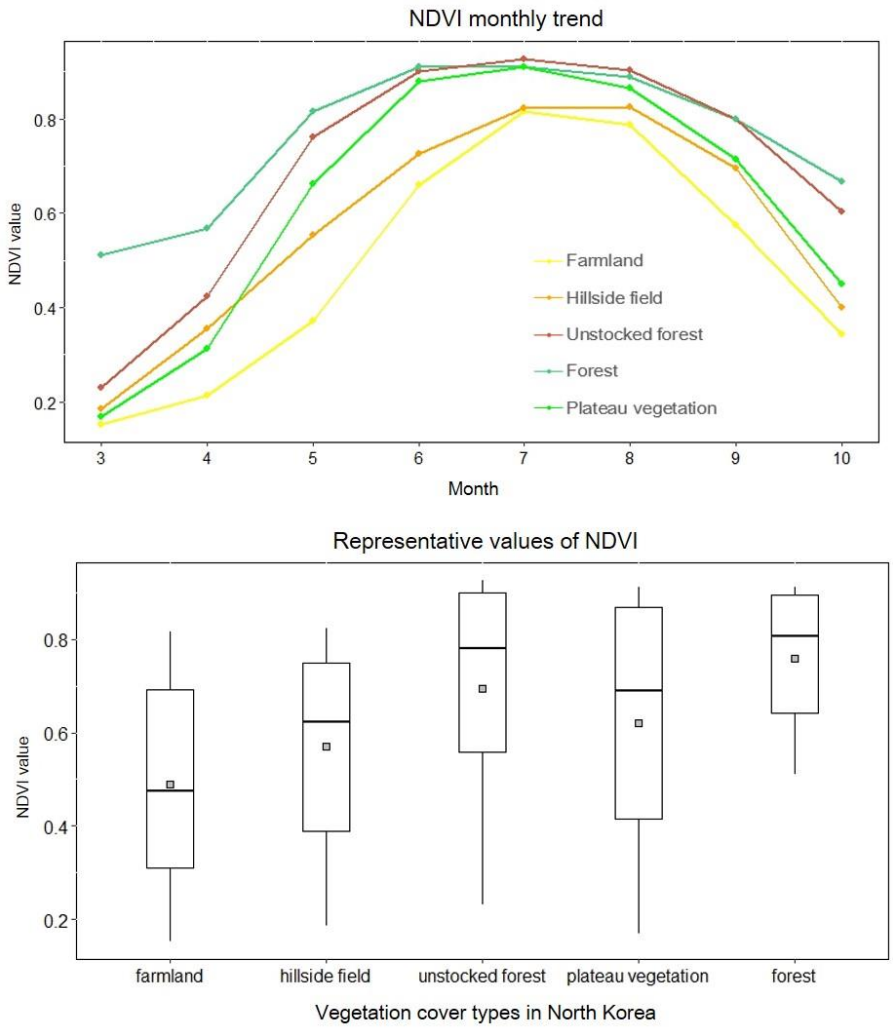

Figure 4. Monthly change and representative values of NDVI by vegetative cover types in North Korea

The monthly NDVI values of each vegetative cover type in North Korea are similar (Figure 4). This means that there are several confusing values occurring between vegetative cover types if one uses a single image. In other words, there is a limit to classifying vegetation types when using a single image, especially in North Korea.

To overcome the reflectance value confusion that occurs when using one image, many researchers have tried to use the representative values of reflectance or NDVI value during the year. The representative values of NDVI by vegetative cover types of North Korea are also presented in Figure 4. We can see that the representative NDVI values of each vegetative cover type are similar. For example, hillside field and plateau vegetation, unstocked forest and forest show similar mean values of NDVI. In addition, forest and plateau vegetation, farmland and hillside field have similar upper extreme values. This shows that there is also a limit to classifying vegetative cover in North Korea by only one type of phenological characteristic.

2. Determine key phenology-based indices

2.1 Data collection and pre-processing

2.1.1 MODIS data collection

The method proposed in this study relies upon the use of multi-temporal and multi-spectral images for classifying deforested areas according to the vegetation, soil, and water phenological characteristics identified. For this, this study the MODIS MOD13Q1 product acquired through USGS Earth Explore (www.earthexpoler.com) was used. MOD13Q1 data were used for deriving phenology-based indices and for predicting fine-resolution data through a spatiotemporal data-fusion model.

MOD13Q1 data were provided every 16 days at 250-m resolution, and included the Normalized Difference Vegetation Index (NDVI); Enhanced Vegetation Index (EVI); blue, red, and near infrared (NIR); and short-wave infrared (SWIR) reflectance. NDVI, RED, Blue, NIR, and SWIR bands were used in this study to extract biomass and chlorophyll content related to biological characteristics (Jensen and Cowen 1997) because most forest and crop plants have a relatively unique growth cycle (Yool et al. 1997). Therefore, this study retrieved the data from the MODIS tiles H27V05, H27V04, and H28V05 (which cover North Korea), from March to October (eight months), considering the growth cycles of the vegetation.

Elevation and slope were added to the classification scheme as predictor variables, which were derived from the SRTM 30-m digital elevation model (DEM). Both elevation and slope were presented using UTM projection with a bilinear interpolation method, and resampled to a 231.7-m cell size to match the MODIS datasets. Thus, the input variables for classification are NDVI (Normalized Difference Vegetation Index), NDSI (Normalized Difference Soil Index), and NDWI (Normalized Difference Water Index) from March to October, and topographic variables such as elevation and slope.

2.1.2 Pre-processing of time series data

The time-series raw data from satellite sensors had signal noise (Clark et al. 2010). We implemented smoothing of the time-series data and extraction of seasonality using TIMESAT v3.2(Eklundh and Jönsson 2015; Jönsson and Eklundh 2004) to reduce the influence of signal noise in the raw NDVI, Red,

NIR, and SWIR data from March to October 2013. This required at least two steps to obtain the phenological dates. First, a spectral profile was built to fit the discrete data into a smoothing curve (Gutman 1991; Holben 1986; Viovy et al. 1992); second, phenological dates were extracted based on the curves by applying certain thresholds or filtering models (Jonsson and Eklundh 2002; Lloyd 1990; Reed et al. 1994; Sellers et al. 1995). The function-fitting parameters used in TIMESAT were for the double logistic function, and the adaption strength was set to 2.0, the season cutoff to 0, and the start and end of the season threshold to 0.2.

Figure 5 shows an example fit to NDVI, Red, NIR and SWIR temporally smoothed from a forest sample. The twelve phenological variables extracted for each growing season included the following: 1) length of the season, 2) base level (average of the left and right minimum values), 3) largest data value for the fitted function during the season, 4) seasonal amplitude, 5) rate of increase at the beginning of the season, 6) rate of decrease at the end of the season, 7) small seasonal integral, 8) large seasonal integral, 9) number of seasons in a calendar year, 10) time of the start of the season, 11) time of the end of the season, and 12) time of the middle of the season. Use of these temporal factors allowed the program to have ample data to fit a full function to the growing seasons of North Korea.

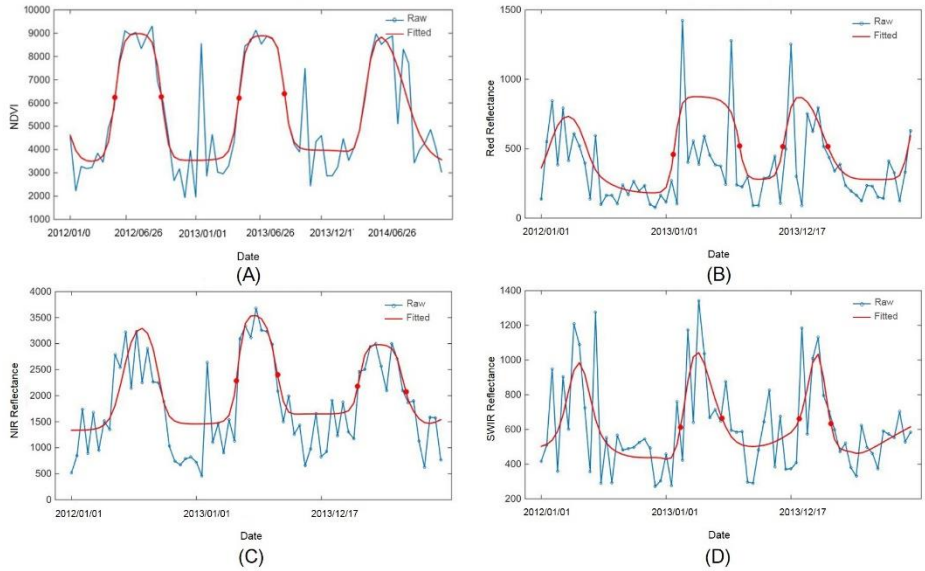

Figure 5. Raw and fitted MODIS NDVI (A), Red reflectance (B), NIR reflectan ce (C), and SWIR reflectance (D): TIMESAT seasonality variables derived fro m the functions are numbered on the figure for the interval from 2012. 1 to 20 13.12.

2.2 Reference data collection

2.2.1 Training samples collection

Representative samples for each class were collected by field survey; reference data from Google Earth; and land-cover maps of North Korea, which were provided by the Korean Forest Service in 2007. Direct collection of regions of interests (ROIs) in the data-scarce, remote areas of North Korea is limited due to political conditions. In this study, only the Chinese side of the North Korea-China border could be accessed for field survey (Figure 5a). On the northern border along the Tumen River, 112 GPS points were collected and we simultaneously observed the land-cover types on the North Korean

side of the river. This study also interpreted the visual criteria of each land-cover class (Table 1) in the satellite imagery of Quickbird and Google Earth (GE, http://www.google.com/earth/). Since GE launched in 2005, many studies have been conducted using GE to explore reference data (Clark et al. 2010; Hu et al. 2013). Hillside field and unstocked forest still have confusing visual characteristics in satellite images. Therefore, the land-cover map of North Korea, classified using spot images, was referenced to distinguish deforestation types.

The sampling method was demonstrated to have high accuracy for use with RF (Ye et al. 2013). All training points were selected across North Korea with point centers at least 500 m apart (Clark et al. 2010). The land-cover types of random points were identified by visual interpretation of each class (Table 1). The sample size per class was set to a minimum of 200 points for classification (Li et al. 2014), and total sample size was 1660 points containing the survey points (Figure 6).

Table 1. Classification types and visual interpretation used for identifying training samples in satellite images

Class	**Description**
Built up	Urban and buildings.
Waterbody	Lakes, reservoirs and rivers.
Paddy	Flooded field used to cultivate rice.
Field	Crop field with annual crops on flatland. It can be distinguished from paddy or other landscapes by the characteristics of plow lines, rectilinear shapes.
Hillside field	Crop field with annual crops on the hillside. It can be detected by 3D view in Google earth that offers elevation information.
Unstocked forest	This class is covered with shrubs or grasses, where crown cover of trees has fallen to < 20% because of slash and burn.

	This class can be confused with hillside field, but it can be detected by the texture and whether there are plow lines or not.
Natural forest	Trees are the major components.
Plateau vegetation	This class is covered with shrubs or grasses. It can be detected by elevation information and the distribution information from advanced research.

2.2.2 Test samples collection

Ground-truth points used for assessing the accuracy of our results were developed using a random-sampling method, which helps ensure that test samples are chosen in an unbiased manner and in proportion to the underlying, but as yet unmapped, land-cover and land use categories (Congalton and Green 2009).

The random points created in ArcGIS 10.1 were overlaid on the GE images identifying land-cover classes using the visual criteria described in Table 1. The random samples of natural forest were overabundant; in contrast, there were few samples for built-up, paddy, plateau vegetation, and water as these areas covered only small fractions of the landscape. Thus, this study implemented a stratified random sampling (Clark et al. 2010) for these classes. The polygons for built-up, paddy, and water categories were extracted from the land-cover map provided by the Korean Forest Service as a reference, and random points for these landscapes were created. Because there was no information regarding the plateau vegetation on the forest map, random points for plateau vegetation were created within the polygons with elevation > 1800 m. Finally, 999 sample points, with a minimum of 50 points in each class, were selected based on the recommendations of Congalton and

Green(Congalton and Green 2009) at intervals greater than 500m.

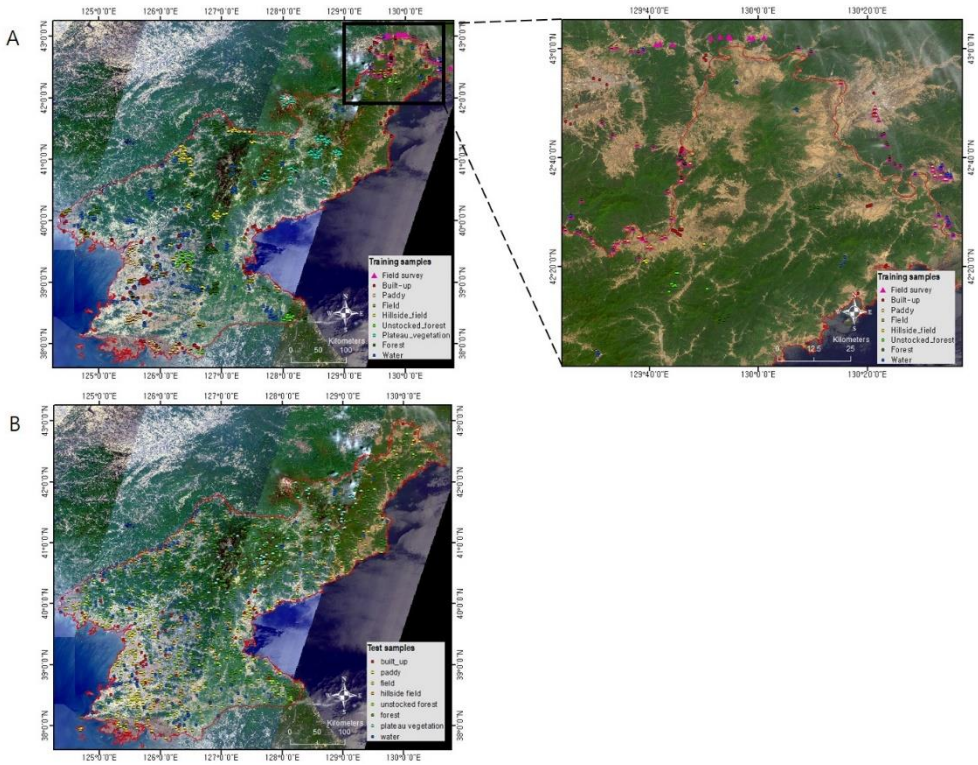

Figure 6. 1660 independent training samples (A) were collected regarding eight land-cover classes in North Korea with field survey. The 999 test points (B) used for the classification accuracy assessment were selected by random sampling. The displayed images are Landsat 8 OLE products.

2.3 Phenology-based indices for classification

2.3.1 Normalized phenology-based indices

Normalized indices show a much higher classification accuracy compared to original un-transformed spectral data. This is because normalization can be used to compensate for changing conditions of illumination, surface slope, and spectral variability due to a reduction in the viewing angle (Simonetti et al. 2014). Such indices can effectively detect changes from early spring

growth to late season maturity and senescence. In this study, multiple indices, NDVI, NDSI and NDWI, were used to enhance the classification accuracy, which indicated the existence of vegetation, soil, and water, respectively (Takeuchi and Yasuoka 2004). The equations of the indices are as follows:

$$\text{NDVI} = \frac{NIR-RED}{NIR+RED} \quad (1)$$

$$\text{NDSI} = \frac{SWIR-NIR}{SWI\ R+NIR} \quad (2)$$

$$\text{NDWI} = \frac{SWIR-RED}{SWIR+RED} \quad (3)$$

where Red, NIR and SWIR are the surface reflectance for bands 1, 2, and 7, respectively, of MODIS.

The NDVI is often used as an indicator to extract seasonal data from the relationships between spectral reflectance and vegetation canopy characteristics (Richard and Poccard 1998; Wang et al. 2005b; White and Nemani 2006). In this case, the R-band was used to represent spectral absorption by vegetation and the NIR-band the reflectance value (Equation 1). Therefore, the NDVI can characterize the properties of vegetation well (Huete et al. 2002; Setiawan et al. 2016). The NDVI is commonly used to complete spatial and temporal comparisons of terrestrial photosynthetic activity; thus, it is among the indicators of the state of land degradation and of the rate of increase or decrease in photosynthesis, which provides biophysical information (Ceccato et al. 2001; Prince and Goward 1995; Tucker 1980).

The NDSI is more sensitive to canopy structure (Deng et al. 2015) because

it identifies areas where soil is the dominant background or foreground material. The NDSI uses the SWIR- and NIR-bands (Equation 2), where SWIR represents the difference in the reflectance values between soil areas (Wolf 2010). Thus, the NDSI is a good indicator for separating areas of vegetation from areas of soil.

The NDWI, using NIR and SWIR reflectance values (Gao 1996)(Equation 3), is proposed for use in remote sensing of the liquid water content of vegetation canopies. It reflects surface canopy moisture and forest humidity (Gao 1996; Jiang et al. 2014). The NDWI has been used for monitoring water stress (Fensholt and Sandholt 2003), and for mapping burnt areas in boreal forest (Fraser and Li 2002). Thus, the changing pattern of the NDWI with the seasons could distinguish areas of natural vegetation, farmland, and soil, as related to moisture.

2.3.2 Random forest algorithm

RF has been used for classifying deforested areas in this study. RF is an ensemble of classification trees intended to improve classification accuracy (Breiman 2001). RF randomly selects samples of variables many times to produce a large number of classification trees. Each tree is individually trained on a bootstrapped sample of the training data and contributes a single vote for assignment of the most frequent class to the input data (Breiman 2001). RF can handle thousands of input features, and has been applied

recently in remote-sensing studies (Pal 2005; Rodriguez-Galiano et al. 2012; Senf et al. 2012).

Multi-temporal satellite images are effective in reducing the uncertainty associated with land-cover change (Grinand et al. 2013). Traditional classification algorithms (such as maximum likelihood) may not be appropriate for the classification of combined multi-date images because of the heterogeneous spectral signature of land-cover categories over large areas. To overcome this problem, roles for the RF classifier have recently emerged in remote sensing, and RF has been applied successfully in classifying complex land-cover status and dynamics.

RF was built using the software R (Team 2009) and the RF package(Liaw and Winener 2002). The number of trees (ntree) was set to 500, which proved to be a sufficient number for previous experiments (Senf et al. 2012). At each node, a number of variables (mtry) were randomly sampled from a random subset of the features, and 100 runs were performed. To estimate the accuracy of trees, the out-of-bag prediction was used to estimate the accuracy of all trees, which represents an unbiased estimate of map accuracy, as long as the reference data were obtained via probability sampling (Senf et al. 2013). To verify the classification result, this study used the confusion matrix to estimate overall, user's and producer's accuracies, and the kappa coefficient (Jensen 2005; Jeong et al. 2016a).

2.4 Deforestation and degradation dynamics from 1990 to 2016

2.4.1 Data collection

To extract degraded areas, this study needed to add a reference for use. This study selected as references and classified the forest during the 1990s because the forest in North Korea has shown a clearly decreasing trend starting from this period (Schoene et al. 2007). We used Landsat TM5 imagery downloaded from the US Geological Survey National Center for Earth Resources Observation and Science via the GLOVIS data portal (http://glovis.usgs.gov). All images in the early 1990s with cloud cover less than 5% for 12 Landsat scene tiles covering North Korea were selected. All Landsat images were atmospherically corrected.

Table 2. Information on remote-sensing data for mapping land cover from 1990 to 2016.

Years	**Remote sensed Products**	**Tiles (Path/Row)**	**Acquired time**
1990s	Landsat TM5 (30m)	115/030; 115/031 115/032; 115/033 116/031; 116/032 116/033; 116/034 117/031; 117/032 117/033; 118/032	1994-07-03; 1994-07-03 1994-07-03; 1991-08-12 1993-05-28; 1993-05-20 1992-06-02; 1992-06-02 1993-05-27; 1993-05-27 1992-06-01; 1990-09-15
2000	MOD13Q1 (250m) (band1, 2, 5, 7)	H27V04; H27V05 H28V05	DOY 065~ 305
2010			
2016			

The MODIS products of 2000, 2010, and 2016 and pre-processing were the

same as shown previously (2.1 MODIS and Landsat image data collection).

2.4.2 Deforestation and degradation mapping

The forest during the 1990s was used as the reference data; thus, we only classified the two kinds of land cover: forest and non-forest. Because the forest in North Korea, plateau forest, forests in the north, and forests in the south, show different reflectance and spatial differences, it is not clear where to find the reference training data for supervised classification, so unsupervised classification methods were considered for mapping. Various clustering algorithms are generally deployed in remote sensing. The two most well-known are the K-means and the ISODATA unsupervised classification algorithms. Both algorithms are strong in clustering, but the ISODATA algorithm supplies better results based on previous studies (EI_Rahman 2016).

Deforestation and degradation mapping using the MODIS products used the RF classification model developed in the previous section to predict land cover during 2000, 2010, and 2016.

Finally, this study used a change-detection method to analyze changed land cover areas, and categorized forest degradation and deforestation types. Because of the lack of reference images for collecting test points in other years, there were limitations in the accuracy assessment of the classification. Here, a change detection method was used to calculate the uncertainties instead of an accuracy assessment (Congalton and Green 2009). Based on the types of deforestation and degradation, this study suggested general strategies

for forest restoration planning.

2.4.3 Computation of deforestation rates

Because this paper used a different method and data to analyze forest during the 1990s than during other years, the information from the 1990s was considered as a separate case. For the purposes of standardization and comparison of statistics, the forest area data and time were used to calculate a standardized deforestation rate using the following formula (Armenteras et al. 2017; Puyravaud 2003):

$$\text{Deforestation rate} = \frac{1}{(t_2 - t_1)} * \text{Ln}(\frac{A_2}{A_1}) * 100$$

where A_1 and A_2 are the forest areas in years t_1 and t_2, respectively. For example, for a period from $t_1 = 1990$ to $t_2 = 2000$, A_1 and A_2 are the values of forest cover during 1990 and 2000. This standardization of deforestation rates makes the annual changes comparable across periods.

Then, to derive the drivers of deforestation and degradation, this paper gathered information considering the scale of the observed changes during the study period. The information included agricultural expansion, policy change and others related to deforestation and degradation in North Korea from previous papers, reports, and news releases.

3. Spatiotemporal data-fusion method for monitoring deforestation and degradation

3.1 Notations and definitions

Before describing the details of the RDSFM, some notations and definitions are provided for convenience.

(x_i, y_i) : coordinate index of the ith pixel;

$C_1(x_i, y_i, b)$: band b value of coarse pixel (e.g., MODIS) at location (x_i, y_i) observed at t1;

$C_2(x_i, y_i, b)$: band b value of coarse pixel (e.g., MODIS) at location (x_i, y_i) observed at t2;

$\mathrm{F}_1(x_{ij}, y_{ij}, b)$: band b value of the jth fine pixel (e.g., Landsat image) within the coarse pixel at location (x_i, y_i) observed at t1;

$\mathrm{F}_2(x_{ij}, y_{ij}, b)$: band b value of the jth fine pixel (e.g., Landsat image) within the coarse pixel at location (x_i, y_i) observed at t2;

m : the number of fine pixels (or subpixels) within one coarse pixel;

i : index of a coarse pixel;

j : index of a fine pixel within one coarse pixel (j=1, …m);

$f_c(x_i, y_j)$: the fraction of class c of the (x_i, y_i) coarse pixel;

$\Delta C(x_i, y_i, b)$: change of band b value of the (x_i, y_i) coarse pixel between

t1 and t2;

$\Delta F(c, b)$: change of band b value of class c at fine resolution between t1 and t2.

3.2 Residual distribution based Spatiotemporal data fusion method

3.2.1 Overview of the unmixing-based data fusion and FSDAF

The unmixing-based data-fusion method was first proposed by Zhukov et al. (1999) for blending images acquired from different sensors and with different spatial resolutions. It applies four steps to predict a fine-resolution image: (1) Classify a fine-resolution image to define endmembers, (2) estimate the fractions of each endmember within each coarse pixel, (3) unmix the coarse pixel at the prediction time within a moving window, and (4) assign reflectance spectra to the fine-resolution pixel.

Unmixing-based methods assign unmixed reflectance to fine pixels based on endmember fractions of each coarse pixel (Zhukov et al. 1999). Unmixing-based fusion methods require that no land-cover type change occurs between the input and prediction dates.

The FSDAF is one of the unmixing-based methods. It estimate the residuals using the result of the unmixing-based method and distributes the residuals to fine pixels. It is a key step to improve the accuracy of temporal prediction. It needs one pair of fine- and coarse-resolution images acquired at t1 and one

coarse-resolution image at t2. The FSDAF can more accurately predict fine-resolution images in heterogeneous areas and it requires minimal input data (Zhu et al. 2016). The FSDAF has six main steps, and the detailed descriptions of each step are found in Zhu et al. (2016).

1) Classify the fine resolution image at t1

To obtain the fraction of each class within one coarse pixel, the fine-resolution image at t1 is classified by unsupervised classification using all image bands. After classification of the fine-resolution image at t1, the class fraction within a coarse pixel was calculated by counting the number of fine pixels of each class:

$$f_c(x_i, y_i) = N_c(x_i, y_i)/m \quad (4)$$

where $N_c(x_i, y_i)$ is the number of fine pixels belonging to class c within the coarse pixel at (x_i, y_i), $f_c(x_i, y_i)$ is the fraction of class c of the (x_i, y_i) coarse pixel, and m is the number of fine pixels within one coarse pixel.

2) Estimate the temporal change of each class

For band b, the temporal change of the coarse pixel at (x_i, y_i) is $\Delta C(x_i, y_i, b) = C_2(x_i, y_i, b) - C_1(x_i, y_i, b)$. According to spectral linear mixing theory, the temporal change of a coarse pixel is the weighted sum of the temporal change of all classes within it as follows:

$$\Delta C(x_i, y_i, b) = \sum_{c=1}^{l} f_c(x_i, y_i) \times \Delta F(c, b), \quad (5)$$

where l is the number of classes. This equation is valid only when no land-cover type change occurs between t1 and t2.

3) Predict the fine-resolution image and residuals from temporal changes

The temporal change of each class can be assigned to relevant fine pixels without considering the within-class variability. If land-cover types do not change between t1 and t2, adding the temporal change to values of fine pixels observed at t1 can obtain the prediction of values of fine pixels at t2 as follows:

$$F_2^{TP}(x_{ij}, y_{ij}, b) = F_1(x_{ij}, y_{ij}, b) + \Delta F(c, b) \; if \; (x_{ij}, y_{ij}) \; belongs \; to \; class \; c \tag{6}$$

where $F_2^{TP}(x_{ij}, y_{ij}, b)$ is referred to as the temporal prediction because it only uses the temporal change information between input and prediction dates rather than any spatial information, such as spatial dependence.

For each coarse pixel, its value is equal to the sum of the values of all the fine pixels inside it and a bias factor ξ, which is the system difference between two sensors caused by differences in bandwidth and solar geometry. This system difference can be considered constant between t1 and t2; thus the values of coarse pixels at t1 and t2 can be written as follows:

$$C_1(x_i, y_i, b) = \frac{1}{m}\sum_{j=1}^{m} F_1(x_{ij}, y_{ij}, b) + \xi \tag{7}$$

$$C_2(x_i, y_i, b) = \frac{1}{m}\sum_{j=1}^{m} F_2(x_{ij}, y_{ij}, b) + \xi. \tag{8}$$

The temporal prediction at t2 is not an accurate prediction where land-cover type change has occurred and large within–class variability exists. In the FSDAF, a residual term R between the true values and temporal prediction of the fine pixels was estimated. Distributing residual $R(x_i, y_i, b)$ to fine pixels

within a coarse pixel is a key step in the FSDAF as follows:

$$R(x_i, y_i, b) = \Delta C(x_i, y_i, b) - \frac{1}{m}\left[\sum_{j=1}^{m} F_2^{tp}(x_{ij}, y_{ij}, b) - \sum_{j=1}^{m} F_1(x_{ij}, y_{ij}, b)\right] \quad (9)$$

4) Obtain TPS interpolation for guiding residual distribution

Residuals of the temporal prediction mainly originate from land-cover type change and within-class variability. However, because the fine-resolution image is unknown at t2, all true information regarding land-cover type change and within-class variability is contained in the coarse-resolution image at t2, which further helps to distribute the residuals from the temporal prediction.

For spatial prediction, the FSDAF used the thin plate spline (TPS) method to downscale the coarse-resolution image at t2. TPS is a spatial interpolation technique for point data based on spatial dependence. The value of each coarse pixel is attributed to the location at the center to obtain a regular point data set. TPS first fits a spatial-dependent function using known point data through minimizing an energy function. Because TPS prediction only uses spatial dependence of the coarse pixel, it produces a smooth result. The strength of TPS prediction is that it maintains the land-cover type change signals and local variability in the result.

5) Distribute residuals to fine pixels

The distribution of residuals from the temporal prediction to individual fine

pixels inside each coarse pixel is the key step to improving the accuracy of the temporal prediction. The FSDAF used a new weighted function to distribute more residuals to the subpixels with larger errors.

In a homogenous landscape, TPS spatial prediction presents the true values of fine pixels at t2, and the error of the temporal prediction can be estimated as follows:

$$\mathrm{E_{ho}}\left(x_{ij}, y_{ij}, b\right) = F_2^{sp}\left(\mathrm{x_{ij}}, \mathrm{y_{ij}}, \mathrm{b}\right) - \mathrm{F_2^{TP}}\left(x_{ij}, y_{ij}, b\right) \qquad (10)$$

However, the error estimated is not valid for fine pixels in heterogeneous landscapes or at edges between two land-cover types, because TPS prediction smoothed these edges in space. Where the landscape is heterogeneous, or at land-cover edges, assuming that all fine pixels within a coarse pixel with equal error is reasonable if there is no other information available as follows:

$$E_{he}\left(x_{ij}, y_{ij}, b\right) = R\left(x_i, y_i, b\right) \qquad (11)$$

To integrate two cases into one weighted function to guide the residual distribution, a homogeneity index was used as follows:

$$HI\left(x_{ij}, y_{ij}\right) = \left(\sum_{k=1}^{m} I_k\right)/m \ , \qquad (12)$$

where $\mathrm{I_k} = 1$ when the kth fine pixels within a moving window with the same land-cover type as the central fine pixel $(\mathrm{x_{ij}}, \mathrm{y_{ij}})$ is being considered, otherwise $\mathrm{I_k} = 0$. HI ranges from 0 to 1, and larger values indicate a more homogenous landscape. The weight for combining the two cases through HI is as follows:

$$CW(x_{ij}, y_{ij}, b) = E_{ho}(x_{ij}, y_{ij}, b) \times HI(x_{ij}, y_{ij}) + E_{he}(x_{ij}, y_{ij}, b) \times (1 - HI(x_{ij}, y_{ij})). \quad (13)$$

The weight is then normalized as follows:

$$W(x_{ij}, y_{ij}, b) = CW(x_{ij}, y_{ij}, b) / \sum_{j=1}^{m} CW(x_{ij}, y_{ij}, b). \quad (14)$$

Then the residual is distributed to the j*th* fine pixel as follows:

$$R(x_{ij}, y_{ij}, b) = m \times R(x_i, y_i, b) \times W(x_{ij}, y_{ij}, b). \quad (15)$$

Summing the distributed residual and the temporal change, the FSDAF obtains the prediction of the total change of a fine pixel between t1 and t2:

$$\Delta F(x_{ij}, y_{ij}, b) = r(x_{ij}, y_{ij}, b) + \Delta F(c, b) \ \ if \ \ (x_{ij}, y_{ij}) \ \ belongs \ to \ class \ c. \quad (16)$$

6) Obtain a robust prediction of a fine image using neighborhood

For reducing the uncertainties in final predictions while mitigating the block effect, the FSDAF used a similar strategy as that of STARFM to obtain a more robust prediction of fine pixel values at t2. The FSDAF used the weight which was determined by the spatial distance between similar pixels and the target pixel. Adding this final estimate of total change to the initial observation at t1 yields the final prediction of the target pixel value at t2 as follows:

$$F_2(x_{ij}, y_{ij}, b) = F1(x_{ij}, y_{ij}, b) + \sum_{k=1}^{n} w_k \times \Delta F(x_k, y_k, b) \quad (17)$$

The strengths of FSDAF are that 1) it needs minimum input data, 2) it is suitable for heterogeneous landscapes, 3) it can predict both gradual change

and land-cover type change.

In FSDAF, the distribution of residual R to fine pixels within a coarse pixel is a key step to improve the accuracy of the prediction. The strategy of distributing residuals uses a homogeneity index, which indicates the homogenous rate of one coarse pixel. However, although estimating and distributing residuals are essential ideas for increasing accuracy in mixed pixels, the prediction accuracy of pixels caused by phenology or land-cover change is even lower, because the weights for distributing residuals are the same in each band, but the range of change of each band has a different trend. As mentioned for FSDAF, the distribution of the residuals from the temporal prediction to individual fine pixels inside each coarse pixel is the key step to improving the accuracy of the temporal prediction. Errors of temporal prediction are mainly caused by land-cover type change and a spectral changed within-class. The FSDAF used the homogeneity index (HI), which ranges from 0 to 1 and indicates the degree of homogeneity and heterogeneity. HI is decided using the pixels within a moving window (its size is one coarse pixel) with the same land-cover type as the target pixel, and the land-cover types are determined by a fine-resolution image at t1; however, misclassification will occur in landscapes with similar reflectance by season, such as bare ground, farmland and grassland, etc.

When applying the FSDAF method to areas with seasonal change, it shows high accuracy in the red band and in pure pixels, such as forest (Figure 7a), but many errors appear in farmland. For the NIR band, prediction errors are

distributed in all test areas, and large errors appear in farmland (Figure 7b). In short, the FSDAF shows strength in predicting homogeneous and heterogeneous pixels, but it did not improve the accuracy of pixels with land-cover change or a spectral change from phenology.

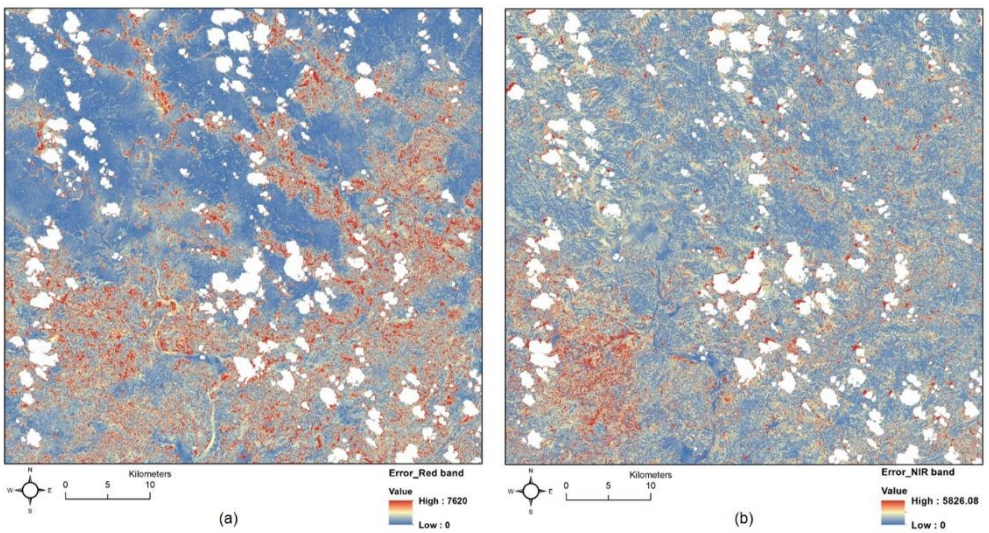

Figure 7. Error distribution in red band (a) and NIR band (b) between FSDAF-predicted and observed values. The time of base images are 9/10/14 and the predict time is 5/21/14. The blanks are pixels with clouds in predicted time.

3.2.2 Residual-distribution-based spatiotemporal data-fusion method

In this study, improvement solutions for the prediction of pixels with land-cover change or spectral change will be proposed, based on distributed residuals.

Most landscapes in temperate zones have phenology characteristics, and the reflectance of each band changes within-class according to the seasonal

change, such as farmland, grassland, wetland, riverside, etc. Figure 8 represent the spectrum of each land cover during different seasons. Figure 8a describes the spectrum in built-up areas; the spectral changes between two seasons is nearly equal to 0. For the vegetation-covered areas of farmland (Figure 8c) and forest (Figure 8b), we can see the most spectral change was in band 5(NIR band) because the NIR band responds sensitively to leaf growth. Figure 8d shows the riverside changed from water to bare ground depending on the water flow; we can see the spectrum completely changed between the two seasons. However, the range of changed values in each band shows a large difference by each land-cover type. This will result in several errors when these land-cover types are mixed in one coarse pixel and distribute the residuals only by heterogeneous degree.

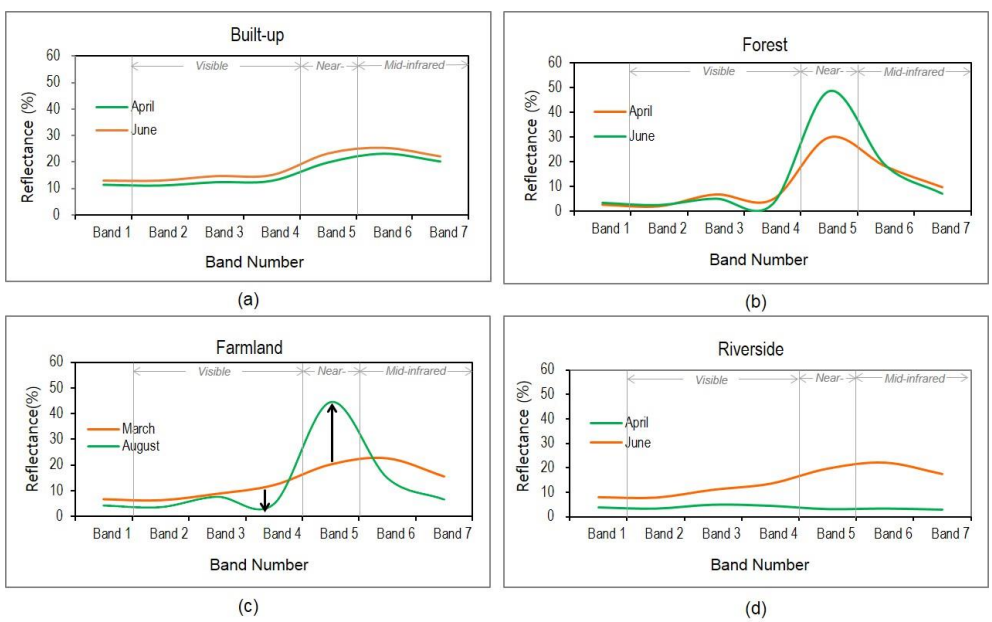

Figure 8. The spectrum of land-cover types during different seasons. The reflectance value of each band was extracted using Landsat 8 OLI.

This study proposed a Residual-Distribution-based Spatiotemporal data-fusion Method (RDSFM), attempting to use the correlation between two images to improve the fusion accuracy for remote-sensing images of different temporal and spatial characteristics. The RDSFM includes five main steps: 1) predict a fine image at t2 using an unmixing-based method, 2) estimate the residuals between real changed values and predicted changed values, 3) estimate the weights based on MAD variates and a heterogeneous index for each subpixel and each band, 4) distribute the residuals to fine pixels, and 5) final prediction using information in the neighborhood.

Detailed descriptions of the steps of the RDSFM are given below. It needs one fine-resolution image and a coarse image at t1, and one coarse-resolution image at the prediction time. The work flow of the method can be seen in Figure 9.

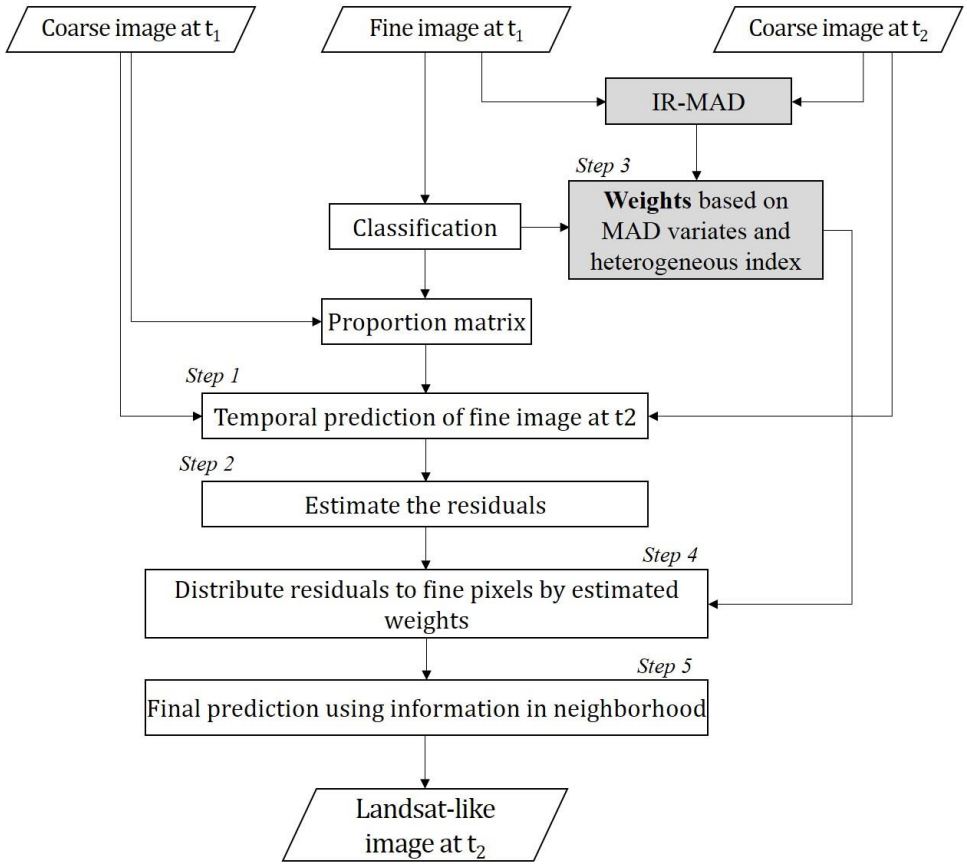

Figure 9. Workflow of the RDSTM

1) Predict fine-resolution image at t2 using the unmixing based method

In this step, the unmixing-based method was used for predicting the temporal change without considering the within-class variability. First, to obtain the fraction of each class within a coarse pixel, the fine-resolution image at t1 is classified by unsupervised classification. This step is the same as the unmixing-based method used in FSDAF (Zhu et al. 2016) (see Equation (4) ~ (6)).

$$F_2^{TP}(x_{ij}, y_{ij}, b) = F_1(x_{ij}, y_{ij}, b) + \Delta F(c, b) \; if \; (x_{ij}, y_{ij}) \; belongs \; to \; class \; c \quad (18)$$

2) Estimate the residuals

The real changed values between t1 and t2 can be written as follows:

$$\Delta C(x_i, y_i, b) = C_2(x_i, y_i, b) - C_1(x_i, y_i, b) \; . \quad (19)$$

The predicted fine-resolution image at t2 is not an accurate prediction if a spectral change has occurred. The predicted change values between the temporal prediction of the fine-resolution image at t2 and the real fine-resolution image at t1 is as follows:

$$\Delta F(x_i, y_i, b) = \frac{1}{m}\sum_{j=1}^{m} F_2^{TP}(x_{ij}, y_{ij}, b) - \frac{1}{m}\sum_{j=1}^{m} F_1 \; (x_{ij}, y_{ij}, b) \; . \quad (20)$$

Between the real changed values and the temporally predicted changed values, there are residuals. These residuals mainly are caused by a spectral change, such as a land-cover type change and within-class variability across the image (Zhu et al. 2016). Distributing residuals $R(x_i, y_i, b)$ to fine pixels within a coarse pixel is important to improve the accuracy of the predict fine pixel value at t2. The residual R between the true changed values and the predicted changed values can be derived as follows:

$$R(x_i, y_i, b) = \Delta C(x_i, y_i, b) - \Delta F(x_i, y_i, b) \; . \quad (21)$$

In FSDAF, residual distribution is based on the degree of heterogeneity distributing the spectral changed values, but it only depends on the classes classified by the fine-resolution image at t1. Because different landscape types have similar reflectance at a particular time, it will be misclassified and

generate errors in some cases.

3) Estimate MAD-based weights using IR-MAD

For distributing the residuals to each subpixel more properly, this study introduced a weight based on multi-variates between the images at t1 and t2. It is estimated by iteratively regularized multi-variate alteration detection (IR-MAD), which detect changes in multi-variate data acquired at two points in time covering the same geographical region (Nielsen 2007).

The IR-MAD method (Nielsen 2007) is adopted for multi-variate calculation, owing to its effectiveness, speed, and fully automatic processing. For IR-MAD it is customary to calculate the difference between two images; the areas that exhibit no or small changes have zero or low absolute values and areas with large changes have large absolute values in the different image.

The main idea of IR-MAD is a simple iterative scheme to place high weights on observations that exhibit little change over time. The IR-MAD algorithm is an established change detection technique based on canonical correlation analysis. Mathematically, the IR-MAD tries to identify linear combinations of two variables, $a^T X$ and $b^T Y$, to maximize the objective function $max_{a,b}\, var(a^T X - b^T Y)$ with $V\{a^T X\} = V\{b^T Y\} = 1$. The dispersion matrix of the MAD variates is as follows:

$$\begin{aligned} D = V\{a^T X - b^T Y\} &= V\{a^T X\} + V\{b^T Y\} - 2cov\{a^T X, b^T Y\} \\ &= 2(1 - corr\{a^T X, b^T Y\}). \end{aligned} \tag{22}$$

A MAD variate is the difference between the highest order canonical

variates and it can be expressed as follows:

$$\begin{bmatrix} X \\ Y \end{bmatrix} \rightarrow \begin{bmatrix} a_p^T X - b_p^T Y \\ \vdots \\ a_1^T X - b_1^T Y \end{bmatrix} \tag{23}$$

where a_i and b_i are the defining coefficients from a standard canonical correlation analysis.

Using a brief derivation, the objective function can be reformulated to minimize the canonical correlation of two variables, that is $min\lambda = corr(a^T X, b^T Y)$, where corr represents a correlation function. If we let the variance-covariance matrix of X and Y be Σ_{XX} and Σ_{YY}, respectively, and their covariance be Σ_{XY}, the correlation can be formulated to Rayleigh quotients as follows:

$$\min \lambda^2 = \frac{a^T \Sigma_{XY} \Sigma_{YY}^{-1} \Sigma_{YX} a}{a^T \Sigma_{XX} a} = \frac{b^T \Sigma_{XY} \Sigma_{XX}^{-1} \Sigma_{YX} b}{b^T \Sigma_{YY} b} \tag{24}$$

Equation (24) is just an eigenvalue problem, that is $\Sigma_{XY} \Sigma_{YY}^{-1} \Sigma_{YX} a = \lambda^2 \Sigma_{XX} a$, and hence the solutions are the eigenvectors of $a_1, \ldots, a_n$ corresponding to the eigenvalues $\lambda_1^2 \geq \cdots \geq \lambda_n^2 \geq 0$ of $\Sigma_{XY} \Sigma_{YY}^{-1} \Sigma_{YX}$ with respect to Σ_{XX}. Now assuming that the MODIS image is preprocessed to be zero mean, we denote $\text{MAD} = a^T X - b^T Y$ as the MAD components of the combined bi-temporal image.

Because the MAD variates are linear combinations of the measured variables, they will have an approximate Gaussian distribution with the central limit theorem. Thus, MAD can represent the relative changes in

subpixels in a coarse-resolution pixel. In this process, the ENVI extension for IR-MAD generated by Mort Canty (2013)[1] was used for running the IR-MAD and obtaining the MAD variates.

MAD values are determined by the correlation between two images; a larger value means much change occurred in the spectrum, indicating changed areas, and lower values means there are no changes in the spectrum and indicate the areas are the same as the previous image. Here, the input data for multi-variate calculation are a fine-resolution image at t1 and coarse-resolution image at t2, which resampled to a fine resolution through a bilinear interpolation method.

4) Distribute the residuals to the fine pixel

Errors in temporal prediction are mainly caused by land-cover type change and within-class variability across the image. Therefore, this study proposed a new weighted function to distribute residuals to subpixels, considering the variates in each band and the heterogeneous degree. This study introduced a multi-variate-based weight as follows:

$$W_{MAD}(x_{ij}, y_{ij}, b) = MAD(x_{ij}, y_{ij}, b) / \sum_{i=1}^{m} MAD\ (x_{ij}, y_{ij}, b) \qquad (25)$$

The HI proposed by Zhu et al. (2016), which represent the degree of heterogeneity, was also used for distributing the residuals.

[1] Open source IDL code : https://mortcanty.github.io/src/idldoc/index.html

$$HI(x_{ij}, y_{ij}) = (\sum_{k=1}^{m} I_k)/m \quad (26)$$

where I_k approaches 1 means the kth fine pixels within a moving window with the same land cover type as the central fine pixel (x_{ij}, y_{ij}) being considered, otherwise I_k approaches 0. HI ranges from 0 to 1, and larger values indicate more homogeneous landscape, and smaller values indicate more heterogeneous. The weight for combining the two cases is:

$$W(x_{ij}, y_{ij}, b) = R(x_{ij}, y_{ij}, b) * \left(1 - HI(x_{ij}, y_{ij})\right) + R(x_{ij}, y_{ij}, b) * W_{MAD}(x_{ij}, y_{ij}, b) \quad (27)$$

The weight is then normalized as follows:

$$W_{Normalized}(x_{ij}, y_{ij}, b) = W(x_{ij}, y_{ij}, b)/\sum_{j=1}^{m} W(x_{ij}, y_{ij}, b) \quad (28)$$

Then, the residual distributed to j*th* fine pixel is as follows:

$$r(x_{ij}, y_{ij}, b) = W_{Normalized}(x_{ij}, y_{ij}, b) * R(x_i, y_i, b) \quad (29)$$

Summing the distributed residual and the temporal change, we can obtain the prediction of the total change of a fine pixel between t1 and t2 as follows:

$$\Delta F(x_{ij}, y_{ij}, b) = r(x_{ij}, y_{ij}, b) + [F_2^{TP}(x_{ij}, y_{ij}, b) - F_1(x_{ij}, y_{ij}, b)] \quad (30)$$

5) Final prediction using information in neighborhood

In theory, adding the total change estimated in Eq. (30) to the value of the fine pixel at t1 can obtain the final prediction at t2. However, because the prediction is processed on a pixel-by-pixel basis, it unavoidably has many

uncertainties caused by errors during the previous steps and noise contained in all input images. Moreover, the distribution of MAD weights implemented with a fine-resolution image and interpolated with a coarse-resolution image leads to uncertainties in detail. Also, a block effect can occur from the residual within each coarse pixel. Many previous spatiotemporal data-fusion methods, such as STARFM, FSDAF, and ESTARFM, used additional neighborhood information to reduce the uncertainties and mitigate block effects in the final prediction (Gao et al. 2006; Zhu et al. 2010; Zhu et al. 2016). In this study, a similar strategy as that of FSDAF to obtain a more robust prediction of fine pixel values at t2 was used.

In the fine image at t1, for a target fine pixel (x_{ij}, y_{ij}), n fine pixels (named as similar pixels including the target pixel itself) with the same class and smallest spectral difference from the target fine pixel within its neighborhood are selected. For the number of similar pixels n, Zhu et al. (2016) recommended selecting 20 similar pixels in practice as follows:

$$S_k = \sum_{b=1}^{B} [\frac{|F_1(x_k, y_k, b) - F_1(x_{ij}, y_{ij}, b)|}{F_1(x_{ij}, y_{ij}, b)}] \quad (31)$$

Then, the weight of each similar pixel is determined by the spatial distance between similar pixels and the target pixel. The spatial distance of kth similar pixel Dk is a relative distance defined in ESTARFM (Zhu et al. 2010) as follows:

$$D_k = 1 + \sqrt{\left(x_k - x_{ij}\right)^2 + \left(y_k - y_{ij}\right)^2} / \left(\frac{w}{2}\right) \quad (32)$$

where w is the size of the moving window and neighborhood. D_k is a relative distance ranging from 1 to $1 + \sqrt{2}$. Assuming that similar pixels are further away and contribute less to the estimated target pixel, the weight for the k*th* similar pixel is calculated as follows:

$$W_k = \left(\frac{1}{D_k}\right) / \sum_{k=1}^{n} \left(\frac{1}{D_k}\right) \quad (33)$$

Change information for all similar pixels is summed by weight to obtain the total change value of the target pixel. Adding this final estimate of total change to a fine-resolution image at t1, the final prediction of the target pixel at t2 can be calculated as follows:

$$F_2\left(x_{ij}, y_{ij}, b\right) = F_1\left(x_{ij}, y_{ij}, b\right) + \sum_{k=1}^{n} W_k \times \Delta F\left(x_{ij}, y_{ij}, b\right) \quad (34)$$

3.2.3 Testing experiment

For the experiments, this study tested Landsat images covering two study areas with contrasting spatial and temporal dynamics, i.e. one with a complex and heterogeneous landscape and another with a land-cover-type change. These two sites have been used to evaluate different spatiotemporal data-fusion methods, including STARFM, ESTARFM, FSDAF, etc. These sites can be used as a benchmark for comparing or testing spatiotemporal data-fusion methods.

At the first site with a complex and heterogeneous landscape, two cloud-

free Landsat 7 ETM+ images covered southern New South Wales, Australia (145.0675ºE, 34.0034ºS). The two Landsat images (Path/Row 93/84) were acquired on November 25, 2001 and January 12, 2002 respectively. The major land cover types in this area are irrigated rice cropland, dryland agriculture, and woodlands. Rice croplands are often irrigated during October and November (Emelyanova et al. 2013; Zhu et al. 2016).

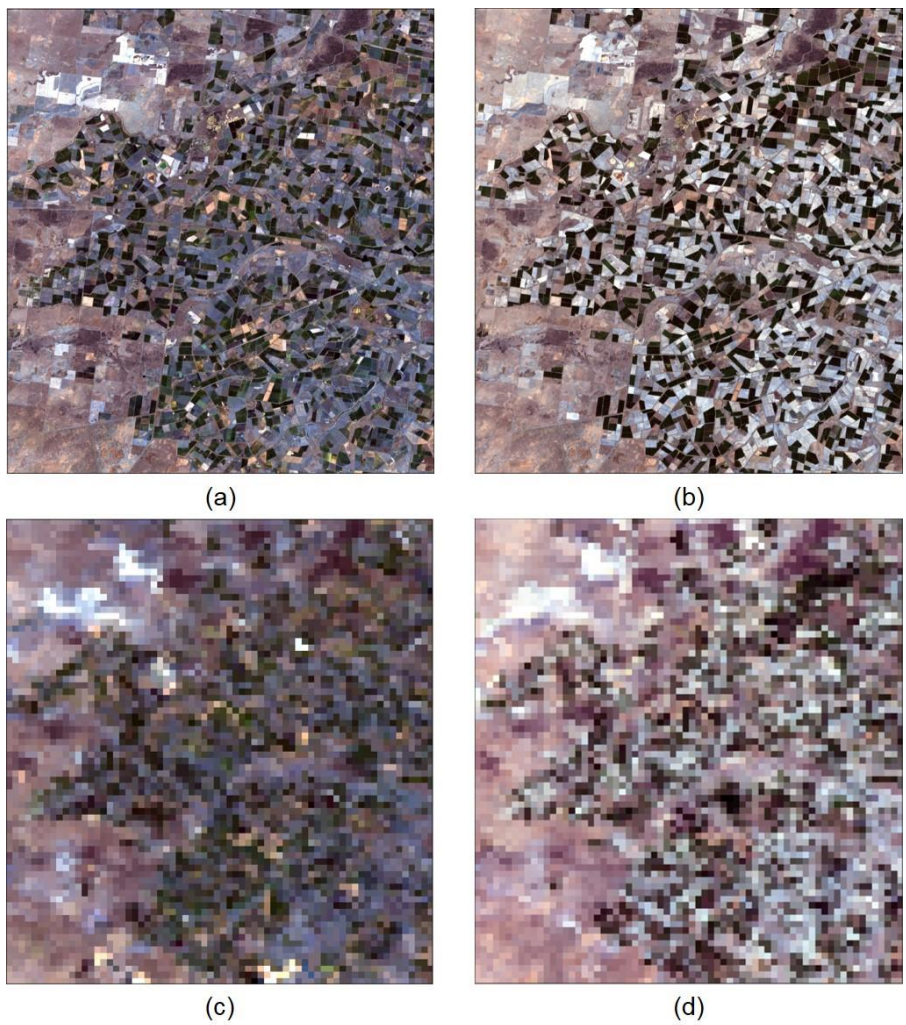

Figure 10. Test data in a complex and heterogeneous landscape: Landsat images acquired on (a) November 25, 2001 and (b) January 12, 2002, (c) and (d) are the

corresponding MODIS images with a 500-m spatial resolution to (a) and (b). All images use red-green-blue as RGB, and MODIS images are resampled to have the same image size as the Landsat images.

The second site with land-cover-type change is in northern New South Wales, Australia (149.2815ºE, 29.0855ºS). This site covers an area of 20 km × 20 km and is relatively homogenous, with large parcels of croplands and natural vegetation. Two Landsat images were acquired on November 26, 2004 and December 12, 2004 (Path/Row 91/80). A large flood occurred in December 2004. From the Landsat image of December 12, 2004, we can see a large inundated area. The flood event caused land-cover-type change to water in some pixels.

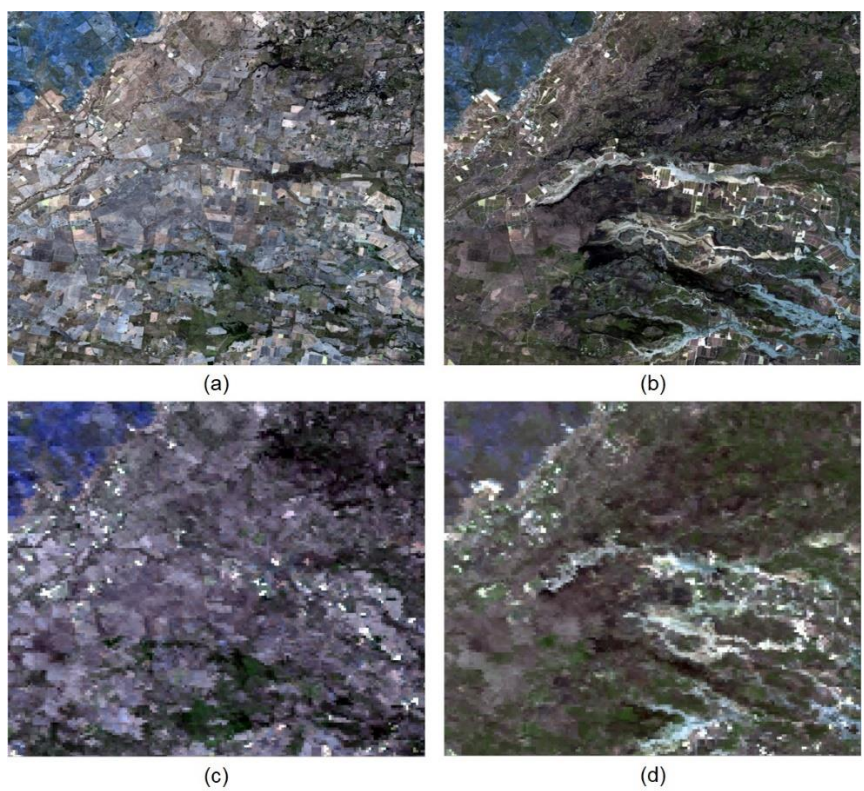

Figure 11. Test data in area with land-cover type change: Landsat images acquired

on (a) November 26, 2004 and (b) December 12, 2004, (c) and (d) are the corresponding MODIS images with a 500-m spatial resolution to (a) and (b). All images use red-green-blue as RGB, and MODIS images are resampled to have the same image size as the Landsat images.

3.2.4 Comparison and evaluation of accuracy assessment

The performance of RDSTM was also compared to the unmixing-based data-fusion algorithm (UBDF) (Zhukov et al. 1999) and FSDAF algorithm (Zhu et al., 2016), because the proposed algorithm is also unmixing-based. The fine-resolution images predicted using the two methods were compared to the true images quantitatively and visually. Several indices were calculated to represent the different aspects of accuracy. Root mean square error (RMSE) was used to gauge the difference between the predicted reflectance and the actual reflectance. Correlation coefficient r was used to show the linear relationship between the predicted and actual reflectance. The functions for RMSE and r are as follows:

$$\mathrm{RMSE} = \sqrt{\frac{\sum_{i=1}^{n}(P_i - O_i)^2}{n}} \tag{35}$$

where n is the number of samples, Pi is the predicted value of pixel I, and Oi is the observed value in pixel i:

$$\mathrm{r} = \frac{\sum_{i=1}^{n}(x_i - \bar{x})(y_i - \bar{y})}{\sqrt{\sum_{i=1}^{n}(x_i - \bar{x})^2}\sqrt{\sum_{i=1}^{n}(y_i - \bar{y})^2}} \tag{36}$$

where xi, yi are the single sample indexed with I, and $\bar{x} = \frac{1}{n}\sum_{i=1}^{n} xi$ (the sample mean), and analogously $\bar{y}$.

The average difference (AD) between the predicted and true images was used to represent the overall bias of predictions. A positive AD indicates that the fused image generally overestimates the actual values, while a negative AD represents underestimation.

In addition to the aforementioned quantitative assessment, a visual assessment index, structure similarity (SSIM) (Wang et al. 2004; Zhu et al. 2016), was also used to evaluate the similarity of the overall structure between the true and predicted images as follows:

$$\text{SSIM} = \frac{(2\mu_X\mu_Y + C_1)(2\sigma_{XY} + C_2)}{(\mu_X^2 + \mu_Y^2 + C_1)(\sigma_X + \sigma_Y + C_2)} \tag{37}$$

where μ_X and μ_Y are means; σ_X and σ_Y are the variance of the true and predicted images, respectively; σ_{XY} is the covariance of the two images; and C_1 and C_2 are two small constants to avoid unstable results when the denominator of Eq. 35 is very close to zero. A SSIM value closer to 1 indicates more similarity between the two images.

3.3 Monitoring deforestation and degradation using RDSFM

The aim of this part is to develop a transparent and cost-effective method to obtain a reliable deforestation and forest degradation map that can be easily applied to other regions in North Korea or other regions that have heterogeneous vegetative cover.

3.3.1 Study area for monitoring

The study area (Figure 12) for monitoring deforestation and degradation is the range of one Landsat image (Path/Row 117/032). The study area includes parts of North Pyongan province, South Pyongan province and Chagang province. Chagang province is one of the mountainous provinces and is 98% forest. North Pyongan province is bordered on the north by China, on the east by Chagang province, and on the south by South Pyongan province. North Pyongan province and South Pyongan province are among the most fragmented areas as result of deforestation and agriculture practices. Because this area is near the Pyeongyang region, the pressure of deforestation has been increasing. For monitoring deforestation and degradation, the study was conducted during 2014, when drought was the worst, so that the vegetation condition decreased while degradation increased due to climate. The reference year chosen was 2001, when the temperature and precipitation were similar to that of average years.

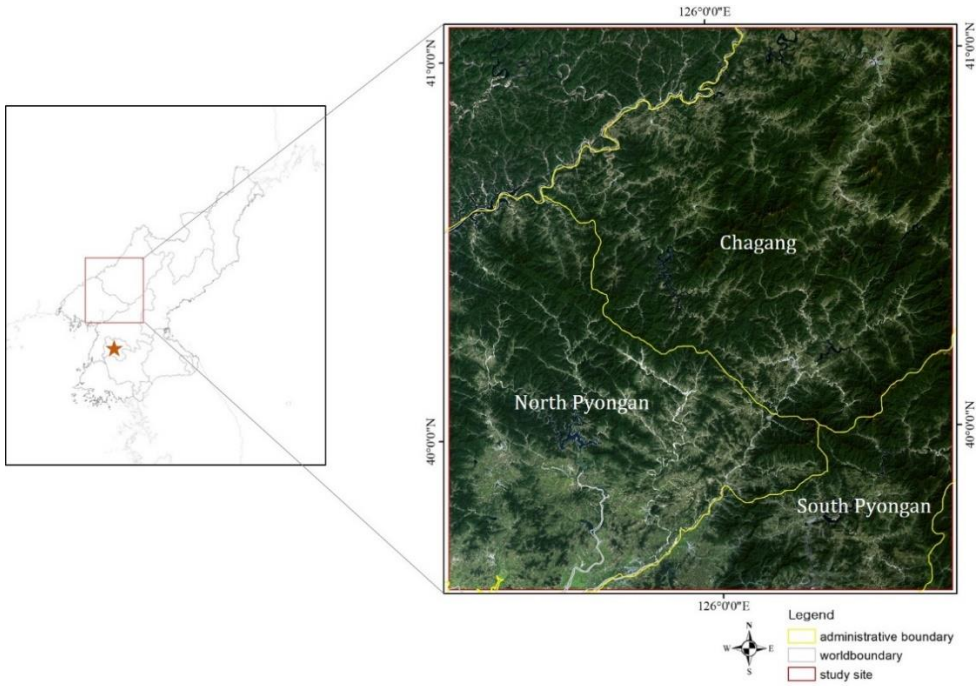

Figure 12. Study area for degradation mapping

To construct time series Landsat-like images monthly, cloud-free Landsat 8 OLI images (band 3~6) covering an area of 148 km × 165 km in southern North Korea was used as the fine image at t1. The false color composite of Landsat images and their corresponding MODIS images are shown in Figure 11. The two Landsat images (Path/Row 117/032) were acquired on September 10, 2014 (Figure. 13a) and May 21, 2014 (Figure. 13b), respectively.

The major land-cover types in this area are irrigated rice cropland, farmland, hillside field, and woodlands. Rice croplands and farmland are irrigated from April to June. In this part, the pair of images on November 10, 2014 and the MODIS image on May 21, 2014 were used to predict the Landsat image in

Figure. 13b.

The Landsat image was atmospherically correlated and converted radiance data to surface reflectance using FLAASH in ENVI 5.4. During the process of RDSFM, Figure. 13a was classified into a maximum of 10 spectral classes using the ISODATA method.

Table 3. Information of test images

Data type	**Acquire time**	**Spatial resolution**	**Cloud**	**Location**	**Band**	**Role**
Landsat 8 OLI	2014.09.10	30m	0%	Path/Row 117/032	Band 3~6	Input/Fine image at t1
	2014.05.21		50%			Accuracy test
MCD43 A4	2014.09.10	480m	-	H27V	Band1, 2, 6, 7	Input/ coarse image at t1
	2014.05.21		-			Input/ coarse image at t2

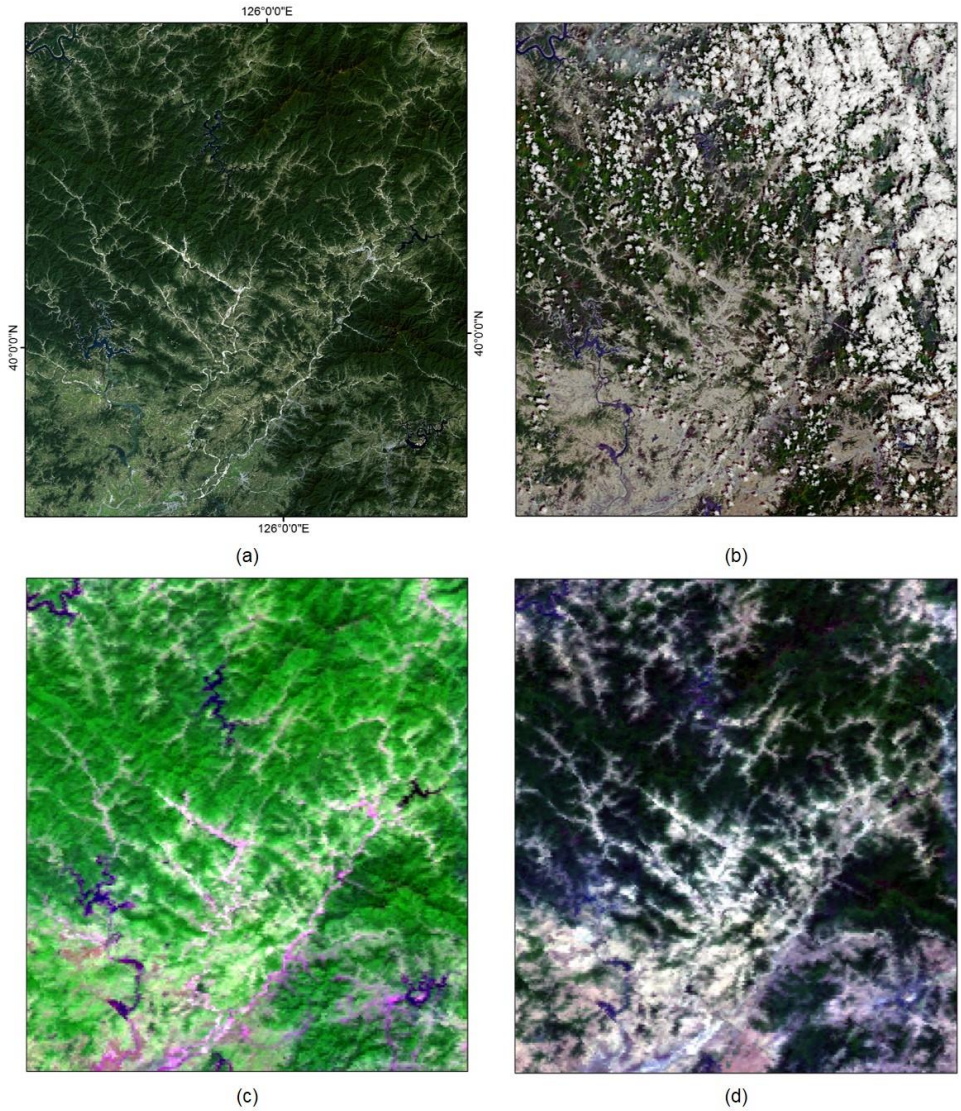

Figure. 13. Test data in the study area with both heterogeneous and spectrum of land-cover changes by phenology: Landsat images (4928 × 5504 pixels) acquired on (a) September 10, 2014 and (b) May 21, 2014. (c) and (d) are 480-m MODIS images. All images using RGB and MODIS images were resampled to the same image size as the Landsat images.

In this part, two Landsat images, acquired on May 21, 2014 and October 28, 2014 were selected to test the fusion accuracy, considering the different time intervals from the input image. To demonstrate the method effectiveness in

heterogeneous and homogeneous landscapes, sample site 1 and sample site 2 were selected, respectively (Figure 14). Sample site1 represents an area that is the most fragmented and heterogeneous. The main landscapes in sample site1 are rice fields, crop fields, a water body and some forest. Sample site 2 represents an area with a homogeneous landscape. The main landscapes in sample site 2 are forest and some farmland. The sample sites were chosen in each image considering the least impacts from cloud cover. Furthermore, the image of the whole study area was verified through R, RMSE, AD and SSIM.

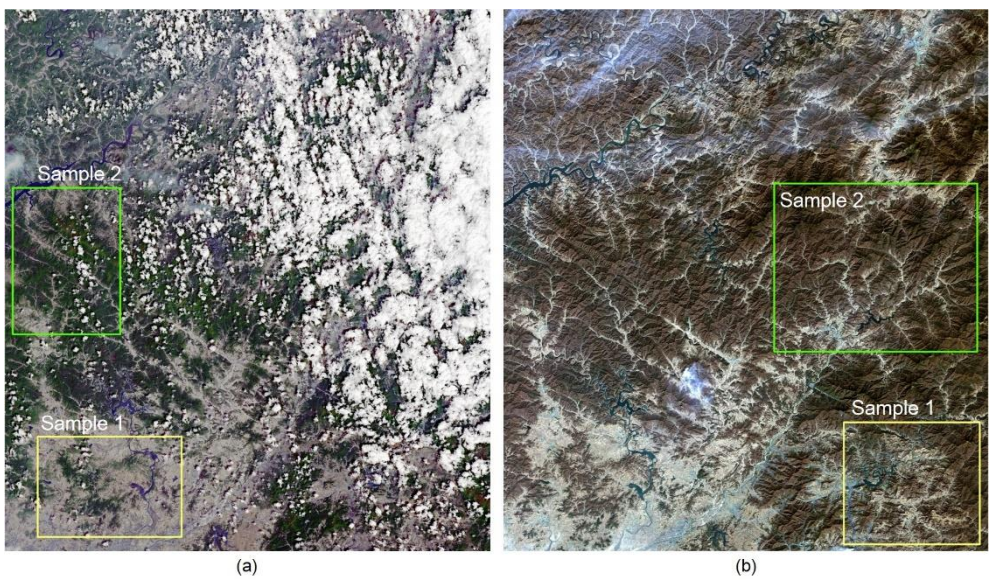

Figure 14. Validation images acquired on (a) May 21,2014 and (b) October 28, 2014.

3.3.2 Application to deforestation and degradation monitoring

To propose a cost-effective method for monitoring land use change, particularly as previously mentioned, key phenological variables for land-cover classification of North Korea derived in the first part, and the

spatiotemporal method proposed in second part, were used for land-cover classification during 2001 and 2014. Through the land-cover classification results of two periods, the degradation that occurred from 2001 to 2014 was detected.

Because there is no reference data for the past time, unsupervised classification methods were considered for mapping. Various clustering algorithms are generally deployed in remote sensing. The two most well-known are the K-means and ISODATA unsupervised classification algorithms. Both algorithms are strong in clustering, but the ISODATA algorithm supplies better results as documented in previous studies (EI_Rahman 2016).

Therefore, an ISODATA classifier was used for mapping land cover during 2001 and 2014. ISODATA computes class means consistently circulated in the data space before iteratively clustering the continuing pixels utilizing least-distance approaches. Every iteration recalculates means as well as reclassifies pixels with respect to the new means, while in the K-means approach, the number of clusters K remains the same throughout the iteration, although it may be found later that more or fewer clusters would fit the data better. This drawback can be overcome in the ISODATA algorithm, which allows the number of clusters to be adjusted automatically during the iteration by merging similar clusters and splitting clusters with large standard deviations.

Ground-truth points used for assessing the accuracy of our results were established using a random-sampling method, which helps ensure that test

samples are chosen in an unbiased manner and in proportion to the underlying, but as yet unmapped, land-cover and land use categories (Congalton and Green 2009).

The random points made in ArcGIS 10.1 were overlaid on the GE images identifying land-cover classes using the visual criteria described in Table 3. The random samples of natural forest were overabundant; in contrast, there were few samples for plateau vegetation, as these areas covered only small fractions of this site. Thus, this study implemented a stratified random sampling(Clark et al. 2010) for these classes. Because there was no information regarding plateau vegetation on the forest map, random points for plateau vegetation were established within the polygons with an elevation > 1,800m. Finally, 331 sample points, with a minimum of 30 points in each class, were selected based on the recommendations of Congalton and Green (Congalton and Green 2009) at intervals over 30m.

To verify the classification result, a confusion matrix was used to estimate overall, user's and producer's accuracies, and the kappa coefficient (Jensen 2005; Jeong et al. 2016a).

Finally, a change detection method was used to analyze the land-cover-change areas, and categorized forest degradation and deforestation types. Through the types of deforestation and degradation, this study suggests general strategies for forest restoration planning.

IV. Results and discussions

1. Key phenological–based indices for classification

1.1 Temporal indices of land-cover classes

Figure 15 shows that the phenological characteristics (via NDVI, NDSI, and NDWI) of the paddies, flatland fields, hillside field, unstocked forest, forest, and plateau vegetation fluctuated during the growing season. The NDVI consistently increased from March to June for forest, unstocked forest and plateau vegetation during the growing season, and decreased during the period from August to October (end of the growing season). For paddy, field and hillside field the growing season extended to July. The highest NDVI value of all land-cover classes was observed during July and August. All landscapes showed slightly different trends of change in the NDVI value. Natural forest had the highest NDVI value during all periods (mainly consisting of trees), while unstocked forest consisting of grasses and shrubs had slightly lower NDVI values, but the curves followed the same general form. In hillside fields, the crops were planted more densely than in the flat fields (Jiang et al. 2014), with resultant NDVI values higher overall by month in comparison to flatland fields. Natural forest showed the highest NDVI value, followed by unstocked forest, plateau vegetation, hillside fields, flat land fields, and paddies.

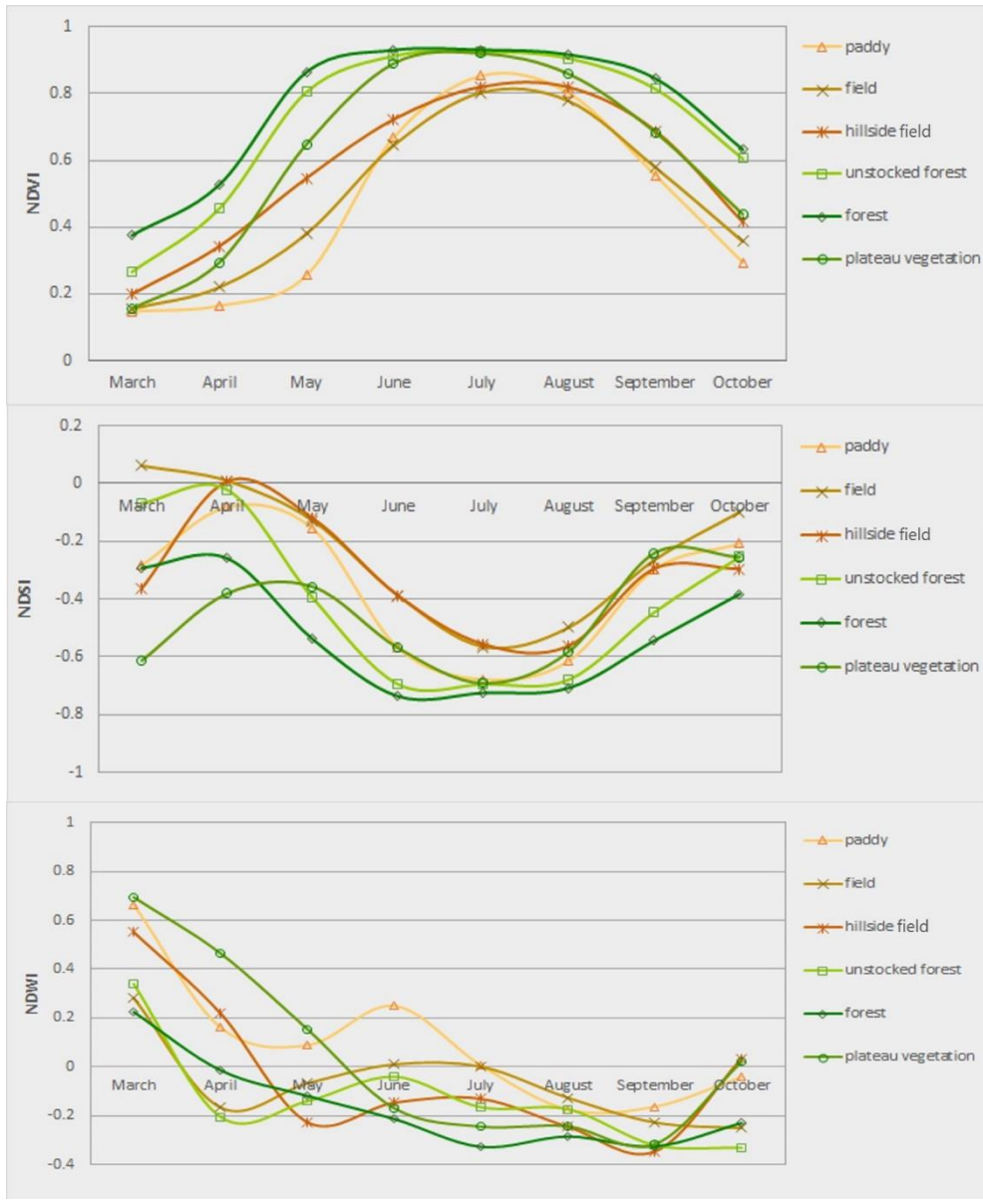

Figure 15. Time series indices of MODIS NDVI, NDSI, and NDWI (derived from Red, NIR, and MIR reflectance) for paddy, field, hillside field, unstocked forest, forest, and plateau vegetation categories. Random samples of 100 points were individually extracted for each type.

NDSI decreased from April to June or July, depending on the landscape type, as the NDVI increased. Hillside fields exhibited the highest NDSI value

among the forest landscapes when farmers were preparing the fields early in the season creating conditions for maximum soil exposure. From March to May, at the start of the growing season, the area of soil exposure in the four types of forest landscapes varied because of the canopy. In this case, the hillside fields had the highest NDSI values, followed by unstocked forest and forest. The highest NDWI value was observed at the start of the growing season because of snow melt when the canopy water content was at a maximum.

When reviewing the three individual graphs in Figure 15, one notices that the six landscape types followed similar trends by index. However, the relative ranking of these landscape types varied according to the index being considered. The largest differences between forest landscape types occurred during different seasons based on the characteristics of each class. For example, hillside field and forest landscape types had similar trends of NDVI during the growing season and at the end of season. During these periods hillside fields had lower NDVI values of approximately 0.2, but in the middle of the season the difference narrowed to approximately 0.1 between the hillside field and forest landscape types. It is important to note that the NDWI of plateau vegetation is higher than that of the other classes because the snow melt rate on the plateau was initially slower than that of the other forest landscape types, and this remained true until May. Also, the NDWI of paddies reached a summer maximum during June because of irrigation.

1.2 Temporal indices of land-cover classes and relevant variables in RF

Using models with 500 trees, the importance of the contribution of each variable to the general classification model was calculated (Breiman 2001). The mean decrease in accuracy displayed in Figure 16 is the contribution of each variable to the classification model generated by considering the seasonal multiple indices and topographic variables. Variables that have high mean decreased accuracy values are considered to be more important for overall or class-level classification (Clark et al. 2010).

According to the mean decrease in accuracy, the relevant variables in the RF classification were elevation, NDSI during the growing season (March–May), NDVI during September, and NDWI during April. In general, elevation contributed significantly to increased classification accuracy for each category (Table 1). Because the plateau vegetation, hillside field, and (flatland) field categories had similar NDVI patterns, but different topography, the priority variable for classifying these vegetation types was elevation. NDSI had a high value for exposed soils, and showed a large difference between vegetation types during March. Because field preparation for crops began during March (Boo et al. 2001), the fields became bare soil and presented the highest NDSI values while the other land-cover types were covered with vegetation or snow at the start of the season. Therefore, during March, NDSI could effectively distinguish (flatland) fields from other vegetation types. At the end of the growing season (September), differences

in NDVI values could be observed between farmland (field and paddy) and forest (forest and unstocked forest). The forests were covered with vegetation while farmland (field and paddy) was ready for harvest. The NDWI value during April contributed to a classification for plateau vegetation. In the plateau area, the rate of snow melt was slower than other landscape types and the NDWI value at the start of the growing season was higher than that for the other types. For this reason, this high value clearly distinguished the plateau sites from the other vegetation types that occurred nearby.

Other variables during each season also contributed to increased accuracy in the classification of each vegetation type. The contributions of these variables are specific to North Korea. For mapping regions where there is heterogeneous vegetative cover, it is necessary to find the variables most effective for classification. Each vegetation type during each season was representative of different vegetation, soil, and water conditions (Takeuchi and Yasuoka 2004), so the phenology-based indices were found to be effective for classifying these vegetation-cover types (Clark et al. 2010; Pan et al. 2010; Richardson and O'Keefe 2009; Senf et al. 2013).

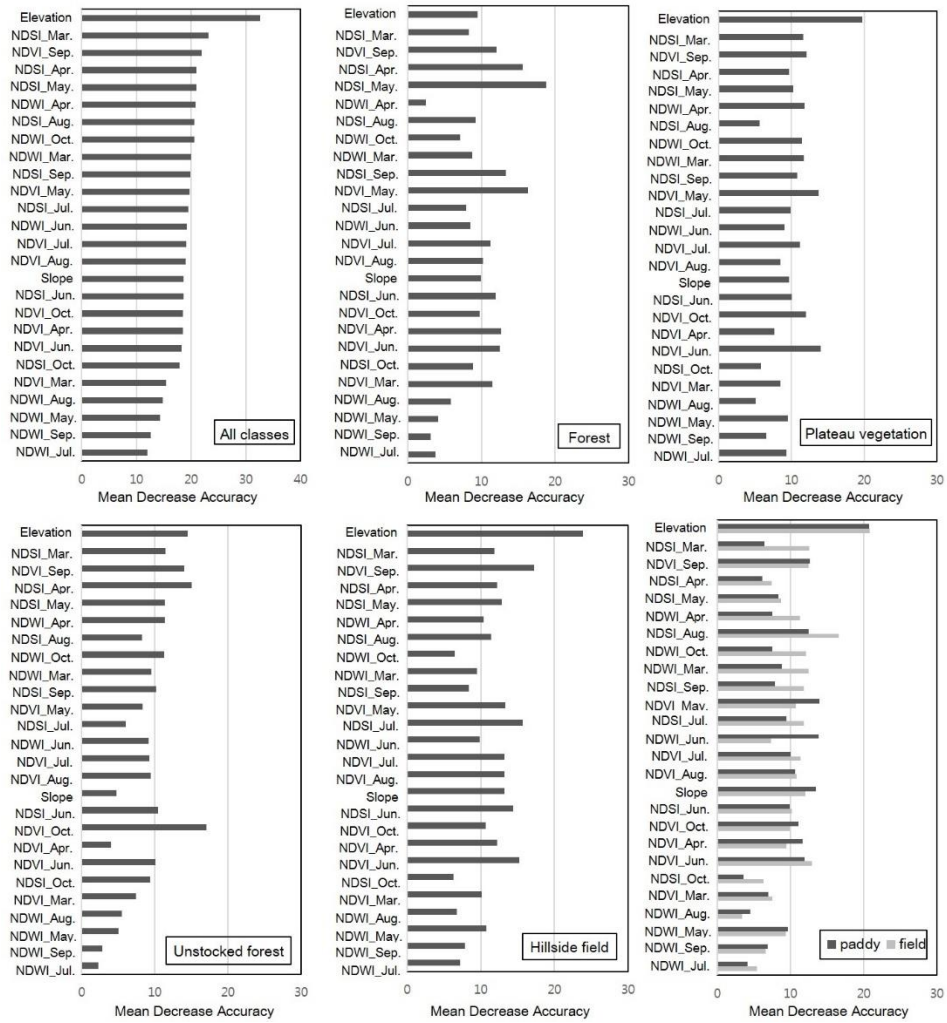

Figure 16. Mean decrease accuracy values of overall and for each class from the RF classification using phenology-based multi-index, and topographic variables.

Therefore, from Figure 16, one can see that NDVI during September; NDSI during March, April, May, August, and September; NDWI during March, April, and October; and elevation are the key variables that contributed more than 20% to classification.

1.3 Classification result and accuracy assessment

Classification results in this study demonstrated that phenology-based indices using RF classification are effective in mapping deforested land, and in understanding complex vegetative cover. High classification accuracies were achieved (Table 4), and it was possible to successfully distinguish areas covered by shrubs, crops, and plateau vegetation; which in turn distinguished unstocked forest, hillside field, and plateau from forest. The producer's accuracy in mapping the hillside field and unstocked forest was 80.3% and 87%, respectively, which indicates deforested areas. The corresponding user's accuracies were 94% and 91.2%. Consequently, the overall accuracy of the resultant map was 89.38%, with a kappa coefficient 0.87 (Table 4). Because the landscape types within forest have similar variation in spectral signatures (Immitzer et al. 2012), hillside field was misclassified as other classes, such as flatland field or unstocked forest. Some areas of water were misclassified as built-up because the sand on the riverside was recognized as bare soil. This is a limitation of classification using data of 250-m resolution. This is a common problem when classifying heterogeneous landscapes using per-pixel classification techniques (Duro et al. 2012; Lu and Weng 2007; Zhang et al. 2014).

Table 4. Confusion matrix for land-cover classification of North Korea

Reference Data / Map results	Built-up	Paddy	Field	Hillside field	Unstocked forest	Forest	Plateau vegetation	Water	Total	User's
Built-up	51	0	4	0	0	0	0	2	57	89.5%
Paddy	0	79	15	3	0	0	0	3	100	79%
Field	0	1	90	8	0	0	0	0	99	90.9%
Hillside field	0	0	0	94	1	0	5	0	100	94%
Unstocked forest	0	0	0	7	93	2	0	0	102	91.2%
Forest	0	0	0	0	12	329	6	0	347	94.8%
Plateau vegetation	0	0	0	0	0	8	69	1	78	88.5%
Water	15	1	3	5	1	4	0	87	116	75%
Total	66	81	112	117	107	343	80	93	999	
Producer's	77.3 %	96.3 %	80.4 %	80.3%	87%	96%	86.3%	93.5%		

OOB estimate of error rate: 4.47%
Accuracy: 89.38%
Kappa: 0.8701

Figure 17a is the final classification map of the vegetative cover in North Korea, and Figure 17b shows the areas of deforestation in North Korea projected in this study. Approximately 4 million ha of forestland appeared deforested representing 34.2% of the total forestland in North Korea. In these areas forest was converted to hillside field (~ 2.7 million ha) and unstocked forest (~ 1.3 million ha) as shown in Figure 17b. Similar results were reported by Jeong (Jeong et al. 2016b), who also observed that approximately 30% of the forest was degraded in North Korea.

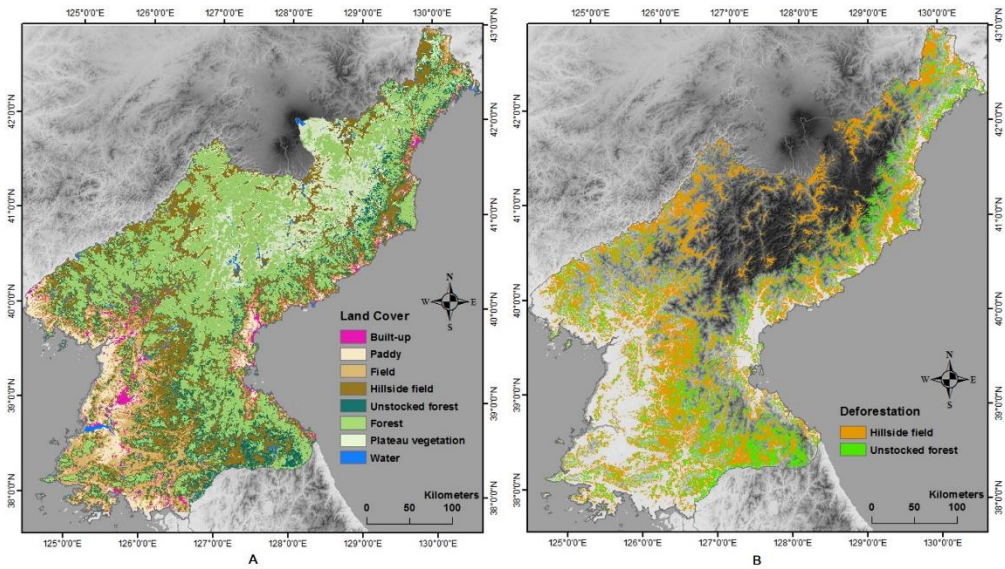

Figure 17. Final land-cover classification map of North Korea: A) Land-cover map in North Korea, B) Distribution of deforested land in North Korea

In North Korea, attempts to separate these cover types using traditional multispectral data or vegetation indices (Landsat, MODIS or NDVI in one-time images) (Cha and Park 2007; Jeong et al. 2016b) have not been successful. The class accuracies indicated that phenology-based indices that also include vegetation, soil, and water information, along with the use of RF consistently increased the individual classification accuracies. Nevertheless, further research is needed to develop a technique to analyze detailed vegetative cover types at high spatial resolution.

2. Deforestation and degradation dynamics from 1990 to 2016

The key phenology-based indices of 2001, 2010, and 2016 were stacked to one layer, respectively, then input into the RF classification model proposed previously, which can predict each year of land cover in North Korea only constructed by the phenology-based indices. The results of mapping land cover in North Korea can be seen in Figure 18. Each vegetative cover type during each season was representative of different vegetation, soil, and water conditions. In temperate climatic regions, the characteristics of vegetation phenology are similar, so that the phenology-based indices proposed in the first part are effective for classifying vegetative cover types during each year.

The results of uncertainty can be seen in Table 5–7. Change detection from the 1990s to 2001 has the largest uncertainty; it was estimated as 16.3% because of the differences in satellite sensor, spatial resolution, and classification method. The classified-type difference between the 1990s and 2001 also contributed to the total uncertainty. The pixels classified as non-forest may contain unstocked forest and hillside farm. However, one cannot classify in detail using Landsat TM5 images with no training data.

The total uncertainties between 2001 and 2010, and 2010 and 2016, were 11.42 % and 7.93%, respectively. From the two cases, we can see the greatest uncertainty occurred in hillside farm and farmland on flatland. Because the hillside farmland and farmland on flatland show similar reflectance and

phenology, confusion values through classification remain.

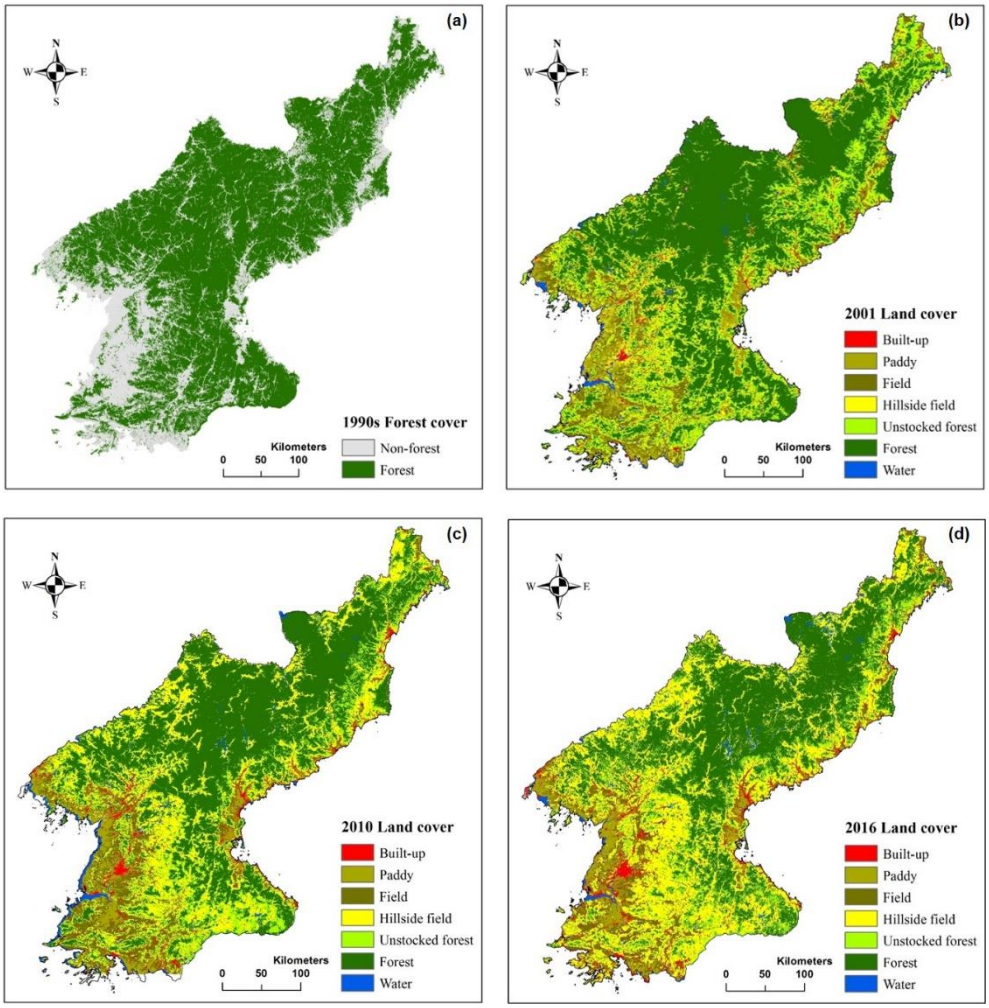

Figure 18. Land-cover map for 2001 (b), 2010 (c), 2016 (d). (a) is the forest cover map for reference of deforestation and degradation.

Table 5. Change detection (km^2) for the period 1990s to 2001. (Natural forest is the sum of plateau vegetation and forest; farmland is the sum of paddy and field. The total area of the study area is 122,778 km^2)

2001 / 1990s	Natural Forest	Unstocked forest	Hillside field	Farmland	Water	Urban	Total in 1990s	Uncerta-inty
Natural forest	57,792 (47.1%)	16,219 (13.2%)	7,821 (6.4%)	2,050 (1.7%)	381 (0.3%)	123 (0.1%)	84,385 (68.7%)	2,431 (2.0%)
Non-forest	4,359 (3.6%)	3,327 (2.7%)	9,896 (8.1%)	17,643 (14.4%)	1,805 (1.5%)	1,363 (1.11%)	38,393 (31.3%)	17,582 (14.3%)
Total in 2001	62,150 (50.7%)	17,717 (15.9%)	17,717 (14.4%)	19,694 (16.0%)	2,185 (1.8%)	1,486 (1.21%)	122,778 (100%)	-
Uncertainty	4,359 (3.6%)	3,327 (2.7%)	9,896 (8.1%)	2,050 (1.7%)	381 (0.3%)	123 (0%)	-	**20,013 (16.3%)**

Note: the table cells with yellow color represent land cover of no-change, the orange color represents forest degradation and deforestation, and the cells with grey color represent the uncertainties in land cover changed.

Table 6. Change detection (km^2) for the period 2001 to 2010. (Natural forest is the sum of plateau vegetation and forest; farmland is the sum of paddy and field. The total area of the study area is 122,778 km^2)

2010 / 2001	Natural Forest	Unstocked forest	Hillside field	Farmland	Water	Urban	Total in 2001	Uncerta-inty
Natural forest	49,136 (40.0%)	6,876 (5.6%)	6,163 (5.0%)	98 (0.1%)	307 (0.3%)	25 (0.02%)	62,605 (51.0%)	405 (0.3%)
Unstocked forest	6,421 (5.2%)	5,230 (4.3%)	7,072 (5.8%)	700 (0.6%)	123 (0.1%)	49 (0.04%)	19,595 (16.0%)	823 (0.7%)
Hillside field	1,682 (1.4%)	1,486 (1.2%)	9,368 (7.6%)	4,138 (3.4%)	479 (0.4%)	577 (0.5%)	17,729 (14.4%)	4,616 (3.8%)
Farmland	221 (0.2%)	196 (0.2%)	5,144 (4.2%)	12,155 (9.9%)	835 (0.7%)	1,130 (0.9%)	19,681 (16.0%)	6,397 (5.2%)
Water	184 (0.2%)	49 (0.04%)	221 (0.2%)	246 (0.2%)	798 (0.7%)	258 (0.2%)	1,756 (1.4%)	958 (0.8%)
Urban	37 (0.03%)	12 (0.01%)	246 (0.2%)	344 (0.3%)	184 (0.2%)	602 (0.5%)	1,424 (1.2%)	823 (0.7%)
Total in 2010	57,681 (47.0%)	13,849 (11.3%)	28,214 (23.0%)	17,680 (14.4%)	2,726 (2.2%)	2,640 (2.2%)	122,778 (100%)	-
Uncertainty	442 (0.4%)	258 (0.2%)	5,611 (4.6%)	5,525 (4.5%)	1,928 (1.6%)	258 (0.2%)	-	**14,021 (11.4%)**

Note: the table cells with yellow color represent land cover of no-change, the orange color

represents forest degradation and deforestation, the cells with green color represent the forest restoration, and the cells with grey color represent the uncertainties in land cover changed.

Table 7. Change detection (km^2) for the period 2010 to 2016. (Natural forest is the sum of plateau vegetation and forest; farmland is the sum of paddy and field. The total area of the study area is 122,778 km^2)

2010 \ 2016	Natural Forest	Unstocked forest	Hillside field	Farmland	Water	Urban	Total in 2010	Uncerta-inty
Natural forest	43,341 (35.3%)	6,593 (5.4%)	7,367 (6.0%)	25 (0.02%)	332 (0.3%)	12 (0.01%)	57,669 (47.0%)	356 (0.3%)
Unstocked forest	4,825 (3.9%)	2,542 (2.1%)	6,421 (5.2%)	49 (0.04%)	37 (0.03%)	12 (0.01%)	13,886 (11.3%)	86 (0.1%)
Hillside field	1,461 (1.2%)	528 (0.4%)	23,377 (19.0%)	1,903 (1.6%)	602 (0.5%)	344 (0.3%)	28,214 (23.0%)	2,505 (2.0%)
Farmland	12 (0.01%)	12 (0.01%)	3,585 (2.9%)	12,266 (10.0%)	172 (0.1%)	1,608 (1.3%)	17,655 (14.4%)	3,782 (3.1%)
Water	74 (0.1%)	74 (0.1%)	589 (0.5%)	638 (0.5%)	970 (0.8%)	417 (0.3%)	2,763 (2.3%)	1,793 (1.5%)
Urban	0 (0.0%)	0 (0.0%)	295 (0.2%)	761 (0.6%)	160 (0.1%)	1,437 (1.2%)	2,652 (2.2%)	1,216 (1.0%)
Total in 2016	49,713 (40.5%)	9,749 (8.0%)	41,634 (33.9%)	15,642 (12.7%)	2,271 (1.9%)	3,831 (3.1%)	122,778 (100%)	-
Uncertai-nty	86 (0.1%)	86 (0.1%)	4,469 (3.6%)	3,376 (2.8%)	1,301 (1.1%)	417 (0.3%)	-	**9,736 (7.9%)**

Note: the table cells with yellow color represent land cover of no-change, the orange color represents forest degradation and deforestation, the cells with green color represent the forest restoration, and the cells with grey color represent the uncertainties in land cover changed.

From Table 5 to 7, the greatest transformation from the 1990s to 2001 is forest to unstocked forest; approximately 16,219 km^2 of forest were deforested to unstocked forest. During this period, the Law of Land in North Korea formulates forest cultivation. A large area of forest was burned in order to clear land.

During the period of 2001–2010, approximately 13,039 km^2 of deforestation

occurred, where forest was converted to hillside field and unstocked forest. Hillside fields are not sustainable, as the ground is damaged resulting in soil and nutrient loss and landslides, as well as increased vulnerability to extreme weather events. Approximately 1,486 km^2 changed from hillside field to unstocked forest during this period, a most serious problem. This occurs because hillside fields are used until their productivity declines and then are abandoned without management. These destructive farming processes are repeatedly undertaken. A new plot is selected and cut down and the forest burned for clear land, then used until the productivity decreases, and abandoned.

From 2010 to 2016, 13,960 km^2 of forest were converted to hillside field and unstocked forest, and 528 km^2 of hillside field converted to unstocked forest. There are several causes for the forest to unstocked forest transformation. It may be caused by natural disasters, such as landslides, floods, or forest fires, because extreme climatic events occurred frequently during this period. Or changes in climatic conditions or landscape fragmentation from anthropogenic pressures may have caused these changes. Unfortunately, this study could not determine the detailed reasons of forest cover change to unstocked forest because the study area is an inaccessible area; thus, there is lack of survey data for forest degradation.

Table 8 . The area of each land-cover type from the 1990s to 2016 (unit: km2)

	1990s	2001	2010	2016
Natural forest	84,385	62,606	57,669	49,713
Unstocked forest	38,393	19,595	13,886	9,749
Hillside field		17,729	28,214	41,634
Farmland		19,681	17,655	15,642
Water		1,756	2,763	2,271
Urban		1,424	2,652	3,831

Table 8 summarizes the area of each land-cover type from Table 5~7, Figure 19, and Figure 20 showing reconstructed results. They represent the forest loss and deforestation trends during the selected periods. One can see most of the decrease in forest was from conversion to unstocked forest and hillside field. The rate of urbanization was much less than the that of the growth of agriculture.

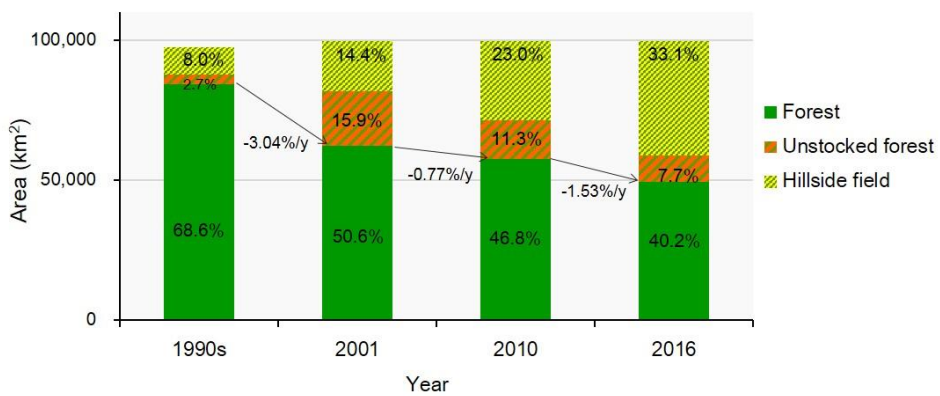

Figure 19. Degradation and deforestation in North Korea from the 1990s to 2016, and the contributions of deforestation and forest degradation.

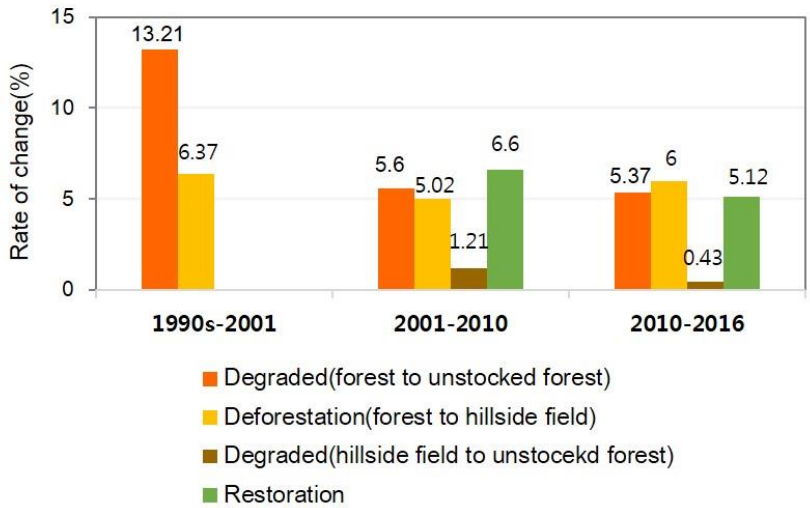

Figure 20. Rate of deforestation and degradation in North Korea form the 1990s to 2016.

According to Table 5–7, we can categorize the degradation and deforestation into three types: degradation from forest to unstocked forest, degradation from hillside field to unstocked forest, and deforestation from forest to hillside field. The area of forest decreased during the study period, while the area of unstocked forest and hillside field increased (Figure 20). From 1990 to 2001, the greatest contribution to deforestation was from forest to unstocked forest. After this, from 2001 to 2016, the change contributing the greatest of amount of degradation was from forest to hillside field. The degradation caused by the change from hillside field to unstocked forest is much less, however, these are potential degradation areas, where forest converted to hillside field occupies 41,634 km^2 of the decreased forest. This means there are much more potential degraded areas if there is no management of the hillside fields.

The forest area of North Korea was 84,385 km^2 during the 1990s, and

remained 49,713 km^2 in 2016. The annual rate of forest loss was 3.04% during the period of the 1990s to 2001; fortunately, the rate of forest loss has decreased, and restoration efforts are encouraged by policy in North Korea.

3. Spatiotemporal data fusion method for monitoring deforestation and degradation

3.1 RDSFM experimental results

Through visually comparing the predicted results via the two methods (Figure 21), one can see that all maintain spatial details. Figure 21b and 21c present a Landsat-like image on January 11, 2002 predicted using the FSDAF and RDSFM. Figure 22 and Figure 23 present the predicted red band and NIR band respectively, which play an important role in analyzing vegetation. From the visual comparison, the images that the two methods predicted are generally similar to the original Landsat image in Figure 21–23. This suggests that the two methods are able to capture the general phenology change of complex and heterogeneous lands.

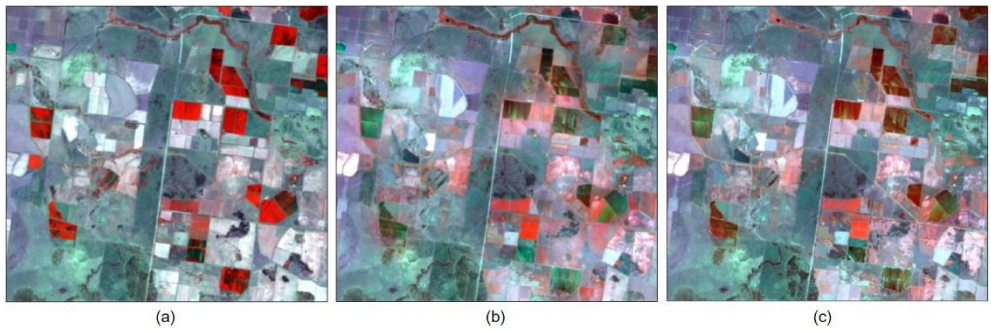

Figure 21. Zoom-in scenes of a complex and heterogeneous site: Original Landsat image of January 11, 2002 (a) and its predicted images suing FSDAF (b) and RDSFM (c)

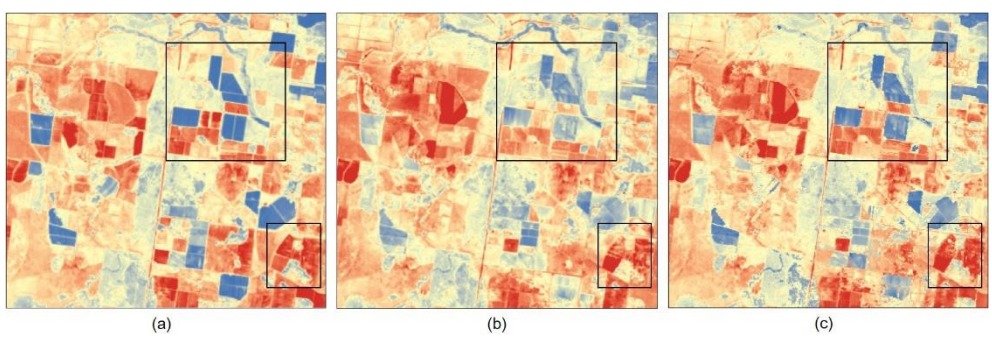

Figure 22. Zoom-in scenes of a complex and heterogeneous site: Original Landsat red band of January 11, 2002 (a) and its predicted red band suing FSDAF (b) and RDSFM (c)

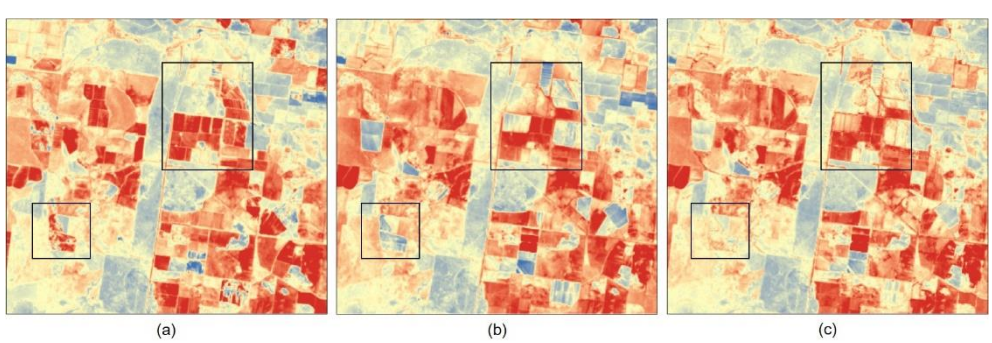

Figure 23. Zoom in scenes of a complex and heterogeneous site: Original Landsat NIR band of January 11, 2002 (a) and its predicted red band suing FSDAF (b) and RDSFM (c)

Comparing the quantitative indices calculated using the original Landsat image at January 11, 2002 (Table 9), one can see that three methods have successfully added certain temporal change information to the input Landsat image to obtain the prediction on January 11, 2002. For the three bands, the fused results of RDSFM have a smaller RMSE and a higher R than those of UBDF and FSDAF, suggesting that the RDSFM predictions are more accurate than those of UBDF and FSDAF. Among the three bands, the NIR band has the greatest difference in accuracy between RDSFM and the other two methods. The acquired time of the two Landsat images was the early growing season of crops; thus, the NIR band and red band experienced a larger reflectance change than that of the other bands. Compared to UBDF and FSDAF, the large improvement in predicting the NIR band and red band suing RDSFM indicates that it is more capable of capturing large temporal change between the input and prediction dates.

Table 9. Accuracy assessment of three data-fusion methods applied to a complex and heterogeneous study area (Figure 21). The units are reflectance (band1: blue band; band2: Green band; band3: Red band; band4: NIR band; band5: SWIR1 band; band6: SWIR2 band; R: correlation coefficient; RMSE: root mean square error; AD: average difference from the true reflectance; SSIM: structural similarity)

		UBDF	**FSDAF**	**RDSFM**
R	band1	0.8300	0.8638	0.8827
	band2	0.7961	0.8551	0.8743
	band3	0.8360	0.8779	0.8978
	band4	0.4965	0.7213	0.7709
	band5	0.8884	0.9354	0.9389
	band6	0.9320	0.9539	0.9558
RMSE	band1	0.0156	0.0140	0.0132
	band2	0.0234	0.0199	0.0187
	band3	0.0329	0.0286	0.0263
	band4	0.0639	0.0462	0.0420
	band5	0.0449	0.0348	0.0332
	band6	0.0329	0.0276	0.0269
AD	band1	0.0032	0.0021	0.0025
	band2	0.0042	0.0023	0.0030
	band3	0.0014	-0.0001	0.0006
	band4	0.0108	0.0024	0.0036
	band5	-0.0050	-0.0092	-0.0071
	band6	-0.0020	-0.0042	-0.0028
SSIM	band1	0.9290	0.9379	0.9415
	band2	0.9093	0.9337	0.9309
	band3	0.8735	0.9065	0.9026
	band4	0.8272	0.8641	0.8515
	band5	0.8356	0.8979	0.8807
	band6	0.8771	0.9130	0.9022

A zoom-in area was also used to highlight the difference between predicted images and the actual image (Figure 24–Figure 26). The predicted image of RDSFM is more similar to the original image than the images predicted using FSDAF in regards to spatial details, which can be seen from the zoom-in images of the red and NIR bands in Figure 25 and Figure 26. Particularly, comparing the zoom-in area of the two original Landsat images, we can see that there is a parcel of lake that changed from non-water to water. For this small parcel, although FSDAF predicted its pixel values well, RDSFM is better at preserving the small changes.

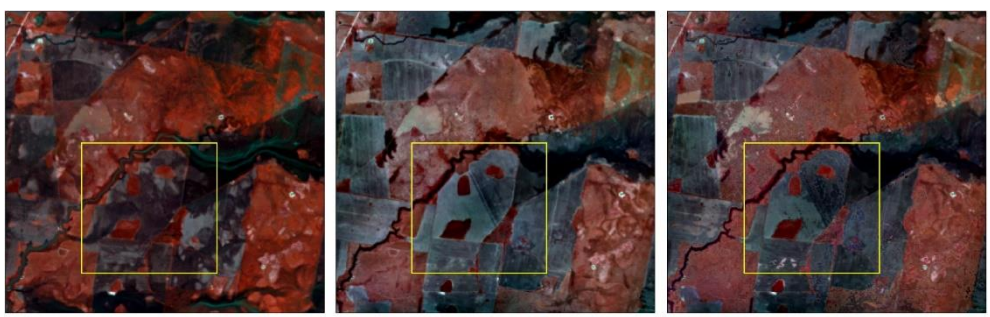

Figure 24. Zoom-in scenes of land-cover change: original Landsat image of November 26, 2004 (a), and predicted images suing FSDAF (b) and RDSFM (c)

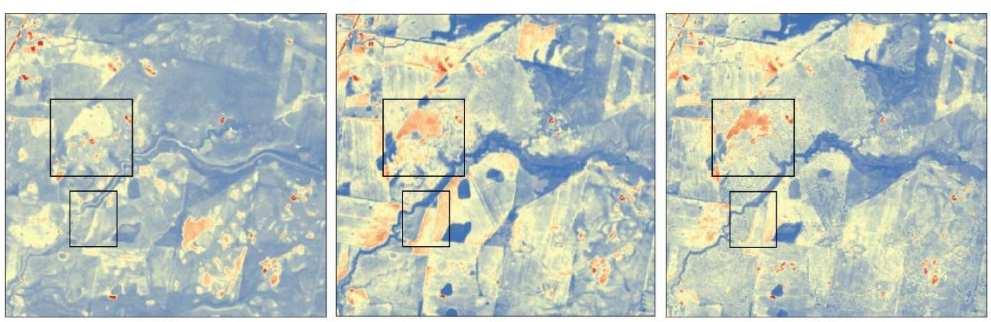

Figure 25. Zoom-in scenes of land-cover change: original Landsat red band of November 26, 2004 (a), and predicted images suing FSDAF (b) and RDSFM (c)

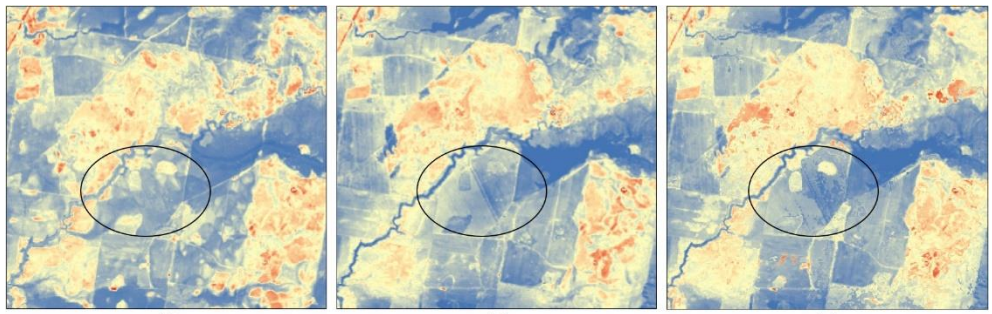

Figure 26. Zoom-in scenes of land-cover change: original Landsat NIR band of November 26, 2004 (a), and predicted images using FSDAF (b) and RDSFM (c)

The quantitative indices calculated from fused results and the original Landsat image on prediction time demonstrate that all data-fusion methods have captured certain temporal change information between the input and prediction images. For the three bands, RDSFM provided the most accurate predictions with the smallest RMSE and highest R and SSIM. For the overall bias of the prediction, the small AD values reveal that all three methods obtained nearly unbiased results.

Table 10. Accuracy assessment of three data-fusion methods applied to a complex and heterogeneous study area (Figure 22). The units are reflectance (band1: blue band; band2: Green band; band3: Red band; band4: NIR band; band5: SWIR1 band; band6: SWIR2 band; R: correlation coefficient; RMSE: root mean square error; AD: average difference from the true reflectance; SSIM: structural similarity)

		UBDF	**FSDAF**	**RDSFM**
R	band1	0.6770	0.7298	0.7353
	band2	0.6461	0.7183	00.7319
	band3	0.6630	0.7450	0.7599
	band4	0.6920	0.8647	0.8637
	band5	0.4423	0.8146	0.8096
	band6	0.5084	0.8034	0.8074
RMSE	band1	0.0185	0.0177	0.0173
	band2	0.0241	0.0232	0.0223
	band3	0.0286	0.0269	0.0256
	band4	0.0483	0.0359	0.0357
	band5	0.0846	0.0544	0.0543
	band6	0.0634	0.0456	0.0442
AD	band1	-0.0041	-0.0041	-0.0039
	band2	-0.0023	-0.0054	-0.0051
	band3	-0.0015	-0.0048	-0.0043
	band4	-0.0096	-0.0139	-0.0130
	band5	-0.0340	-0.0211	-0.0196
	band6	-0.0210	-0.0166	-0.0156
SSIM	band1	0.9006	0.9094	0.9126
	band2	0.8881	0.8965	0.8988
	band3	0.8680	0.8814	0.8829
	band4	0.7826	0.8382	0.8175
	band5	0.6210	0.7142	0.6877
	band6	0.6272	0.7272	0.7150

3.2 Construct monthly Landsat-like images in part of North Korea

In this part, RDSFM proposed in the previous chapter was used to construct monthly Landsat-like images from March to October of 2001 and 2014. The blended images can be seen in Figure 27 and Figure 28. By visually comparing the predicted results, one can see that all can maintain spatial and seasonal details.

From the quantitative indices calculated using the original Landsat image on May 21, 2014 and October 28, 2014 (Table 11), one can see that RDSFM successfully added certain temporal change information to the input Landsat image to obtain the prediction on the two images. The R correlation value between the real Landsat images and predicted Landsat-like images is higher than 0.8, and the SSIM, which represents the structural similarity, is close to 0.9. This means the predicted images are relatively close to the real Landsat images.

For sample site 1, the most heterogeneous and with high spectral changes, the R correlation value is lower than value of all the points and sample site 2, especially the NIR band. Similar results can be seen in Table 9. However, improvements in the NIR band prediction were evident and the results of RDSFM were higher than those of the other methods, so that the predicted results in this part are relatively credible.

For sample site 2, where most areas are homogeneous, the R correlation

value between the atmospherically corrected Landsat images and predicted Landsat-like images is close to 0.9. In addition, the values of RMSE, AD, and SSIM suggest that it predicted accurately in a homogeneous landscape area.

Table 11. Accuracy assessment of two data fusion methods applied to pixels at all points, sample 1 and sample 2. Sample1 is for heterogeneous areas, main land cover is farmland; sample2 is for homogeneous areas, main land cover is forest.

Date		**2014/05/29**				**2014/10/28**			
Indicator		**R**	**RMSE**	**AD**	**SSIM**	**R**	**RMSE**	**AD**	**SSIM**
All	Red	0.880	0.027	0.003	0.834	0.818	0.028	0.011	0.899
	NIR	0.850	0.061	0.005	0.853	0.826	0.063	-0.044	0.828
	SWIR1	0.855	0.037	0.005	0.875	0.878	0.058	0.024	0.841
	SWIR2	0.813	0.036	0.002	0.824	0.824	0.055	0.030	0.870
Sampl esite 1	Red	0.726	0.0469	0.009	0.809	0.721	0.029	0.009	0.868
	NIR	0.703	0.0109	0.006	0.846	0.708	0.065	-0.040	0.902
	SWIR1	0.809	0.064	0.020	0.869	0.785	0.060	0.019	0.769
	SWIR2	0.742	0.061	0.006	0.889	0.740	0.053	0.023	0.840
Sampl esite 2	Red	0.847	0.026	-0.002	0.824	0.830	0.027	0.004	0.979
	NIR	0.905	0.063	0.004	0.887	0.825	0.072	-0.05	0.896
	SWIR1	0.936	0.030	0.002	0.897	0.891	0.066	0.018	0.949
	SWIR2	0.869	0.035	0.001	0.821	0.874	0.052	0.021	0.977

The two Landsat images were acquired during different seasons and temporal interval; the base image (F1) for prediction was acquired in September, while the test image (F2) was acquired in May and October. All quantitative indices for accuracy assessment show consistent and high accuracy. This means that the RDSFM is not related to the temporal interval between the input and predicted image, but it is affected by the degree of

heterogeneity.

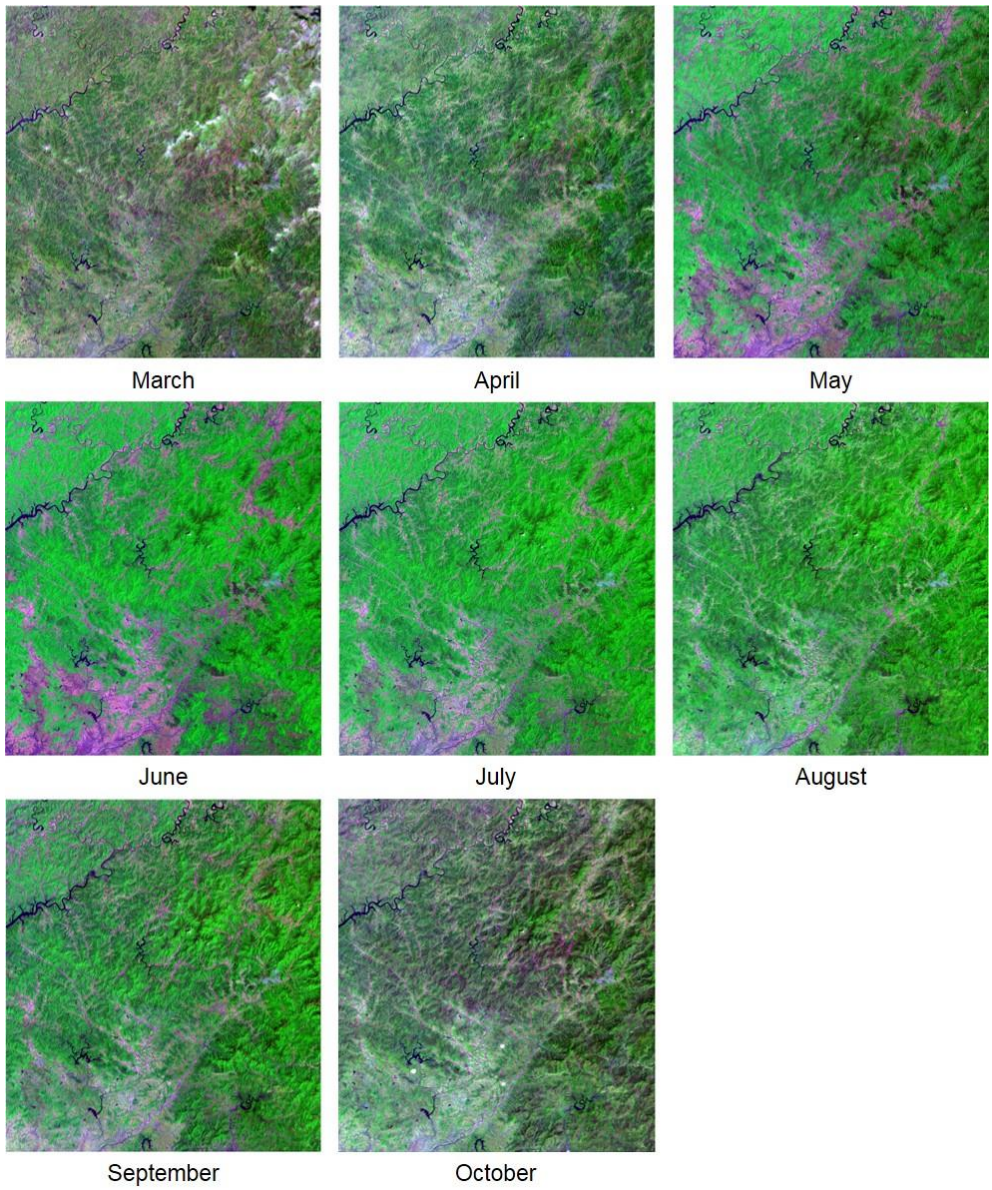

Figure 27. The predicted Landsat-like images from March to October of 2001. All images use red-NIR-green as RGB

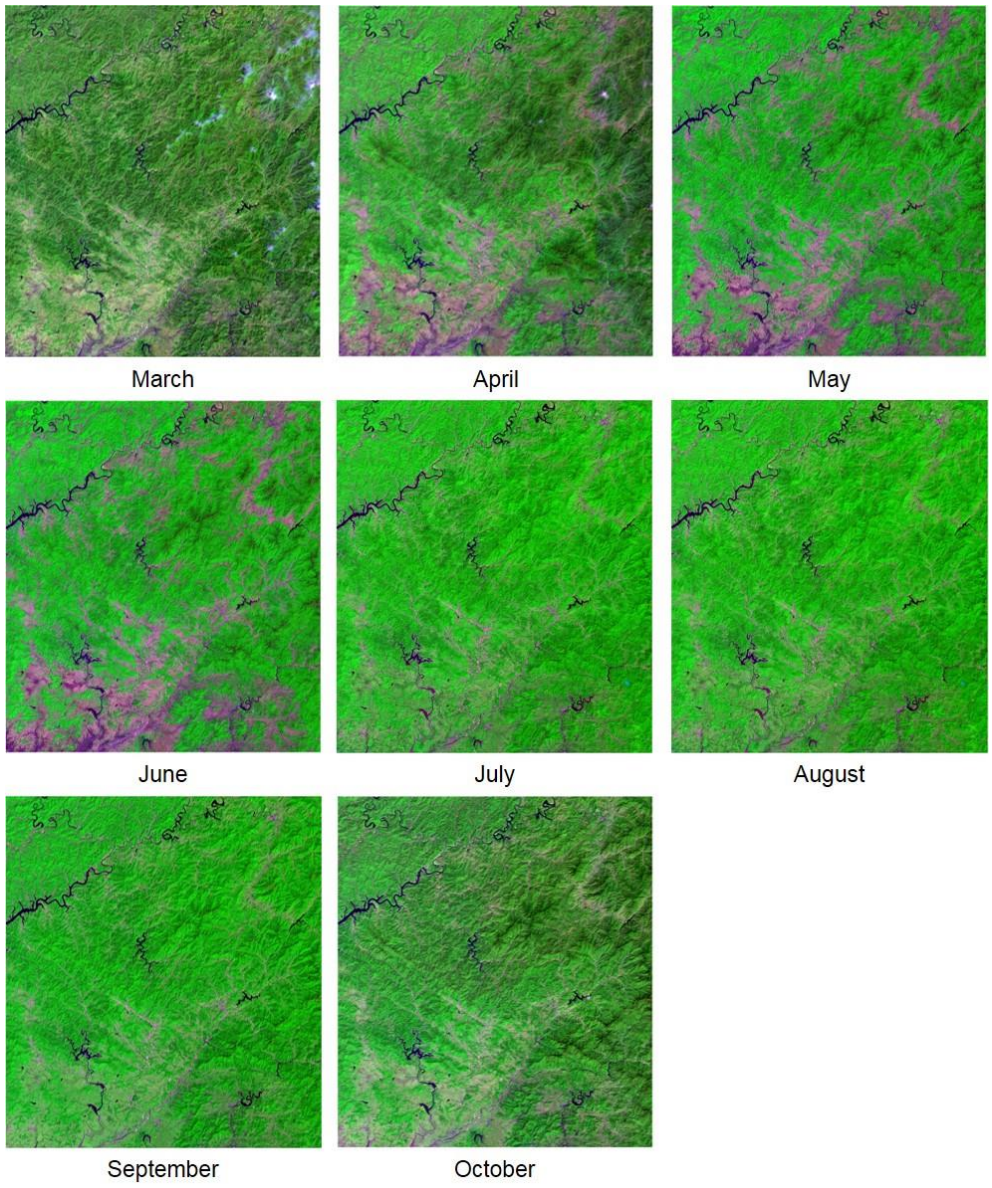

Figure 28. The predicted Landsat-like images from March to October of 2014. All images use red-NIR-green as RGB

3.3 Application to deforestation and degradation monitoring

According to the results of the first part, the key variables for classification of land cover in North Korea are NDSI during the growing season (from March to May), NDVI at the end of the season (September), and NDWI at the start of season and end of the season (March to April, and October). Each vegetative cover type during each season was representative of different vegetation, soil, and water conditions; thus, the phenology-based indices proposed in the first part are effective for classifying vegetation-cover types. These variables have more than 20% relative importance in North Korea.

To combine these key variables in fine resolution, the RDSFM proposed in the second part, was found to be effective in spectral change where there is heterogeneity and changes in phenology. The key phenology-based indices suggested in the first part were built using the RDSFM, and each variable in fine resolution is as below (Figure 29, 30). Finally, these key phenology-based indices were stacked to one layer, and applied to classification.

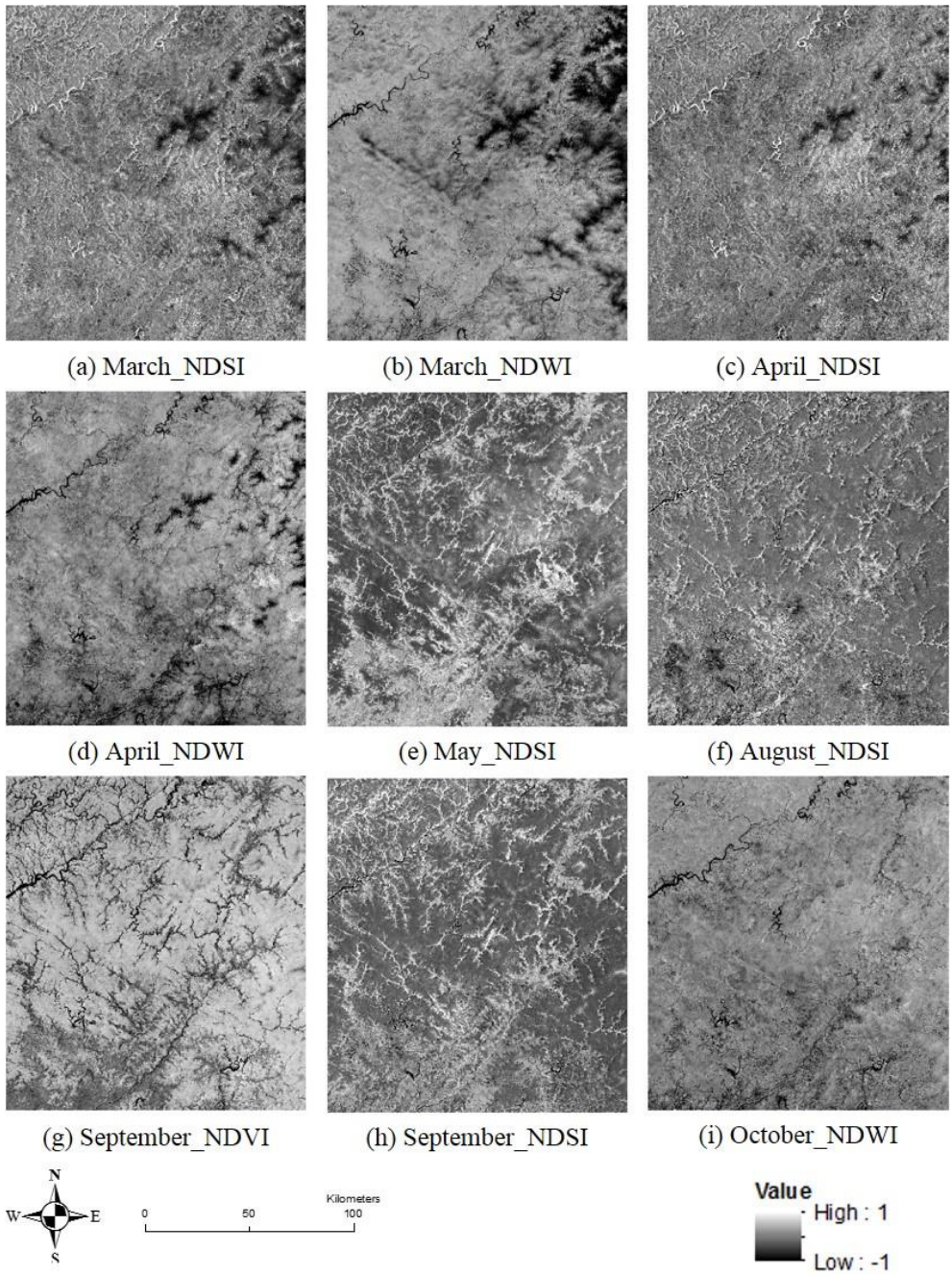

Figure 29. Phenological variables at fine spatial resolution for 2001

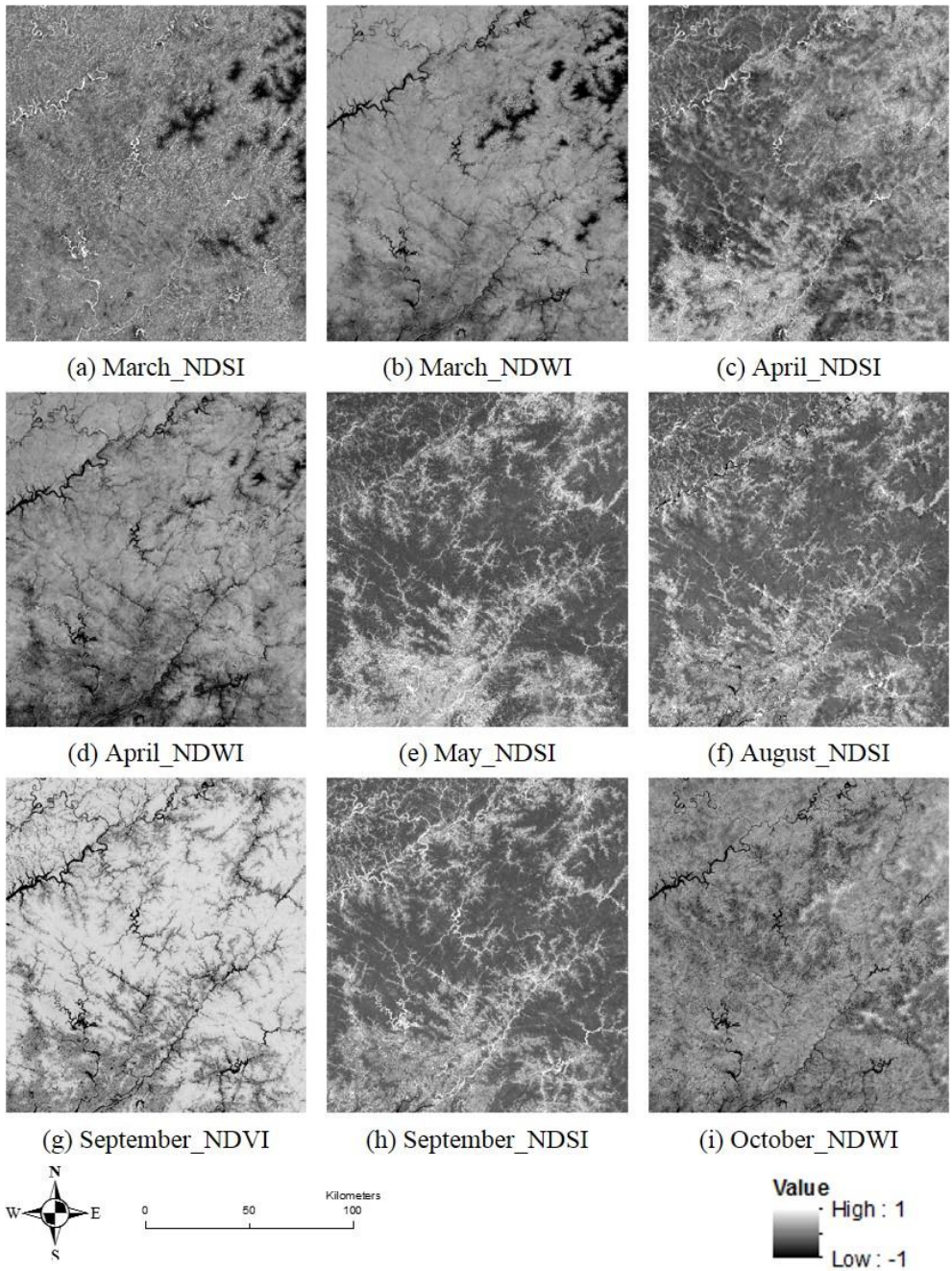

Figure 30. Phenological variables at fine spatial resolution for 2014

Table 12. Confusion matrix for land-cover classification of the study area during 2014

Reference data / Map results	Plateau vegetation	Forest	Unstocked forest	Hillside field	paddy	field	Water	Total	User's
Plateau vegetation	21	2	1	0	0	0	0	24	87.5%
Forest	0	103	1	0	0	0	0	104	99.0%
Unstocked forest	0	3	33	6	0	1	0	43	76.7%
Hillside field	0	0	1	50	6	1	0	58	86.2%
Paddy	0	3	0	1	30	5	0	39	76.9%
Field	0	0	0	7	8	14	0	29	48.3%
Water	0	0	0	0	0	0	34	34	100%
Total	21	111	36	64	46	21	34	331	
Producer's	100%	92.8 %	91.7%	78.1%	65.2 %	66.7 %	100 %		

Overall accuracy : 0.861
Kappa: 0.829

Classification results demonstrated that using phenology-based indices constructed by RDSFM and unsupervised classification are effective in mapping deforested areas, and in understanding complex vegetative cover. High classification accuracies were achieved (Table 12), and it was possible to successfully distinguish areas covered by crops, low canopy areas, and plateau vegetation; which in turn distinguished unstocked forest, hillside field, and plateau from forest and farmland on flatland. The producer's accuracy in mapping the hillside field and unstocked forest was 78.1% and 91.7%, respectively, which indicates deforested areas. The corresponding user's accuracies were 86.2% and 76.7%. The errors of omission were higher than the errors of commission in prediction of hillside field, which suggests that

hillside field was rarely predicted where field and unstocked forest was observed. In unstocked forest prediction, the errors of commission were significantly higher than the errors of omission, which suggests unstocked forest were misclassified to hillside field. Consequently, the overall accuracy of the resultant map for 2014 was 86.1%, with a kappa coefficient 0.829. The land-cover maps for 2001 and 2014 are shown in Figure 31 and Figure 32.

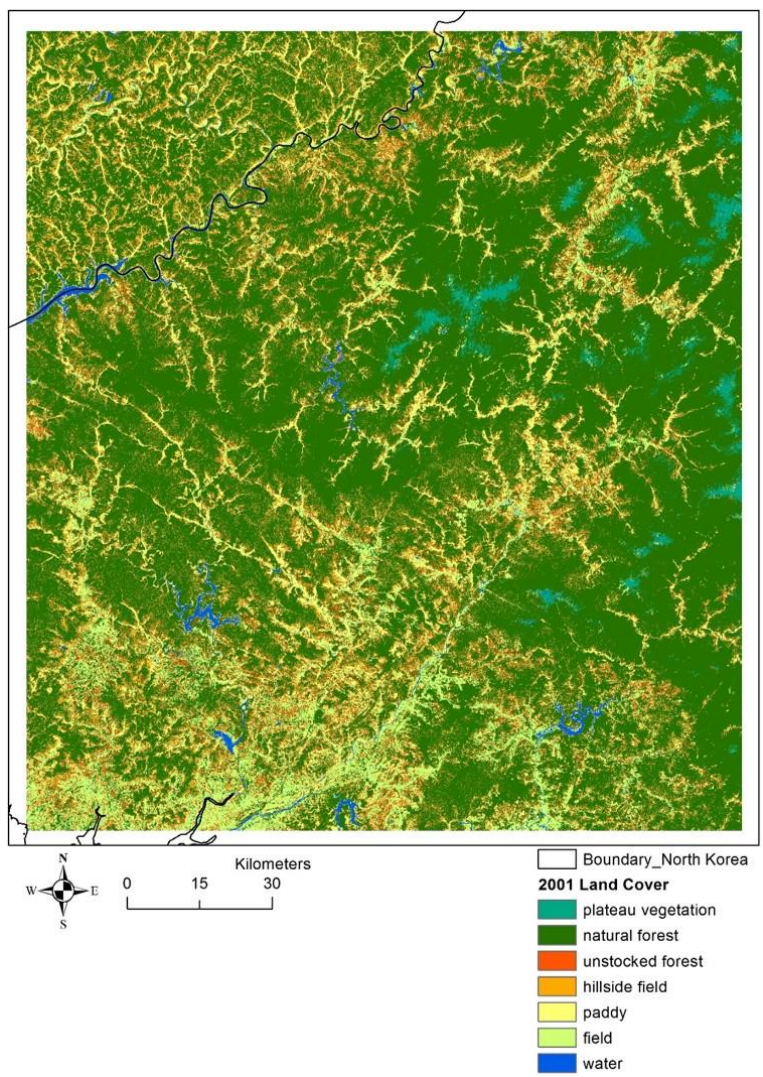

Figure 31. Land cover map in 2001

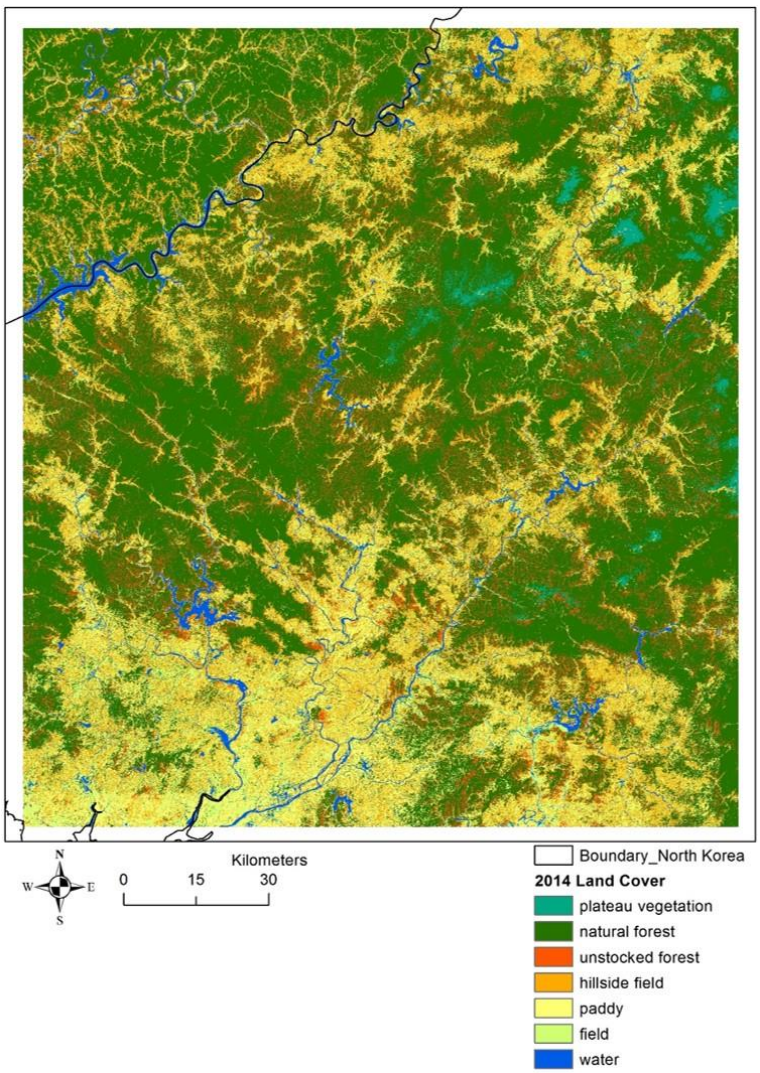

Figure 32. Land cover map in 2014

The map of land-cover change occurring from 2001 to 2014 is as shown in Figure 33. In this study, the phenology-based indices which represent vegetation growth, exposure of soil, water, and moisture of vegetation were used for classification. Thus, the areas that have healthy vegetation and high canopy cover and also have satisfactory moisture of vegetation are first classified to forest. This classification for deforestation and degradation

considered the vegetation, canopy, and moisture conditions of vegetative cover to be more accurate than previous studies that only considered NDVI (Cha and Park 2007; Yoo et al. 2011).

In Table 13 we can see the change rate of each landscape. The gray cells represent an uncertainty in land cover change. The greatest uncertainty appears in farmland classification. Two reasons can be considered. First, the uncertainty may be due to similar characteristics between farmland and hillside field during the two periods. Second, there is also a possibility that errors were caused due to the noise of the data during the blending of the Landsat and MODIS images.

The greatest transformation is forest to unstocked forest; approximately 1,660 km^2 of forest were degraded to unstocked forest. There are several reasons for the forest to unstocked forest transformation. It may be due to natural disasters, such as landslides, floods, or forest fires. It may be a result of changes in climatic conditions or landscape fragmentation, or it could be caused by anthropogenic pressures, such as cutting down trees for fuel, or burning forest for clear land, etc. Unfortunately, this study could not determine the detailed reasons of forest cover change to unstocked forest because the study area is in an inaccessible area; thus, there is lack of survey data for forest degradation.

From 2001 to 2014, approximately 1,562 km^2 of deforestation occurred in the study are, which was forest converted to hillside field. It is a serious problem in North Korea, because hillside fields are created by sacrificing

forest ecosystems. Hillside fields are not sustainable, as the ground is degraded resulting in soil and nutrient loss and landslides, and they are also heavily influenced by extreme weather events.

Table 13. Change rate of each landscape (Natural forest is the sum of plateau vegetation and forest; farmland is the sum of paddy and field. The total area in the study area is 24,411.3 km^2)

2014 / 2001	Natural Forest	Unstocked forest	Hillside field	Farmland	Water	Total in 2001	Uncert a-inty
Natural forest	46.7%	6.8%	6.4%	6.9%	0.3%	67.1%	7.2%
Unstocked forest	1.1%	0.2%	2.8%	2.8%	0.2%	7.1%	3%
Hillside field	4.1%	0.7%	1.3%	0.9%	0.2%	7.2%	5.2%
Farmland	2.0%	0.3%	5.8%	7.7%	1.6%	17.5%	8.7%
Water	0.1%	0.0%	0.0%	0.1%	0.9%	1.1%	0.2%
Total in 2014	54.0%	8.0%	16.4%	18.4%	3.2%	100%	24.3%
Uncertai-nty	6.2%	0.3%	5.8%	10.7%	2.3%	25.3%	

Note: the table cells with yellow color represent land cover of no-change, the orange color represents forest degradation and deforestation, the cells with green color represent the forest restoration, and the cells with grey color represent the uncertainties in land cover changed.

The most serious problem is hillside field transformed to unstocked forest. Approximately 171 km^2 of hillside field was transformed to unstocked forest from 2001 to 2014study area. This occurred because hillside field was used until its productivity declined and then abandoned without management. These destructive farming processes are repeatedly occurring; a new plot is selected and cut down, the forest burned for clear land, it is used until its productivity decreases, and then it is abandoned.

Degradation and deforestation were categorized into three types:

degradation from forest to unstocked forest, degradation from hillside field to unstocked forest, and deforestation from forest to hillside field. A map of each type of degradation and deforestation is as shown in Figure 33.

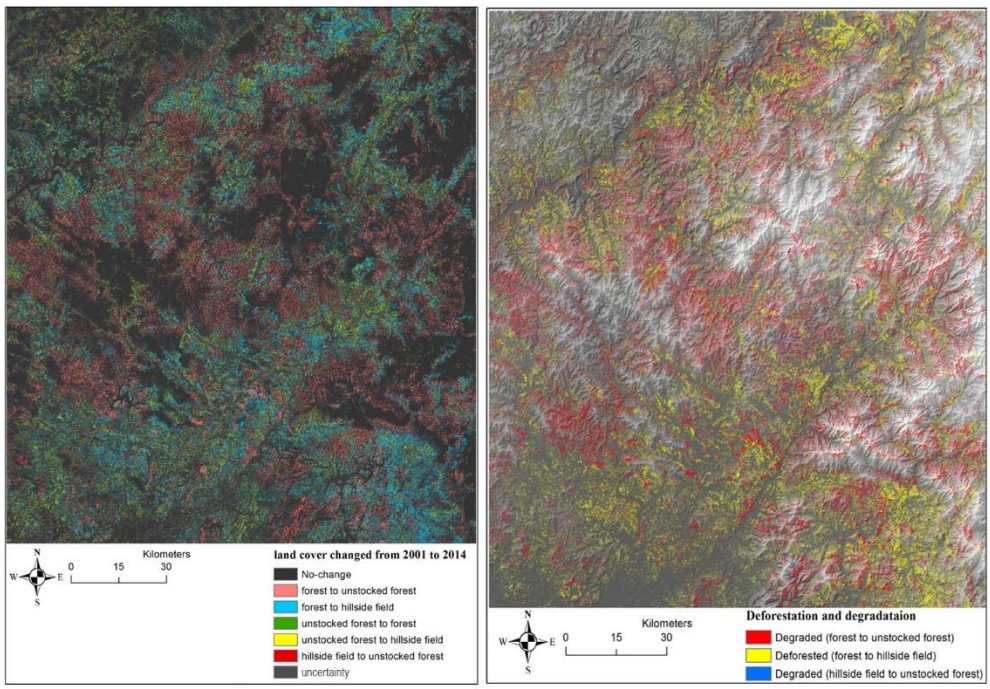

Figure 33 Land-cover changes (a), and deforestation and degradation (b) from 2001 to 2014.

The area of forest decreased during the study period, while unstocked forest and hillside field increased. The conversions contributing the greatest amount of degradation was forest to unstocked forest (49.3%). The degradation caused by conversion of hillside field to unstocked forest is much less, but the potential degradation area, where the forest has been converted to hillside field, occupies 46% of the decreased forest. This means there is much more potential degraded area if there is no management of the hillside field.

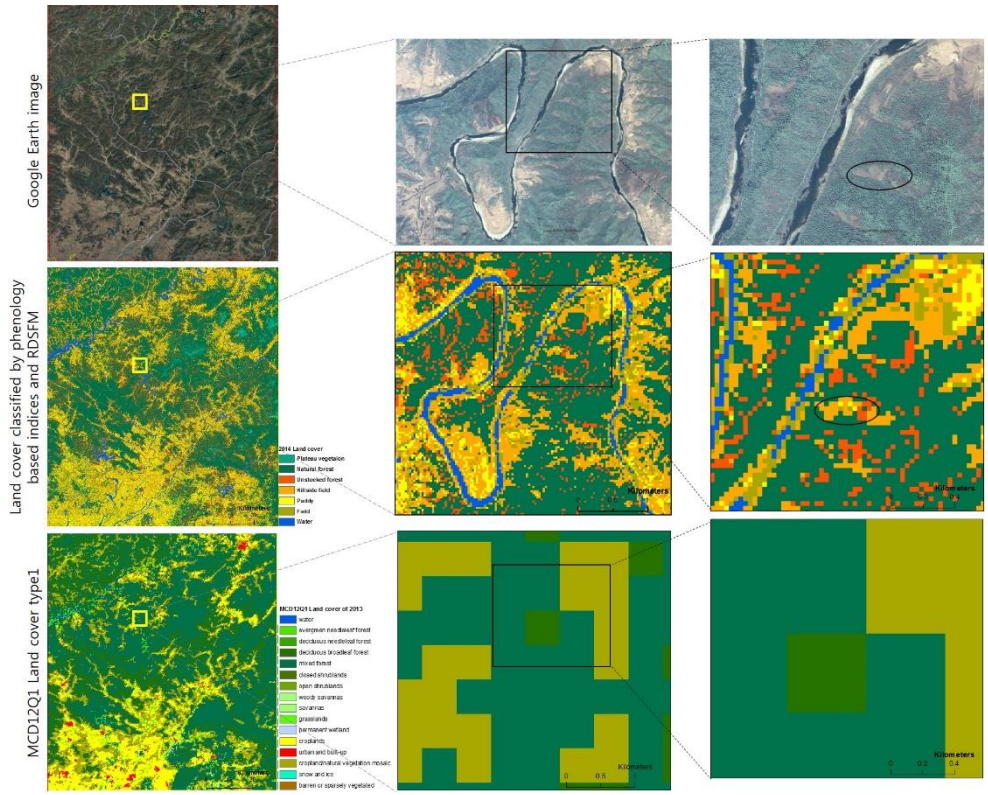

Figure 34. Comparison of the land-cover mapping using phenology-based indices and RDSFM (30 m) with GE image and MCD12Q1 land cover (500 m).

Comparing the quality of the mapping deforestation and degradation result with the MCD12Q1 yearly land cover and GE image, the land-cover result derived using our method is closer to reality. Reviewing the zoom-in image (Figure 34), MCD12Q1 did not reflect the deforestation situation of North Korea. The land-cover types included in the zoomed image range are forest, hillside field, unstocked forest, river, and farmland on flatland. However, for the MCD12Q1 the land-cover types in the zoomed-in image are only classified as mixed forest, deciduous broadleaf forest, and cropland, whereas

the results in this study mostly reflected the vegetative cover types in North Korea, although this may be because of the gap in spatial resolution. In this study we also used the MCD43A4 products, whose spatial resolution is 500 m, the same as MCD12Q1. Moreover, the land-cover types defined in MCD12Q1 cannot reflect the regional scale because it is for global land cover. Thus, the mapping and monitoring method proposed in this study can more effectively reflect the land-cover situation at a regional scale with fine spatial and temporal resolution.

4. Discussions

4.1 Mapping deforestation and degradation using key phenology-based indices

The key phenology-based indices and classification model proposed in this study were applied to classify the deforestation and degradation in 2001, 2010, and 2016 and with fine resolution in 2001 and 2014. This study demonstrated that the proposed phenology-based indices effectively mapped the deforestation in each year with low uncertainty.

However, large uncertainties occurred in mapping land cover for 2001. This is because the climate was different from 2013, when the RF classification model was developed. Because the field survey was completed during 2013 and 2014, the variables of the classification model for mapping deforestation and degradation were standard for 2013. The phenology-based indices of 2013, 2010, and 2016 have a small temporal interval, but a relatively large difference exists between 2001 and 2013.

The solution for improving the classification model is observing the phenology every year, and if the phenology for the target year is different from the variables of the established model, it is better to re-construct the classification model and search for the most contributing variables for the target year.

In North Korea, attempts to separate these cover types using traditional multispectral data or vegetation indices (Landsat, MODIS or NDVI in one-

time images) (Cha and Park 2007; Jeong et al. 2016b) have not been successful. The accuracies of each class indicated that phenology-based indices containing vegetation, soil, and water information, along with the use of RF, consistently increased the individual classification accuracies. Nevertheless, further research and field survey are needed to improve the technique for classifying vegetative cover types at high spatial resolution.

4.2 Compare RDSFM and FSDAF

To monitor rapid land surface dynamics with temporal change, spatiotemporal data-fusion methods have been developed to blend satellite images of different spatial and temporal resolutions. However, previous methods have had difficulties predicting pixel values in land-cover-change areas during the period between the input and prediction dates. To overcome this limitation, this study proposed a new spatiotemporal data-fusion method using residual distribution between fine and coarse images, termed RDSFM, to blend temporally sparse fine-resolution images with temporally dense coarse-resolution images. RDSFM integrates ideas from IR-MAD, which can detect the spectral changed pixels without supervision; the unmixing-based method; and HI, which was proposed in FSDAF and predicted in high accuracy in mixed coarse pixels, into one framework. All results demonstrate that RDSFM can achieve higher accuracy, and better predicted large-spectrum-change areas.

The spectral change of each pixel solved in RDSFM is more robust than that

of other methods because the strategy of weights is based on MAD. MAD addresses detection of nontrivial change in multiple bands and bi-temporal data based on a statistical technique. The data applied for the IR-MAD method are a fine-resolution image at t1 and a coarse-resolution image at t2, for detecting temporal changes. The fine-resolution image at t1 and coarse-resolution image at t1 also applied to IR-MAD for detecting the changes occurring from different sensors. One combines the MADs to calculate the weight based on MAD. Figure 35b and Figure 36b show the distribution of MAD variates of the red and NIR bands between input time and prediction time. One can see the distribution of change detection from the original Landsat image at t1 and t2 (Figure 35b and Figure 36b) are similar to the distribution of estimated MAD between t1 and t2. Through this, we can provide the different weights based on the weight of MAD and can solve the limitations due to the reflectance of each band pixel changing differently. In FSDAF, the weights for residual distribution are the same value for each band based on the degree of heterogeneous. However, not all of the reflectance of the bands is changing in the same range with temporal change. As seen in Figure 7, the reflectance of band 5 is decreasing while the reflectance of other bands is increasing. The weight based on MAD, proposed in this study, can solve this limitation, and can distribute the temporal change more realistically.

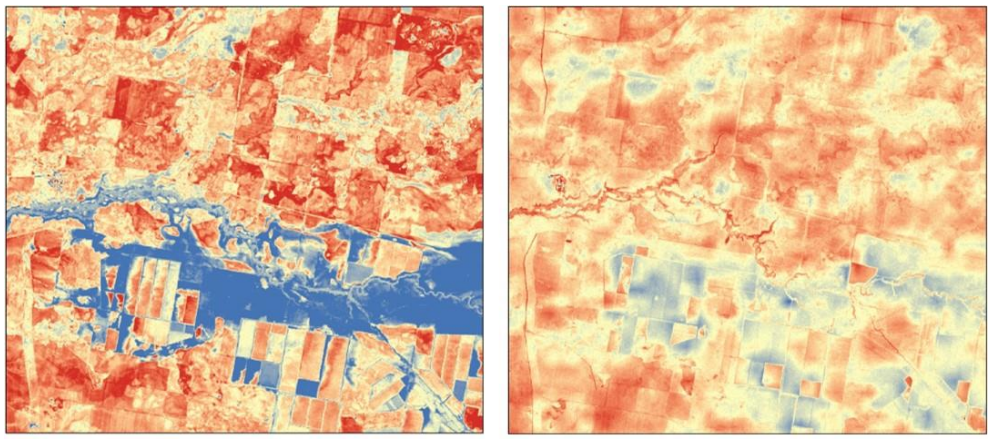

(a) (b)

Figure 35. Change detection of a land-cover-change site from original Landsat red band from November 26, 2004 to December 12, 2004(a), and the estimated MAD variate of the red band(b)

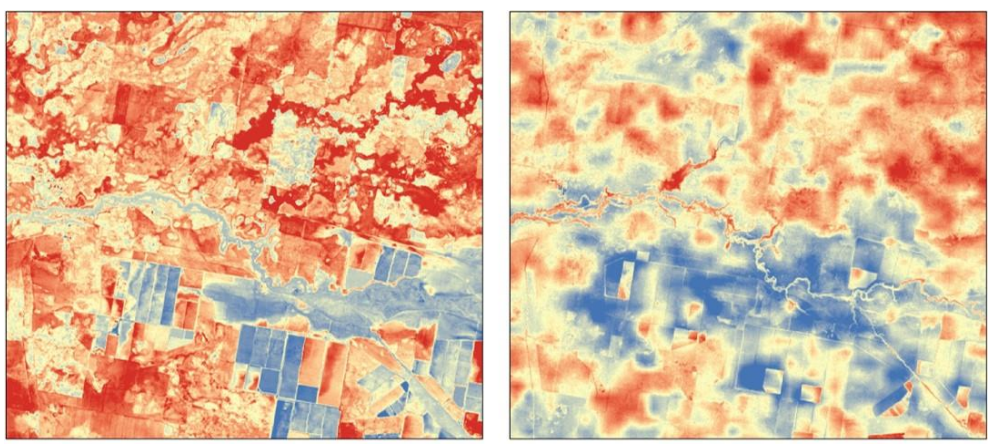

(a) (b)

Figure 36. Change detection of land-cover-change site from the original Landsat NIR band form November 26, 2004 to December 12, 2004 (a), and the estimated MAD variate of the NIR band (b).

Compared to the results of FSDAF, the quantitative indices of the red band or other bands show similar predicted results as seen in Table 9 and 10. The final results of RDSFM combine two changes in the distribution results distributed by the homogeneous index and the weight based on MAD. In

heterogeneous landscapes, if one pixel has little variation between t1 and t2, the final result has the possibility to be biased toward HI. On the contrary, if one pixel has a large variation between t1 and t2, the final result has a possibility of depending on the weight of MAD. Therefore, in some cases, some bands do not change much through temporal change, then the blending result depends on HI, and the final result will be similar to that of the FSDAF, which also uses an HI index for heterogeneous landscape prediction. The weights-based MAD is most effective in the NIR band, the band with a large difference in reflectance value depending on the season, and shows higher accuracy than FSDAF. This is because the MAD can detect temporal differences in each band, and can more accurately predict the pixels that have a spectral change.

Although RDSFM can predict both heterogeneous landscapes and spectral change between the input and prediction dates, it cannot capture miniscule changes in spectral change by land-cover change. For example, if only a few fine pixels underwent a land-cover-type change and the change is invisible in the interpolated coarse-resolution image. Moreover, because RDSFM is designed based on IR-MAD, some other products, such as NDVI and LST, do not directly apply. RDSFM requires a minimum of three bands for blending (Nielsen 2007; Wang et al. 2015).

4.3 Deforestation and degradation drivers in North Korea

Over the past 50 years, North Korea has experienced intensive forestry and agricultural development that has significantly reduced the area of natural forest. In the early 1990s, forest covered 68.7% of North Korea, which decreased to 51% by 2001, and to 47% by 2010. This study estimated that the remaining forest extent covers 40.5% of North Korea. Slowing of forest cover loss is partly the result of a greatly diminished resource base. A summary of the direct causes of forest cover change over the past 50 years in North Korea is provided in Table 14.

The direct drivers of forest cover loss over 50 years are agriculture and logging. The farming methods and post-management in North Korea have accelerating forest reduction. To cultivate forest to farmland, trees are cut down and burned in order to clear land. The cleared land is used until its productivity declines and then it is left without post-management, degrading the ground and leading to soil erosion. As a result, degradation has occurred and considerable forest is now denuded. Poor agriculture techniques and post-management are the main drivers of degradation up to the present.

Of the dominant drivers of forest cover loss, including agricultural extraction and logging, the underlying causes of forest cover loss in North Korea are related to policy and economic status (Schwekendiek 2010).

Considering the scale of the observed changes over the study period, it is clear that large-scale commercial logging and expending farmland in hilly

areas are the main drivers of North Korea forest loss. Because forest cultivation was a part of the government program to expand productive farmlands, many were poorly built in forest and poorly managed, resulting in forest degradation and low productivity (Kang and Choi 2013). Logging and forest cultivation continued and more seriously until 2000 because of serious financial difficulty. The forest loss rate reached 3.13%/year and more than 18% of the forest was deforested, and the damage caused by natural hazards began to increase. In 1995 and 1996, floods resulted in the displacement of 5.4 million people, destruction of 330,000 ha of agricultural land, and loss of 1.9 million tons of grain (Kang and Choi 2013; Noland et al. 2001). Such floods were caused by downpours with decades-long cycles, but the damage was exacerbated due to environmental degradation (Kang and Choi 2013; Kim and Ryu 2009; Myeong 2014). Efforts for forest restoration from 2000 through today have created a policy of forest restoration and a request for assistance to the international society. From 2000 to 2010, the rate of forest loss decreased to 0.88%, and 6.6% of the forest was restored. However, poor forest management technology and continuous natural hazards, such as floods and drought, resulted in a forest loss rate increase to 1.43% from 2010 to 2016. Isolation from the international community resulted in assistance and exchange of techniques of forest restoration stopping. Government efforts for improving techniques of forest management and forest restoration are material to maintaining the remaining forest.

Most of North Korea is mountainous land, and because it is within a

monsoon climatic zone, it is inevitably exposed to floods. Forest cover reduces natural damage by preventing soil erosion and storing water. However, the forest in North Korea cannot supply ecosystem services, due to serious damage. The restoration of forest ecosystems and the prevention of soil loss are the most important issues in North Korea. The results of this study are expected to contribute to planning for forest ecosystem restoration and management and establishment of a sustainable society.

Table 14. A summary of forest cover loss drivers in North Korea over 50 years (Engler et al. 2014; Kang and Choi 2013; Kim and Ryu 2009; Lee et al. 1999; Myeong 2014; Myeong et al. 2008; Noland et al. 2001; Park and Lee 2014; Schwekendiek 2010; VOA 2016/9/17; Zheng et al. 1997) .

Periods	Main drivers	Indirect drivers
Beyond our time frame for analysis		
- 1960	• Wood production based for est management • Indiscriminate forest cultiva tion • Slash and burn for farming	• Policy of encourage forest culti vation • Economic rehabilitation of war devastation
1960-1990	• Large-scale logging and for est cultivation • Slash and burn for farming • Large-scale natural hazard (flood and land slide)	• Population growth and increase d food consumption • A shortage of food and energy • Forest cultivation is formulated by Law of Land
During our time frame for analysis		
1990-2000	• Uncontrolled forest cultivat ion and logging • Vegetation roots for food • Large-scale natural hazard (flood and land slide)	• Financial difficulty from 1980s • Food and energy shortage got worsen • Socialist state collapse and inte rnational isolation • Trade between DPRK and othe r socialist states stopped
2000-2010	• Establishment of Forest Ma nagement Planning • Importing foreign vegetatio n species	• Policy for forest restoration • Request for assistance to intern ational society • Technique exchange
2010-present	• Natural hazard (flood and land slide) • Droughts	• Policy for forest restoration • Poor forest management technol ogy • Isolation from the international community due to nuclear deve lopment

V. Conclusions

In this study, a cost-effective method for classification and monitoring of forest-cover dynamics in high spatial and temporal resolution was proposed. Finally, the answers to the research questions are as follows.

1) What is the optimal combination of variables for effectively mapping confusing vegetative cover?

To classify types of deforested and degraded areas and to increase the accuracy of classification over previous studies, this study investigated a way to combine phenology-based index distinctions derived from the MODIS product and RF, as well as ways to distinguish complex, heterogeneous land cover in forests, such as hillside field and unstocked forest, from plateau vegetation and natural forest. The outcomes of this study extend beyond those of most previous studies, which have usually been focused only on dryland forest. Previous work also involved the use of single-image classifications based only on spectral data to distinguish types of deforestation, and consequently had difficulty capturing the heterogeneous spectral signature of land-cover categories over large areas.

The outcomes of this study can be summarized as follows. First, the seasonal patterns indicated by the three indices (NDVI, NDSI, and NDWI) showed differences typical of each type of vegetative cover in forest land; thus, it was possible to overcome the reflectance value confusion that occurs when using only one image, and to increase the classification accuracy.

Second, to classify complex land cover and dynamics, RF proved to be a useful tool for classifying a variety of input features. The results highlighted the types of deforested land and their distribution in North Korea. That classification result showed an overall accuracy of 89.38% when phenology-based multi-indices were combined with RF. Third, the phenology-based indices highly contributing to classification, over 20%, are NDSI during the growing season (from March to May), NDVI at the end of the season (September), and NDWI at the start and end of the season (March to April and October). The combination of these variables is effective for classifying or monitoring vegetative cover. Our method greatly improved the classification accuracies for classification of heterogeneous vegetative cover and presented deforested areas more reliably. Therefore, it should be useful in continuing to monitor variation in forest areas during forest restoration efforts in North Korea. The ecological impacts of forest degradation in the study area should also be urgently considered.

2) How can one improve spatiotemporal data-fusion accuracy in land cover that changes by season?

To construct continuous satellite data in fine resolution, using the most accessible datasets, a spatiotemporal data-fusion method was developed to blend satellite images in heterogeneous and spectrum-changed areas. However, previous methods have difficulties in predicting spectrum-changed pixels in fine resolution, where each band value changes in a different range during the period between the input and prediction dates.

To overcome this limitation, this study proposed RDSFM to blend temporally fine-resolution data with temporally dense coarse-resolution data. RDSFM integrates ideas from unmixing-based methods and the homogeneous index in FSDAF, IR-MAD, and the weighted function-based method into one framework. RDSFM was tested on a real landscape and compared to the referred to spatiotemporal method, FSDAF and UBFM (unmixing-based data-fusion method). The results of the accuracy assessment demonstrate that RDSFM has higher accuracy, especially in fragmented areas and in the NIR band, and maintains more spatial details.

The spectral change of each pixel solved in RDSFM is more robust than that of the other methods because the strategy of weights is based on MAD. MAD addresses detection of nontrivial change in multiple bands and bi-temporal data based on canonical correlation analysis. To estimate the MAD-based weights, the MAD for detecting the temporal change used a fine-resolution image at t1 and a coarse-resolution image at t2. This can effectively detect the relative alteration of each band in one coarse pixel. This method can help predict the pixel value well in the areas of spectrum-changed land cover or within-class variance. RDSFM, similar to other spatiotemporal data-fusion methods, can be applied to analyze land-cover dynamics, monitor vegetation phenology, and detect land-cover change and degradation occurrence.

3) What is the extent of degraded forest and deforestation in North Korea? How have degradation rates changed from 1990 to 2016, and what are the drivers?

The area of forest during the 1990s was 84,385 km^2. By 2001, the forest area had decreased to 62,606 km^2, while the area of hillside field and unstocked forest was 17,729 km^2 and 19,595 km^2, respectively. By 2010, the area of forest was 57,669 km^2, and hillside field and unstocked forest had increased to 28,214 km^2 and 13,886 km^2 respectively. By 2016, the remaining forest was 49,713 km^2, and the hillside field and unstocked forest was 41,634 km^2 and 9,749 km^2, respectively.

Of the dominant drivers of forest cover loss, including agricultural extraction and logging, the underlying causes of forest cover loss in North Korea are related to policy and economic status (Schwekendiek 2010).

Because forest cultivation was a part of a government program to expand productive farmlands, many were poorly built in forest and poorly managed, resulting in forest degradation and low productivity (Kang and Choi 2013). Logging and forest cultivation continued and more seriously until 2000 because of more serious financial difficulty. The forest loss rate reached 3.04%/year and more than 18% of the forest was deforested, and damage caused by naturals hazard began to increase. Efforts in forest restoration began in 2000 through policies for forest restoration and a request for assistance to the international community. From 2000 to 2010, the rate of forest loss decreased to 0.77%, and 6.6% of the forest was restored. However, poor forest management technology and continuous natural hazards, such as floods and droughts, resulted in the forest loss rate increasing to 1.53% from the 2010 to 2016. Isolation from the international community stopped

assistance and exchange of techniques of forest restoration. Government efforts for improving techniques of forest management and forest restoration are material to maintaining the remaining forest.

4) Are the proposed methods effective in detecting deforestation and degradation?

Using stacked phenology-based multi-variables with RDSFM is a powerful means of reducing classification errors, and enables better characterization of complex land-cover change status at 30-m resolution. The classification result showed an overall accuracy of 86.1% when using the simple unsupervised classifier. It is clearly effective and convenient to perform annual land-cover change analysis and to produce a transition matrix with no information.

Comparing the quality of the mapping deforestation and degradation result to that of the MCD12Q1 yearly land cover and GE above, it was demonstrated that the land cover result derived using the proposed method is closer to reality. The land-cover types included in the zoomed image range are forest, hillside field, unstocked forest, river, and farmland on flatland. Although this may be because of the difference in spatial resolution, in this study we also used the MCD43A4 products, at a spatial resolution of 500m, which is the same as the MODIS land-cover products. Moreover, the land-cover types defined in global land-cover products, such as MCD12Q1, do not reflect at a regional scale because it is for global land cover. Thus, the mapping and monitoring method proposed in this study can more effectively reflect the land-cover situation at a regional scale with fine spatial and temporal resolution.

The mapping and monitoring methods proposed in this study can apply to several fields, especially in optimized forest management and planning, which satisfy several objectives (such as agriculture, extreme climatic events, adaption and biodiversity, etc.). A land-cover map specifying the deforestation and degradation areas is fundamental data for prioritized restoration. It is important to conduct continuous forest inventories reflecting regional characteristics, such as deforestation and degradation in North Korea. This study is expected to contribute to effective forest management and in developing a sustainable environment in North Korea.

BIBLIOGRAPHY

Abood, S.A., Lee, J.S.H., Burivalova, Z., Garcia-Ulloa, J., & Koh, L.P. (2015). Relative Contributions of the Logging, Fiber, Oil Palm, and Mining Industries to Forest Loss in Indonesia. *Conservation Letters, 8*, 58-67

Adam, E., Mutanga, O., Odindi, J., & Abdel-Rahman, E.M. (2014). Land-use/cover classification in a heterogeneous coastal landscape using RapidEye imagery: evaluating the performance of random forest and support vector machines classifiers. *International Journal of Remote Sensing, 35*, 3440-3458

Akçakaya, H.R., Alberti, M., Baxter, C.K., Beck, J.L., Beissinger, S.R., Bekessy, S., Brook, B.W., Ceder, K., Chisholm, R., Comnick, J.M., Cushman, S.A., Dettmers, R., Dickson, B.G., Dijak, W.D., Donovan, M.L., Early, R.J., Estey, M.E., Fitzgerald, J., Flather, C.H., Gitzen, R.A., Gobster, P.H., Gordon, A., Granfors, D.A., Gustafson, E.J., Haight, R.G., Haufler, J.B., He, H.S., Hepinstall, J.A., Herter, D.R., Hicks, L.L., Johnson, R.R., Jones, T., Kernohan, B.J., Larsen, D.R., Larson, M.A., Linden, D.W., Marzluff, J.M., McCarter, J.B., McKelvey, K.S., McKenzie, D., Millspaugh, J.J., Nelson, C.S., Nicholson, E., Niemuth, N.D., Noon, B.R., Oliver, C.D., Pearce, J., Possingham, H.P., Probst, J.R., Raymond, C.L., Reynolds, R.E., Rittenhouse, C.D., Roloff, G.J., Rowland, M.M., Rustay, C., Ruth, J.M., Shifley, S.R., Shriner, S.A., Stabins, H.C., Strong, M.L., Suring, L.H., Thogmartin, W.E., Thompson, F.R., Venier, L., Vogel, W.O., Wangler, B., Will, T.C., Wilson, K.R., Wintle, B., & Wisdom, M.J. (2009). List of Contributors, xv-xx

Armenteras, D., Espelta, J.M., Rodríguez, N., & Retana, J. (2017). Deforestation dynamics and drivers in different forest types in Latin America: Three decades of studies (1980–2010). *Global Environmental Change, 46*, 139-147

Asner, G.P., Knapp, D.E., Broadbent, E.N., Oliveira, P.J.C., Keller, M., & Silva, J.N. (2005). Selective Logging in the Brazilian Amazon. *Science, 310*, 480-482

Baccini, A., Goetz, S.J., Walker, W.S., Laporte, N.T., Sun, M., Sulla-Menashe, D., Hackler, J., Beck, P.S.A., Dubayah, R., Friedl, M.A., Samanta, S., & Houghton, R.A. (2012). Estimated carbon dioxide emissions from tropical deforestation improved by carbon-density maps. *Nature Clim. Change, 2*, 182-185

Baeza, M.J., Valdecantos, A., Alloza, J.A., & Vallejo, V.R. (2007). Human disturbance and environmental factors as drivers of long-term post-fire regeneration patterns in Mediterranean forests. *Journal of Vegetation*

Science, 18, 243-252

Bartholomé, E., & Belward, A.S. (2005). GLC2000: a new approach to global land cover mapping from Earth observation data. *International Journal of Remote Sensing, 26*, 1959-1977

Bhatia, R., & Thorne-Lyman, A.L. (2002). Food shortages and nutrition in North Korea. *The Lancet, 360*, s27-s28

Boo, K., Kim, U., Kim, J., Kim, C., Soo, I., Park, G., Park, G., Park, S., Sohn, H., Yu, B., Lee, K., Lee, S., Im, S., & Choi, J. (2001). *Agriculture in North Korea: the real state and development direction*. (1st ed.). Seoul, South Korea: SNU Press

Breiman, L. (2001). Random Forests. *Machine Learning, 45*, 5-32

Buma, B., & Wessman, C.A. (2011). Disturbance interactions can impact resilience mechanisms of forests. *Ecosphere, 2*, art64

Carleer, A., & Wolff, E. (2004). Exploitation of Very High Resolution Satellite Data for Tree Species Identification. *Photogrammetric Engineering and Remote Sensing, 70(1)*, 135-140

Ceccato, P., Flasse, S., Tarantola, S., Jacquemoud, S., & Grégoire, J.-M. (2001). Detecting vegetation leaf water content using reflectance in the optical domain. *Remote Sensing of Environment, 77*, 22-33

Cha, S., & Park, C.H. (2007). The Utilization of Google Earth Images as Reference Data for The Multitemporal Land Cover Classification with MODIS Data of North Korea. *Korean Journal of Remote Sensing, 23(5)*, 483~491

Cha, S., Seo, D., & Park, C. (2009). Monitoring Vegetation Phenology Using MODIS in Northern Plateau Region, North Korea. *Korean Journal of Remote Sensing, 25(5)*, 399-409

Chazdon, R.L. (2008). Beyond Deforestation: Restoring Forests and Ecosystem Services on Degraded Lands. *Science, 320(5882)*, 1458-1460

Clark, M.L., Aide, T.M., Grau, H.R., & Riner, G. (2010). A scalable approach to mapping annual land cover at 250 m using MODIS time series data: A case study in the Dry Chaco ecoregion of South America. *Remote Sensing of Environment, 114*, 2816-2832

Clerici, N., Weissteiner, C.J., & Gerard, F. (2012). Exploring the Use of MODIS NDVI-Based Phenology Indicators for Classifying Forest General Habitat Categories. *Remote Sensing, 4*, 1781-1803

Congalton, R.G., & Green, K. (2009). *Assessing the Accuracy of Remotely Sensed Data: Principles and Practices*. (2nd edition ed.). Boca Raton CRC Press

de Jong, R., de Bruin, S., de Wit, A., Schaepman, M.E., & Dent, D.L. (2011). Analysis of monotonic greening and browning trends from global NDVI time-series. *Remote Sensing of Environment, 115*, 692-702

Demir, B., Bovolo, F., & Bruzzone, L. (2013). Updating Land-Cover Maps by

Classification of Image Time Series: A Novel Change-Detection-Driven Transfer Learning Approach. *IEEE Transactions on Geoscience and Remote Sensing, 51*, 300-312

Deng, Y., Wu, C., Li, M., & Chen, R. (2015). RNDSI: A ratio normalized difference soil index for remote sensing of urban/suburban environments. *International Journal of Applied Earth Observation and Geoinformation, 39*, 40-48

Duro, D.C., Franklin, S.E., & Dubé, M.G. (2012). A comparison of pixel-based and object-based image analysis with selected machine learning algorithms for the classification of agricultural landscapes using SPOT-5 HRG imagery. *Remote Sensing of Environment, 118*, 259-272

Dymond, C.C., Mladenoff, D.J., & Radeloff, V.C. (2002). Phenological differences in Tasseled Cap indices improve deciduous forest classification. *Remote Sensing of Environment, 80*, 460-472

EI_Rahman, S.A. (2016). Hyperspectral Image Classification Using Unsupervised Algorithms. *International Journal of Advanced Computer Science and Application, 7(4)*, 198-205

Eisavi, V., Homayouni, S., Yazdi, A.M., & Alimohammadi, A. (2015). Land cover mapping based on random forest classification of multitemporal spectral and thermal images. *Environ Monit Assess, 187*, 291

Eklundh, L., & Jönsson, P. (2015). TIMESAT 3.2 Software Manual. *Lund and Malmö University, Sweden*

Emelyanova, I.V., McVicar, T.R., Van Niel, T.G., Li, L.T., & van Dijk, A.I.J.M. (2013). Assessing the accuracy of blending Landsat–MODIS surface reflectances in two landscapes with contrasting spatial and temporal dynamics: A framework for algorithm selection. *Remote Sensing of Environment, 133*, 193-209

Engler, R., Teplyakov, V., & Adams, J.M. (2014). An assessment of forest cover trends in South and North Korea, from 1980 to 2010. *Environmental Management, 53*, 194-201

FAO (2010). Global Forest Resources Assessment 2010: THE DEMOCRATIC PEOPLE'S REPUBLIC OF KOREA. In, *COUNTRY REPORT*. Rome

Fensholt, R., & Proud, S.R. (2012). Evaluation of Earth Observation based global long term vegetation trends — Comparing GIMMS and MODIS global NDVI time series. *Remote Sensing of Environment, 119*, 131-147

Fensholt, R., & Rasmussen, K. (2011). Analysis of trends in the Sahelian 'rain-use efficiency' using GIMMS NDVI, RFE and GPCP rainfall data. *Remote Sensing of Environment, 115*, 438-451

Fensholt, R., Rasmussen, K., Nielsen, T.T., & Mbow, C. (2009). Evaluation of earth observation based long term vegetation trends — Intercomparing NDVI

time series trend analysis consistency of Sahel from AVHRR GIMMS, Terra MODIS and SPOT VGT data. *Remote Sensing of Environment, 113*, 1886-1898

Fensholt, R., & Sandholt, I. (2003). Derivation of a shortwave infrared water stress index from MODIS near- and shortwave infrared data in a semiarid environment. *Remote Sensing of Environment, 87*, 111-121

Franklin, S.E., Connery, D.R., & Williams, J.A. (1994). Classification of alpine vegetation using Landsat Thematic Mapper SPOT HRV and DEM data. *Canadian Journal of Remote Sensing/Journal Canadien de Te´le´tection, 20*, 49-58

Fraser, R.H., & Li, Z. (2002). Estimating fire-related parameters in boreal forest using SPOT VEGETATION. *Remote Sensing of Environment, 82*, 95-110

Friedl, M.A., Mclver, D.K., Hodges, J.C.F., Zhang, X.Y., Muchoney, D., Strahler, A.H., Woodcock, C.E., Gopal, S., Cooper, A., Baccini, A., Gao, F., & Schaaf, C. (2002). Global land cover mapping from MODIS: algorithms and early results. *Remote Sensing of Environment, 83*, 287-302

Fu, D., Chen, B., Wang, J., Zhu, X., & Hilker, T. (2013). An Improved Image Fusion Approach Based on Enhanced Spatial and Temporal the Adaptive Reflectance Fusion Model. *Remote Sensing, 5*, 6346-6360

Funk, C., & Budde, M.E. (2009). Phenologically-tuned MODIS NDVI-based production anomaly estimates for Zimbabwe. *Remote Sensing of Environment, 113*, 115-125

Gómez, C., White, J.C., & Wulder, M.A. (2016). Optical remotely sensed time series data for land cover classification: A review. *ISPRS Journal of Photogrammetry and Remote Sensing, 116*, 55-72

Gao, B.-c. (1996). NDWI—A normalized difference water index for remote sensing of vegetation liquid water from space. *Remote Sensing of Environment, 58*, 257-266

Gao, F., Masek, J., Schwaller, M., & Hall, F. (2006). On the blending of the Landsat and MODIS surface reflectance: predicting daily Landsat surface reflectance. *IEEE Transactions on Geoscience and Remote Sensing, 44*, 2207-2218

Gartzia, M., Alados, C.L., Pérez-Cabello, F., & Bueno, C.G. (2013). Improving the Accuracy of Vegetation Classifications in Mountainous Areas. *Mountain Research and Development, 33*, 63-74

Gevaert, C.M., & García-Haro, F.J. (2015). A comparison of STARFM and an unmixing-based algorithm for Landsat and MODIS data fusion. *Remote Sensing of Environment, 156*, 34-44

Grimm, R., Behrens, T., Märker, M., & Elsenbeer, H. (2008). Soil organic carbon concentrations and stocks on Barro Colorado Island — Digital soil

mapping using Random Forests analysis. *Geoderma, 146*, 102-113

Grinand, C., Rakotomalala, F., Gond, V., Vaudry, R., Bernoux, M., & Vieilledent, G. (2013). Estimating deforestation in tropical humid and dry forests in Madagascar from 2000 to 2010 using multi-date Landsat satellite images and the random forests classifier. *Remote Sensing of Environment, 139*, 68-80

Gutman, G.G. (1991). Monitoring Land Ecosystems Using the Noaa Global Vegetation Index Data Set. *Global and Planetary Change, 90*, 195-200

Hilker, T., Wulder, M.A., Coops, N.C., Linke, J., McDermid, G., Masek, J.G., Gao, F., & White, J.C. (2009). A new data fusion model for high spatial- and temporal-resolution mapping of forest disturbance based on Landsat and MODIS. *Remote Sensing of Environment, 113*, 1613-1627

Hill, R.A., Wilson, A.K., George, M., & Hinsley, S.A. (2010). Mapping tree species in temperate deciduous woodland using time-series multi-spectral data. *Applied Vegetation Science, 13*, 86-99

Holben, B.N. (1986). Characteristics of Maximum-Value Composite Images from Temporal Avhrr Data. *International Journal of Remote Sensing, 7*, 1417-1434

Hosonuma, N., Herold, M., De Sy, V., De Fries, R.S., Brockhaus, M., Verchot, L., Angelsen, A., & Romijn, E. (2012). An assessment of deforestation and forest degradation drivers in developing countries. *Environmental Research Letters, 7*, 044009

Hu, Q., Wu, W., Xia, T., Yu, Q., Yang, P., Li, Z., & Song, Q. (2013). Exploring the Use of Google Earth Imagery and Object-Based Methods in Land Use/Cover Mapping. *Remote Sensing, 5*, 6026-6042

Huang, B., & Zhang, H. (2014). Spatio-temporal reflectance fusion via unmixing: accounting for both phenological and land-cover changes. *International Journal of Remote Sensing, 35*, 6213-6233

Huete, A., Didan, K., Miura, T., Rodriguez, E.P., Gao, X., & Ferreira, L.G. (2002). Overview of the radiometric and biophysical performance of the MODIS vegetation indices. *Remote Sensing of Environment, 83*, 195-213

Immitzer, M., Atzberger, C., & Koukal, T. (2012). Tree Species Classification with Random Forest Using Very High Spatial Resolution 8-Band WorldView-2 Satellite Data. *Remote Sensing, 4*, 2661-2693

Jönsson, P., & Eklundh, L. (2004). TIMESAT—a program for analyzing time-series of satellite sensor data. *Computers & Geosciences, 30*, 833-845

Jacques, D.C., Kergoat, L., Hiernaux, P., Mougin, E., & Defourny, P. (2014). Monitoring dry vegetation masses in semi-arid areas with MODIS SWIR bands. *Remote Sensing of Environment, 153*, 40-49

Jensen, J.R. (2005). *Introductory Digital Image Processing: A Remote Sensing*

Perspective. Prentice Hall

Jensen, J.R., & Cowen, D.C. (1997). *Remote Sensing of Urban/Suburban Socio-economic Attributes. Proceedings Land Satellite Information in the Next Decade II*. Bethesda, Maryland: American Society for Photogrammetry & Remote Sensing

Jeong, S.G., Mo, Y., Kim, H.G., Park, C.H., & Lee, D.K. (2016a). Mapping riparian habitat using a combination ofremote-sensing techniques. *International Journal of Remote Sensing, 37*, 1069-1088

Jeong, S.G., Park, C.H., & Kim, S.W. (2006). Land cover classification of the Korean Peninsula Using Linear Spectral Mixture Analysis of MODIS Multi-temporal Data. *Korean Journal of Remote Sensing, 22(6)*, 553-563

Jeong, S.G., Park, J., Park, C.H., & Lee, D.K. (2016b). Terrace Fields Classification in North Korea Using MODIS Multi-temporal Image Data. *Journal of the Korea Society of Environmental Restoration Technology, 19*, 73-83

Jiang, Y., Wang, T., de Bie, C.A.J.M., Skidmore, A.K., Liu, X., Song, S., Zhang, L., Wang, J., & Shao, X. (2014). Satellite-derived vegetation indices contribute significantly to the prediction of epiphyllous liverworts. *Ecological Indicators, 38*, 72-80

Jin, H., & Eklundh, L. (2014). A physically based vegetation index for improved monitoring of plant phenology. *Remote Sensing of Environment, 152*, 512-525

Jonsson, P., & Eklundh, L. (2002). Seasonality extraction by function fitting to time-series of satellite sensor data. *Ieee Transactions on Geoscience and Remote Sensing, 40*, 1824-1832

Joshi, C., Leeuw, J.D., Skidmore, A.K., Duren, I.C.v., & van Oosten, H. (2006). Remotely sensed estimation of forest canopy density: A comparison of the performance of four methods. *International Journal of Applied Earth Observation and Geoinformation, 8*, 84-95

Jucker Riva, M., Daliakopoulos, I.N., Eckert, S., Hodel, E., & Liniger, H. (2017). Assessment of land degradation in Mediterranean forests and grazing lands using a landscape unit approach and the normalized difference vegetation index. *Applied Geography, 86*, 8-21

Jung, h. (2015). Construction and Unitilization of Environmental Information in Inaccessible Terrain: Focused on Construction of Land Cover Map. In, *Research Report 2015-10*: Korea Environment Institute

Kalensky, Z., & Scherk, R.R. (1975). Accuracy of forest mapping from Landsat computer compatible tapes. In, *Proceedings of the 10th international Symposium on Remote Sensing of Environment* (pp. 1159-1167). Ann Arbor, Michigan

Kang, S., & Choi, W. (2013). Forest cover changes in North Korea since the 1980s.

Regional Environmental Change, 14, 347-354

Ke, Y., Quackenbush, L.J., & Im, J. (2010). Synergistic use of QuickBird multispectral imagery and LIDAR data for object-based forest species classification. *Remote Sensing of Environment, 114*, 1141-1154

Kim, E.S., Lee, S.H., & Cho, H.K. (2010). Segment-based Land Cover Classification using Texture Information in Degraded Forest Land of North Korea. *Korean Journal of Remote Sensing, 26(5)*, 477~487

Kim, J., & Ryu, M. (2009). Analysis of weather forecast and relevant technologies to deal with natural disaster in North Korea. *North Korean Stud Rev, 13(2)*, 97-122

Kiptala, J.K., Mohamed, Y., Mul, M.L., Cheema, M.J.M., & Van der Zaag, P. (2013). Land use and land cover classification using phenological variability from MODIS vegetation in the Upper Pangani River Basin, Eastern Africa. *Physics and Chemistry of the Earth, Parts A/B/C, 66*, 112-122

Kosmas, C., Detsis, V., Karamesouti, M., Kounalaki, K., Vassiliou, P., & Salvati, L. (2015). Exploring Long-Term Impact of Grazing Management on Land Degradation in the Socio-Ecological System of Asteroussia Mountains, Greece. *Land, 4*, 541

Kumar, R., & Jyoti Das, A. (2014). Climate Change and its Impact on Land Degradation: Imperative Need to Focus. *Journal of Climatology & Weather Forecasting, 2*

LCLUC. Deforestation in North Korea. In

Lee, D.K., Oh, Y.C., & Kim, J.U. (2007). A study on forest changes for A/R CDM in North Korea. *J. Korean Env. Res. & Reveg. Tech., 10(2)*, 97~104

Lee, K., Joung, M., & Yoon, J. (1999). Content and characteristics of forest cover change in North Korea. *Jour. Korean For. Soc., 88(3)*, 352-363

Lee, M., Kim, N., Lee, G., & Han, U. (2005). A study on the surface erosion by the development of cropland on the hillslope in the west coast area of North Korea using Quick Bird satellite images. *J Korean Assoc Reg Geogr, 11(4)*, 453-462

Li, C., Wang, J., Wang, L., Hu, L., & Gong, P. (2014). Comparison of Classification Algorithms and Training Sample Sizes in Urban Land Classification with Landsat Thematic Mapper Imagery. *Remote Sensing, 6*, 964-983

Liaw, A., & Winener, M. (2002). Classificatn and regression by randomForest. *R News, 2/3*, 18-22

Liu, L., Liang, L., Schwartz, M.D., Donnelly, A., Wang, Z., Schaaf, C.B., & Liu, L. (2015). Evaluating the potential of MODIS satellite data to track temporal dynamics of autumn phenology in a temperate mixed forest. *Remote Sensing of Environment, 160*, 156-165

Lloyd, D. (1990). A Phenological Classification of Terrestrial Vegetation Cover

Using Shortwave Vegetation Index Imagery. *International Journal of Remote Sensing, 11*, 2269-2279

Lu, D., & Weng, Q. (2007). A survey of image classification methods and techniques for improving classification performance. *International Journal of Remote Sensing, 28*, 823-870

MA (2005). Ecosystems and human well-being: Scenarios. In. Washington, D.C.

Margono, B.A., Turubanova, S., Zhuravleva, I., Potapov, P., Tyukavina, A., Baccini, A., Goetz, S., & Hansen, M.C. (2012). Mapping and monitoring deforestation and forest degradation in Sumatra (Indonesia) using Landsat time series data sets from 1990 to 2010. *Environmental Research Letters, 7*, 034010

Martin, M.E., Newman, S.D., Aber, J.D., & Congalton, R.G. (1998). Determining Forest Species Composition Using High Spectral Resolution Remote Sensing Data. *Remote Sensing of Environment, 65*, 249-254

Matricardi, E.A.T., Skole, D.L., Cochrane, M.A., Pedlowski, M., & Chomentowski, W. (2007). Multi-temporal assessment of selective logging in the Brazilian Amazon using Landsat data. *International Journal of Remote Sensing, 28*, 63-82

Miettinen, J., Stibig, H.-J., & Achard, F. (2014). Remote sensing of forest degradation in Southeast Asia—Aiming for a regional view through 5–30 m satellite data. *Global Ecology and Conservation, 2*, 24-36

Mon, M.S., Mizoue, N., Htun, N.Z., Kajisa, T., & Yoshida, S. (2012). Factors affecting deforestation and forest degradation in selectively logged production forest: A case study in Myanmar. *Forest Ecology and Management, 267*, 190-198

Morris, R.J. (2010). Anthropogenic impacts on tropical forest biodiversity: a network structure and ecosystem functioning perspective. *Philos Trans R Soc Lond B Biol Sci, 365*, 3709-3718

Myeong, S. (2014). Flood Vulnerability and Deforestation: a case study of North Korea. In: Korea Environment Institute

Myeong, S., Hong, H., Choi, H., & Jung, J. (2008). Estimation of flood vulnerable areas in North Korea and collabration strategies between South Korea and North Korea. In, *KEI-2008-RE-16*: Korea Environment Institute

Nielsen, A.A. (2007). The Regularized Iteratively Reweighted MAD Method for Change Detection in Multi- and Hyperspectral Data. *IEEE Transactions on Image Processing, 16*, 463-478

Noland, M., Robinson, S., & Wang, T. (2001). Famine in North Korea: Causes and Cures. *Econ Dev Cul Chang, 49*, 741-767

Pal, M. (2005). Random forest classifier for remote sensing classification. *International Journal of Remote Sensing, 26*, 217-222

Pan, X.-Z., Uchida, S., Liang, Y., Hirano, A., & Sun, B. (2010). Discriminating different landuse types by using multitemporal NDXI in a rice planting area. *International Journal of Remote Sensing, 31*, 585-596

Panta, M., Kim, K., & Joshi, C. (2008). Temporal mapping of deforestation and forest degradation in Nepal: Applications to forest conservation. *Forest Ecology and Management, 256*, 1587-1595

Park, M., & Lee, H. (2014). Forest Policy and Law for Sustainability within the Korean Peninsula. *Sustainability, 6*, 5162-5186

Prince, S.D., & Goward, S.N. (1995). Global Primary Production: A Remote Sensing Approach. *Journal of Biogeography, 22*, 815-835

Puyravaud, J.-P. (2003). Standardizing the calculation of the annual rate of deforestation. *Forest Ecology and Management, 177*, 593-596

Reed, B.C., Brown, J.F., Vanderzee, D., Loveland, T.R., Merchant, J.W., & Ohlen, D.O. (1994). Measuring Phenological Variability from Satellite Imagery. *Journal of Vegetation Science, 5*, 703-714

Renó, V.F., Novo, E.M.L.M., Suemitsu, C., Rennó, C.D., & Silva, T.S.F. (2011). Assessment of deforestation in the Lower Amazon floodplain using historical Landsat MSS/TM imagery. *Remote Sensing of Environment, 115*, 3446-3456

Richard, Y., & Poccard, I. (1998). A statistical study of NDVI sensitivity to seasonal and interannual rainfall variations in Southern Africa. *International Journal of Remote Sensing, 19*, 2907-2920

Richardson, A.D., & O'Keefe, J. (2009). Phenological Differences Between Understory and Overstory, 87-117

Rishmawi, K., & Prince, S. (2016). Environmental and Anthropogenic Degradation of Vegetation in the Sahel from 1982 to 2006. *Remote Sensing, 8*, 948

Rodriguez-Galiano, V.F., Ghimire, B., Rogan, J., Chica-Olmo, M., & Rigol-Sanchez, J.P. (2012). An assessment of the effectiveness of a random forest classifier for land-cover classification. *ISPRS Journal of Photogrammetry and Remote Sensing, 67*, 93-104

Sasaki, N., & Putz, F.E. (2009). Critical need for new definitions of "forest" and "forest degradation" in global climate change agreements. *Conservation Letters, 2*, 226-232

Schoene, D., Killmann, W., Lüpke, H.v., & LoycheWilkie, M. (2007). Definitional issues related to reducing emissions from deforestation in developing countries In, *Forest and Climate Change Working Paper5*. Rome

Schwekendiek, D. (2010). Regional variations in living conditions during the North Korean food crisis of the 1990s. *Asia Pac J Public Health, 22*, 460-476

Sellers, P.J., Tucker, C.J., Collatz, G.J., Los, S.O., Justice, C.O., Dazlich, D.A., & Randall, D.A. (1995). A Global 1-Degrees by 1-Degrees Ndvi Data Set

for Climate Studies .2. The Generation of Global Fields of Terrestrial Biophysical Parameters from the Ndvi (Vol 15, Pg 3519, 1995). *International Journal of Remote Sensing, 16*, 1571-1571

Senf, C., Hostert, P., & van der Linden, S. (2012). Using MODIS time series and random forests classification for mapping land use in South-East Asia, 6733-6736

Senf, C., Pflugmacher, D., van der Linden, S., & Hostert, P. (2013). Mapping Rubber Plantations and Natural Forests in Xishuangbanna (Southwest China) Using Multi-Spectral Phenological Metrics from MODIS Time Series. *Remote Sensing, 5*, 2795-2812

Setiawan, Y., Kustiyo, K., & Darmawan, A. (2016). A simple method for developing near real-time nationwide forest monitoring for Indonesia using MODIS near- and shortwave infrared bands. *Remote Sensing Letters, 7*, 318-327

Shen, M., Tang, Y., Chen, J., Zhu, X., & Zheng, Y. (2011). Influences of temperature and precipitation before the growing season on spring phenology in grasslands of the central and eastern Qinghai-Tibetan Plateau. *Agricultural and Forest Meteorology, 151*, 1711-1722

Simonetti, E., Simonetti, D., & Preatoni, D. (2014). Phenology-based land cover classification using Landsat 8 time series. In, *JRC Technical Reports*: European Commission

Song, H., & Huang, B. (2013). Spatiotemporal Satellite Image Fusion Through One-Pair Image Learning. *IEEE Transactions on Geoscience and Remote Sensing, 51(4)*, 1883-1896

Souza, J.C., Siqueira, J., Sales, M., Fonseca, A., Ribeiro, J., Numata, I., Cochrane, M., Barber, C., Roberts, D., & Barlow, J. (2013). Ten-Year Landsat Classification of Deforestation and Forest Degradation in the Brazilian Amazon. *Remote Sensing, 5*, 5493-5513

Takeuchi, W., & Yasuoka, Y. (2004). Development of normalized Vegetation, soil and water indices derived from satellite remote sensing data. *Journal of the Japan society of photogrammetry and remote sensing, 43(6)*, 7-19

Tang, L., Shao, G., Piao, Z., Dai, L., Jenkins, M.A., Wang, S., Wu, G., Wu, J., & Zhao, J. (2010). Forest degradation deepens around and within protected areas in East Asia. *Biological Conservation, 143*, 1295-1298

Team, R.D.C. (2009). *R: A language and envirionment for statistical computing*. Vienna, Austria: R Foundation for Statistical Computing

Thompson, I.D., Guariguata, M.R., Okabe, K., Bahamondez, C., Nasi, R., Heymell, V., & Sabogal, C. (2013). An Operational Framework for Defining and Monitoring Forest Degradation. *Ecology and Society, 18(2)*, 20

Tuanmu, M.-N., Viña, A., Bearer, S., Xu, W., Ouyang, Z., Zhang, H., & Liu, J. (2010). Mapping understory vegetation using phenological characteristics derived

from remotely sensed data. *Remote Sensing of Environment, 114*, 1833-1844

Tucker, C.J. (1980). Remote sensing of leaf water content in the near infrared. *Remote Sensing of Environment, 10*, 23-32

Viovy, N., Arino, O., & Belward, A.S. (1992). The Best Index Slope Extraction (Bise) - a Method for Reducing Noise in Ndvi Time-Series. *International Journal of Remote Sensing, 13*, 1585-1590

VOA, V.O.A. (2016/9/17). 「유엔 실사팀"북한 홍수피해 50~60년만에 최악, 당국 종합대책 시급"」. In

Wang, B., Choi, S.-K., Han, Y.-K., Lee, S.-K., & Choi, J.-W. (2015). Application of IR-MAD using synthetically fused images for change detection in hyperspectral data. *Remote Sensing Letters, 6*, 578-586

Wang, C., Qi, J., & Cochrane, M. (2005a). Assessment of Tropical Forest Degradation with Canopy Fractional Cover from Landsat ETM+ and IKONOS Imagery. *Earth Interactions, 9(22)*, 1-18

Wang, Q., Adiku, S., Tenhunen, J., & Granier, A. (2005b). On the relationship of NDVI with leaf area index in a deciduous forest site. *Remote Sensing of Environment, 94*, 244-255

Wang, Z., Bovik, A.C., Sheikh, H.R., & Simoncelli, E.P. (2004). Image Quality Assessment: From Error Visibility to Structural Similarity. *IEEE Transactions on Image Processing, 13*, 600-612

White, M.A., & Nemani, R.R. (2006). Real-time monitoring and short-term forecasting of land surface phenology. *Remote Sensing of Environment, 104*, 43-49

Wilson, E.H., & Sader, S.A. (2002). Detection of forest harvest type using multiple dates of Landsat TM imagery. *Remote Sensing of Environment, 80*, 385-396

Wolf, A. (2010). Using WorldView 2 Vis-NIR MSI Imagery to Support Land Mapping and Feature Extraction Using Normalized Difference Index Ratios. In. Longmont CO

Wolter, P.T., Mladenoff, D.J., Host, G.E., & Crow, T.R. (1995). Improved Forest Classification in the Northern Lake States Using Muti-Temporal Landsat Imagery. *Photogrammetric Engineering and Remote Sensing, 61(9)*, 1129-1143

Yan, E., Wang, G., Lin, H., Xia, C., & Sun, H. (2015). Phenology-based classification of vegetation cover types in Northeast China using MODIS NDVI and EVI time series. *International Journal of Remote Sensing, 36*, 489-512

Yang, X., & Lo, C.P. (2002). Using a time series of satellite imagery to detect land use and land cover changes in the Atlanta, Georgia metropolitan area.

International Journal of Remote Sensing, 23, 1775-1798

Ye, Y., Wu, Q., Zhexue Huang, J., Ng, M.K., & Li, X. (2013). Stratified sampling for feature subspace selection in random forests for high dimensional data. *Pattern Recognition, 46*, 769-787

Yeom, J., Han, K., Lee, C., Park, Y., & Kim, Y. (2008). A Detection of Vegetation Variation Over North Korea using SPOT/VEGETATION NDVI. *Journal of the Korean Association of Geographic Information Studies, 11(2)*, 28-37

Yoo, S.J., Lee, W.K., Lee, S.H., Kim, E.S., & Lee, J. (2011). Approach for Suitable Site Selection and Analysis for Reforestation CDM using Satellite Image and Spatial Data in North Korea. *Journal of the Korean society for geo-spatial information system, 19(3)*, 3-11

Yool, S.R., Makaio, M.J., & Watts, J.M. (1997). Techniques for computer-assisted mapping of rangeland change. *Journal of Range Management, 50(3)*, 307-314

Zhang, J., Li, P., & Wang, J. (2014). Urban Built-Up Area Extraction from Landsat TM/ETM+ Images Using Spectral Information and Multivariate Texture. *Remote Sensing, 6*, 7339-7359

Zheng, D., Wallin, O.D., & Hao, Z. (1997). Rates and patterns of landscape change between 1972 and 1988 in the Changbai Mountain area of China and North Korea. *Landscape Ecology, 12*, 241-254

Zhu, X., Chen, J., Gao, F., Chen, X., & Masek, J.G. (2010). An enhanced spatial and temporal adaptive reflectance fusion model for complex heterogeneous regions. *Remote Sensing of Environment, 114*, 2610-2623

Zhu, X., Helmer, E.H., Gao, F., Liu, D., Chen, J., & Lefsky, M.A. (2016). A flexible spatiotemporal method for fusing satellite images with different resolutions. *Remote Sensing of Environment, 172*, 165-177

Zhu, Z., Woodcock, C.E., & Olofsson, P. (2012). Continuous monitoring of forest disturbance using all available Landsat imagery. *Remote Sensing of Environment, 122*, 75-91

Zhukov, B., Oertel, D., Lanzl, F., & Reinhackel, G. (1999). Unmixing-Based Multisensor Multiresolution Image Fusion. *IEEE Transactions on Geoscience and Remote Sensing, 37(3)*, 1212-1226

Zurita-Milla, R., Clevers, J., & Schaepman, M.E. (2008). Unmixing-Based Landsat TM and MERIS FR Data Fusion. *IEEE Geoscience and Remote Sensing Letters, 5*, 453-457

Abstract in Korean

산림생태계는 인류에 여러 가지 생태계 서비스를 제공한다. 그러나 장기간의 인위적 압력과 산불, 산사태, 가뭄 등과 같은 자연 재해, 더불어 기후변화와 같은 비생물적 요인 변화로 인하여 산림 생태계가 제공하는 생태계 서비스는 점차 감소된다. 북한은 전 세계에서 산림 황폐율이 높은 나라 중 하나이며, 개간된 산지와 황폐된 산림의 증가는 북한 산림 생태계와 인근 주민 생활에 위협을 주는 가장 주요한 요소이다. 이러한 산림 파괴는 북한의 낙후한 농업기술로 인하여 발생되었다고 할 수 있다. 산지의 개간으로 인하여 토양층이 얇아지고 농작물의 생산력이 감소되며 결국에는 방치되어 황폐지로 이어진다. 북한의 이러한 산림 훼손으로 인해 자연 재해에 취약하며 매년 홍수, 산사태, 산불 등 재해로 인한 심각한 피해가 보고되고 있다. 특히 강우로 인한 토양 유실 또는 산사태 등은 매년 심각해지며 토양 자체의 생산성을 감소시켜 조림사업을 시행하더라도 생태계 복원이 어렵게 된다. 따라서 우선 복원지역 선정, 체계적인 복원계획 및 관리방안을 수립하기 위하여 황폐된 산림과 개간된 산림을 지속적으로 모니터링하는 것이 필수적이다.

토지피복 또는 산림 황폐지 및 산림 개간 지역을 모니터링하는 것은 많은 과학분야에서 사용되는 가장 기본적인 정보 중 하나로, 북한과 같이 접근이 어렵고 사용 가능한 데이터가 부족한 지역을

높은 공간 해상도로 주기적이고 정확하게 분석하는 것은 여전히 도전적인 과제이며 북한 지역 연구에서 필요한 연구이다. 이를 위해 본 연구에서는 정밀 공간해상도로 주기적인 산림피복을 정확하게 분류하고 모니터링하기 위한 비용대비 효율적인 방법을 제안하고자 한다.

우선, 산림 황폐지역인 무입목지와 개간된 산림지역인 개간산지를 반사 값이 유사한 산림 또는 농지로부터 높은 정확도로 분류하기 위하여 식생 계절 기반의 다중 지표의 최적의 조합을 제안하였다. 선행 연구에서는 산림 파괴 지역을 분류하기 위해 단일 영상의 스펙트럼을 기반으로만 분류하였기에 넓은 지역의 토지 피복 유형의 이질적인 스펙트럼 특징을 파악하는 것이 어려웠다. 본 연구 결과는 기존의 연구에서 위의 한계점으로 인해 황폐지역 구분 시 오직 산림과 건초지 분류에 초점을 맞춘 연구의 한계점을 해결하였다.

그 결과를 요약하면 다음과 같다. 1) 식생의 성장, 식생의 캐노피, 식생의 수분 상태를 표현하는 지수인 NDVI, NDSI, NDWI 의 계절적인 변화 특성은 반사 값이 유사한 피복에서 전형적인 계절적인 차이를 보였으며 이는 단일 영상을 사용했을 때의 반사 값의 유사성으로 나타난 오류를 해결해주고 분류의 정확도를 높였다. 2) 이질적이고 복잡한 토지피복과 변화를 분석하기 위한 랜덤포레스트는 많은 변수를 입력했을 때 가장 효과적인 도구인 것으로 나타났다. 계절 특성을 반영하는 식생 지수와 랜덤포레스트를 결합하여 분류한

결과 89.38%의 높은 정확도로 나타났다. 3) 분류에 20% 이상으로 크게 기여한 식생 지수는 3 월에서 5 월까지 식생 성장 기간의 NDSI, 계절이 끝나는 기간인 9 월 NDVI, 그리고 계절 초기와 마지막 시점인 3 월, 4 월, 10 월의 NDWI 인 것으로 나타났다. 이 변수들의 조합은 북한의 산림 황폐지역 또는 파괴지역을 구분하거나 모니터링하는데 효과적이다. 본 연구결과는 이질적인 경관에서 식생 피복을 분류하는데 있어 정확도를 크게 제고하였고 개간산지와 무입목지 분류의 신뢰성을 제시하였다. 따라서 본 연구에서 제시한 변수의 조합은 산림 파괴지역 또는 황폐지역을 주기적으로 모니터링 하는데 유용할 것으로 보인다.

둘째, 본 연구에서 제시한 변수의 조합과 랜덤 포레스트 분류 모형을 2001 년, 2010 년, 2016 년에 적용하여 각 년도의 토지피복을 분류하였고 1990 년대의 산림과 비교하여 각 년대의 황폐율을 계산하였다. 분류 결과 각 분류 과정에 나타난 불확실성은 7.93%~16.3%로 나타났다. 특히 2001 년 분류 결과에서 비교적 큰 불확실성이 나타났는데 이는 분류 모형 구축 시기인 2013 년은 2001 년에 비해 식생 계절 특징이 약간의 변화로 인해 불확실성이 16.3%로 가장 크게 나타난 것으로 사료된다. 산림 감소율은 1990~2001 년에는 3.13%/년으로 가장 큰 감소율로 나타났고, 2001~2010 년에는 0.88%/년으로 감소율이 대폭 감소된 것을 볼 수 있었다. 이는 북한 정부에서 산림 복원 계획과 국제사회에 대한 기술

교류 추진으로 인해 황폐율이 감소된 것으로 사료된다. 2010~2016 년의 산림 감소율은 1.43%/년으로 다시 증가 추세를 보였지만, 이는 2010 년 이후 기후는 평년기후와 달리 극한 기상이 자주 발생하며 이러한 기상 요건이 산림 황폐화를 가속하는데 일조한 것으로 사료된다.

셋째, 가장 얻기 쉬운 데이터를 활용하여 정밀하고 연속적인 위성 영상 데이터를 구축하기 위하여 본 연구에서는 두 영상의 변량을 통한 시공간 데이터 융합 기법인 RDSFM (Residual Distribution-based Spatiotemporal Data-Fusion Method)를 제안하였다. 기존의 시공간 융합 기법은 입력 시간과 예측 시간 사이 발생한 스펙트럼 변화지역을 예측하는데 어려움이 있었다. 특히 식생 피복 같은 경우 계절 변화에 따라 각 밴드 값의 반응 방향과 변화 레인지는 서로 다를 수 있다. 이러한 한계점을 해결하기 위해 본 연구에서는 두 개 서로 다른 시간대의 영상의 스펙트럼 상관관계를 통해 각 밴드의 최대 변량을 기반한 가중치로 잔여 값들을 분배하여 예측하는 RDSFM 을 제시하였다. RDSFM 은 FSDAF 기법에서 제기한 이질성지수, IR-MAD, unmixing 기반 기법과 가중 함수 기법들을 하나의 프레임워크로 통합하였다. 본 연구에서는 실제 위성영상으로 테스트하여 예측 결과를 UBDF, FSDAF 기법과 비교하였다. 예측 정확도 비교 결과 RDSFM 이 더 높은 예측 정확도로 나타났으며

특히 파편화된 경관 및 NIR 밴드 예측에서 더 높은 정확도를 보여주고 있다.

RDSFM 이 FSDAF 보다 더 높은 정확도로 예측한 이유는 두 영상의 상관성을 통해 계산된 MAD 변량에 기반한 가중치를 부여함으로써 나타난 결과로 보여진다. MAD 는 정준상관분석에 기반한 변수 집단을 비교하여 무감독으로 변화된 지역을 탐지한다. MAD 기반의 가중치를 추정하기 위하여 우선 t1(입력 데이터 시간)에서의 정밀해상도 영상과 t2(예측 데이터 시간)에서의 거친 해상도 영상과의 변화를 탐지하였고, 두 센서간의 차이로 인하여 나타나는 변화를 덜어내기 위하여 t1 에서의 정밀해상도 영상과 거친 해상도 영상과의 변화를 탐지하여 계산되었다. 이는 거친 해상도 픽셀에서 각 밴드 subpixel 의 상대적인 변화를 효과적으로 감지할 수 있으며, 토지피복 변화 또는 클래스 내 스펙트럼 변화에 의한 픽셀 값을 예측하는데 도움이 된다. RDSFM 은 기타 시공간 융합 기법보다 더 높은 예측 정확도로 토지피복 변화를 분석하고, 식생의 계절적인 변화를 모니터링하며, 산림 황폐지역을 감지하는 등 다양한 영역에 효과적으로 활용할 수 있다.

마지막으로 위에서 제안한 방법들의 유효성을 판단하기 위하여 여러 식생 피복 유형이 가장 혼합되어 있는 지역에서 가장 심플한 분류 방법인 무감독 분류를 활용하여 2001 년과 2014 년에 발생한 황폐지역과 파괴된 지역을 구분함으로써 본 연구에서 제시한 방법의

간편성과 효율성을 증명하였다. 분류에 효과적인 계절 특성에 기반한 다중 식생변수들은 RDSFM 을 통해 구축된 변수 조합은 분류 오류를 줄이는데 가장 효과적인 방법이며 토지피복변화 및 황폐지역을 30m 의 공간해상도에서 분석 가능하다. 이러한 방식으로 2001 년과 2014 년 사이에 발생한 황폐지역을 산림에서 무입목지로 변화된 지역, 산림에서 개간산지로 변화된 지역, 개간산지에서 무입목지로 변화된 지역 세 가지로 구분하였다. 무감독 분류를 활용한 분류 결과 약 86.1%의 분류정확도를 나타냈으며 이는 매년 현지 조사 데이터가 없이 토지피복 변화를 분석하는데 비용대비 효과적임을 보여주고 있다.

종합하면, 식생계절 기반의 변수의 조합과 RDSFM 기법은 산림 피복 변화의 분류 및 모니터링에 있어 공간적 및 시간적 해상도를 향상시킬 수 있다. 또한 본 연구는 산림 황폐지역을 세분화하는 것이 체계적인 복원 계획 및 산림 생태계 분석에서 필요함을 제시하였다.

주요어 : 산림 황폐화, 산림 파괴, 랜덤 포레스트, 무감독 변화 탐지기법, 불혼합 기반 데이터 융합, 데이터 융합, 산림 피복 변화 모니터링

학번: 2014-31476